HIGH RESOLUTION LAKE-BASED MAGNETIC MAPPING

HIGH RESOLUTION LAKE-BASED MAGNETIC MAPPING AND MODELLING OF BASEMENT STRUCTURES WITH EXAMPLES FROM KÜÇÜKÇEKMECE LAGOON, TURKEY AND CHARITY SHOAL, LAKE ONTARIO

By Philip Suttak, B.Sc. (Hons)

A Thesis

Submitted to the School of Graduate Studies

In Partial Fulfillment of the Requirements

for the Degree

Master of Science

MASTER OF SCIENCE (2013) McMaster University
(Earth and Environmental Science) Hamilton, Ontario

TITLE: High-resolution lake-based magnetic mapping and modelling of basement structures, with examples from Küçükçekmece Lagoon, Turkey and Charity Shoal, Lake Ontario

AUTHOR: Philip Suttak, B.Sc. (McMaster University)

SUPERVISOR: Dr. Joseph Boyce

NUMBER OF PAGES: ix, 113

Abstract

Magnetic surveys are one of the principal geophysical methods employed to map the structure of basement rocks deeply buried below cover strata. In resource studies, aeromagnetic surveys are commonly acquired at regional scales (100-1000's km^2) while very few studies have attempted to resolve basement structures at site-scale (<10 km^2). In this study, high-resolution lake-based magnetic survey methods were evaluated for mapping of deeply-buried basement faults (Küçükçekmece Lagoon, Turkey; 6 km^2) and a suspected meteorite impact crater (Charity Shoal, Lake Ontario; 9 km^2). Total magnetic intensity (TMI) surveys were acquired using a single Overhauser magnetometer with 50-150 m line spacing. Interpretation of the magnetic data was aided by forward modelling of TMI data and depth to basement estimates using Euler and analytic signal methods.

Total magnetic intensity (TMI) maps of Küçükçekmece Lagoon identify several north-northwest trending (340-350°) magnetic lineaments that are aligned with strike-slip faults mapped from offshore seismic data. The pattern of magnetic anomalies in the lagoon is consistent with extensional normal faulting of bedrock and lake sediments. The orientation of en-echelon extensional faults is consistent with a transtensional regime, produced by active northwest-trending strike-slip splay faults of the North Anatolian Fault Zone (NAFZ).

Magnetic results from Charity Shoal reveal a large (>1400 nT) parabolic-shaped magnetic anomaly centered over the crater basin and an annular magnetic high (40-50 nT) corresponding with the basin rim. Euler depth to basement estimates indicate a crater depth of >600 m. Forward 2-D models verify that the observed TMI anomaly requires a deep (>450 m) depression in Precambrian basement or a source body (diatreme) with a remanent magnetization opposing the main field. Modelling results exclude the origin of the CSS as a shallow glacial erosional or karst sinkhole feature and are most consistent with a pre-Paleozoic meteorite impact in the Precambrian basement.

Acknowledgements

Research and graduate scholarship support provided by a Natural Sciences and Engineering Research Council of Canada (NSERC) Discovery Grant to J. Boyce and a grant from Istanbul University (Scientific Research Projects Coordination Unit, project #13154) to H. Alp. Research was facilitated by an academic software grant from Geosoft Ltd. and field equipment was provided by Marine Magnetics Ltd.

I'd like to thank Joe Boyce for believing in my academic potential and for having me as a graduate student these past two years. Your support and guidance was invaluable to my academic and personal growth.

I would like to thank Ulrich Riller for several discussions on fault kinematics and assistance developing my kinematic theories.

I would like to thank Doug Hrvoic for assistance with fieldwork and the field equipment.

I would like to thank the Graduate Think Tank for discussions on Charity Shoal. Especially fellow office mates Shawn Collins, Heidi Daxberger, Brady Gregory, Bobby Hendricks, Ilya Inozemtsev, Shawn Kovacs, and Rebecca Moumblow.

I would like to thank my family, especially my parents, for all the love and support. Since day one you have been pushing me to achieve.

Finally I would like to thank Christina Ioannou for the love and support I have received throughout the last two years.

Table of Contents

List of Figures and Tables

Chapter One

Chapter Two

CHAPTER THREE

Chapter One: Introduction

1. Introduction

Airborne magnetic survey methods are employed widely for mapping of geologic structure at site to regional scales in mineral exploration and geological studies (Boyce and Morris, 2002; Del Negro and Napoli, 2002; Dehler and Potter, 2002; Grauch et al., 2004). In marine settings, where drilling is costly, marine magnetic surveys can be used in combination with reflection seismic studies to characterize seabed geology (Jones, 2001). Ship-borne total magnetic intensity (TMI) and gradient measurements are increasingly employed in offshore oil and gas exploration to assist in characterizing sedimentary basins and depth to basement (Jacques et al., 2003). Marine magnetic surveys have also been applied successfully for site-scale investigations for archaeology, mapping of contaminated lakes sediments and detailed mapping of basement faults (Boyce et al., 2004; Boyce et al., 2009; Pozza et al., 2004; Weiss et al., 2007). Pozza (2002) employed high-resolution lake-based magnetic surveys for mapping of Precambrian basement structures in Lake Simcoe, in southern Ontario, Canada. Surveys were conducted with 75-100 m line spacing with the objective of mapping bedrock faulting associated with a Late Proterozoic shear zone. His results identified several northeast and north-south trending faults in the basement rocks that were previously unrecognized in the regional airborne (800-1000 m line spacing, 300 m flight elevation) Provincial aeromagnetic dataset. Pozza's (2002) study demonstrates that many buried fault structures in Precambrian basement rocks are below the resolution of available regional airborne datasets. An important implication of this is that the seismic hazard assessments based on regional aeromagnetic data underestimate the distribution of brittle fault zones and the seismic risk potential (Boyce and Morris, 2002; Boyce et al., 2002). Boyce et al. (2002) advocated the use of high-resolution marine/airborne magnetic surveys in combination with near-surface seismic reflection data as an improved method for delineating and mapping fault zones.

In this thesis, lake-based magnetic survey methods were evaluated for mapping and modelling of basement faults (Küçükçekmece Lagoon, Turkey) and to better resolve the origin of a suspected meteorite impact crater (Charity Shoal, Lake Ontario; 9 km^2). Geophysical surveys were conducted in Küçükçekmece Lagoon in July 2011 as a collaborative study with the University of Istanbul (Dr. H. Alp). The study was aimed at better resolving the location of basement fault structures below the heavily populated urban area (Avcılar; Fig. 1) in western İstanbul. Previous offshore seismic work had identified several northwest-trending branches of the Northern Anatolian Fault Zone (NAFZ) in the Marmara Sea and it was speculated that these faults may have ruptured and contributed to severe damage in Avcılar during the 17 August 1999 İzmit (M_b = 7.6) earthquake event (Gökaşan et al., 2002; 2003). Geophysical survey work was conducted in Küçükçekmece Lagoon in order to identify the possible northwestward extension of the NAFZ fault splays. Prior to this study, no magnetic or reflection seismic survey work had been conducted in the lagoon or onland in Avcılar to locate and map the suspected faults. The lagoon was selected as a favourable site for survey work as the basement geology includes high magnetic susceptibility Paleozoic-Mesozoic metamorphic and metasedimentary rocks and sediments (Strandja Massif, Istanbul Zone). The study is of importance, as it provides the first evidence for active (Holocene-recent) faults in the lake bed. The fault structures, imaged in single-channel seismic profiles, are spatially coincident with magnetic lineaments and may indicate zones of active rupture during the destructive 1999 İzmit earthquake.

A second study, conducted in eastern Lake Ontario (Fig. 2), investigated the Charity Shoal Structure (CSS). The CSS is a speculated meteorite impact structure located on the lakebed of Lake Ontario about 25 km south of Kingston, Ontario (Holcombe et al., 2001; 2013; Suttak et al., 2013). The CSS comprises a 1400 m wide crater-like feature with a 15-20 m deep central basin and well defined bedrock rim that rises within 2-3 m of the water surface. The enigmatic structure has a well-defined streamlined ‘tail’ composed of bedrock and/or glacial drift and has been modified to some extent by glacial abrasion and erosion

during the last Late Wisconsinan glacial cycle. Holcombe et al. (2013) interpreted the CSS as an Ordovician-age meteorite impact based on multi-beam bathymetric data and stratigraphic inferences. Subsurface data, required to interpret the depth and geometry of the CSS were not available. Other possible origins of the structure include a glacial erosional, volcanic intrusive or synclinal feature (fold) in the Precambrian basement (Holcombe, 2001; Suttak et al., 2013). The CSS has also been proposed as a possible post-Paleozoic impact crater, linked to a Younger Dryas (ca. 12.9 Ka) extinction event by Firestone et al. (2007). Lake-based magnetic and sub-bottom seismic surveys were conducted in July 2012 to investigate the subsurface geology of the CSS. The geophysical results indicate the structure is >450 m deep and is seated in the Late Proterozoic basement. These results are important as they rule out the origin of the CSS as a late post-glacial impact event.

2. Objectives

The overall aim of this thesis is to evaluate high-resolution marine magnetic methods for site-scale imaging and mapping of buried basement structures. The thesis is structured as two stand-alone papers, describing marine magnetic investigations conducted in Küçükçekmece Lagoon, Avcılar, Turkey (Chapter #2) and in northeastern Lake Ontario, Canada (Chapter # 3).

Chapter #2 documents the mapping of basement fault structures below Küçükçekmece Lagoon and their relation to the North Anatolian Fault Zone (NAFZ). The specific objectives were:

1) to map the structure of the Paleozoic-age Istranca basement and overlying sedimentary cover using magnetic survey methods
2) to document evidence for near-surface faulting in the lake basin Holocene sediments in shallow seismic and magnetic data,
3) to determine structural relations between faulting in Küçükçekmece Lagoon and northwest-trending faults on the north slope of the basin, in the Sea of Marmara,
4) to determine the depth to the Istranca metamorphic basement rocks.

Figure 1. Chapter Two study area located in the Marmara Sea region of northwest Turkey.

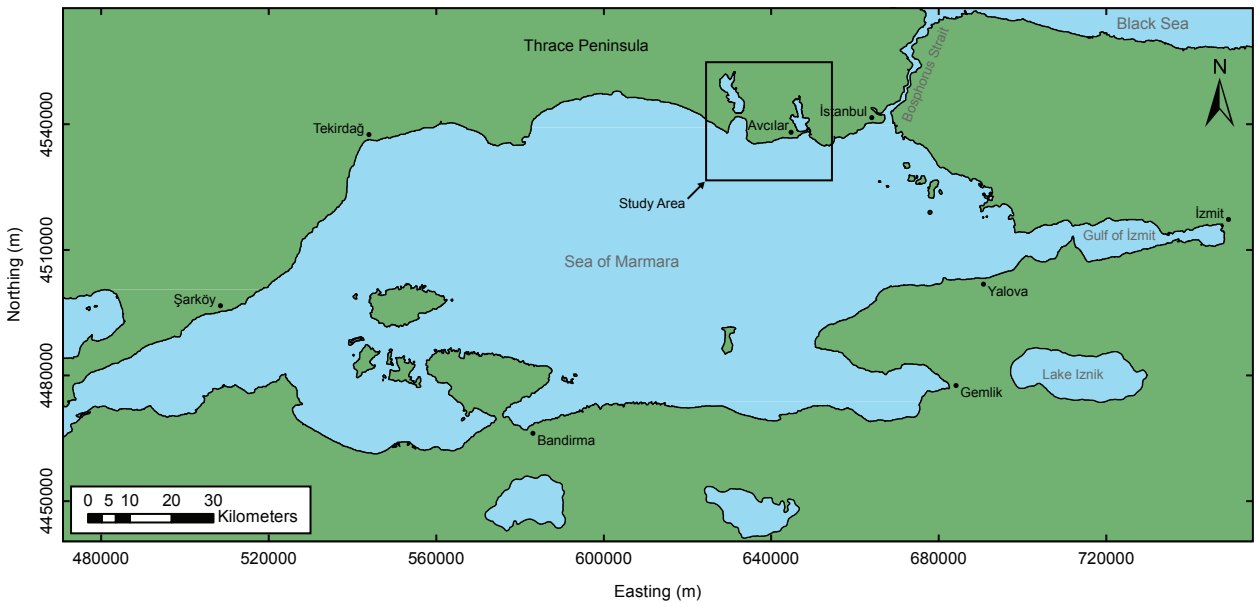
Thrace Peninsula
Black Sea
Bosphorus Strait
N
Tekirdağ
Avcılar
İstanbul
Study Area
İzmit
Gulf of İzmit
Sea of Marmara
Şarköy
Yalova
Lake Iznik
Gemlik
Bandirma
0 5 10 20 30
Kilometers
Northing (m)
4540000
4510000
4480000
4450000
480000
520000
560000
600000
640000
680000
720000
Easting (m)

Figure 2. Chapter Three study area located in southeast Ontario, Canada.

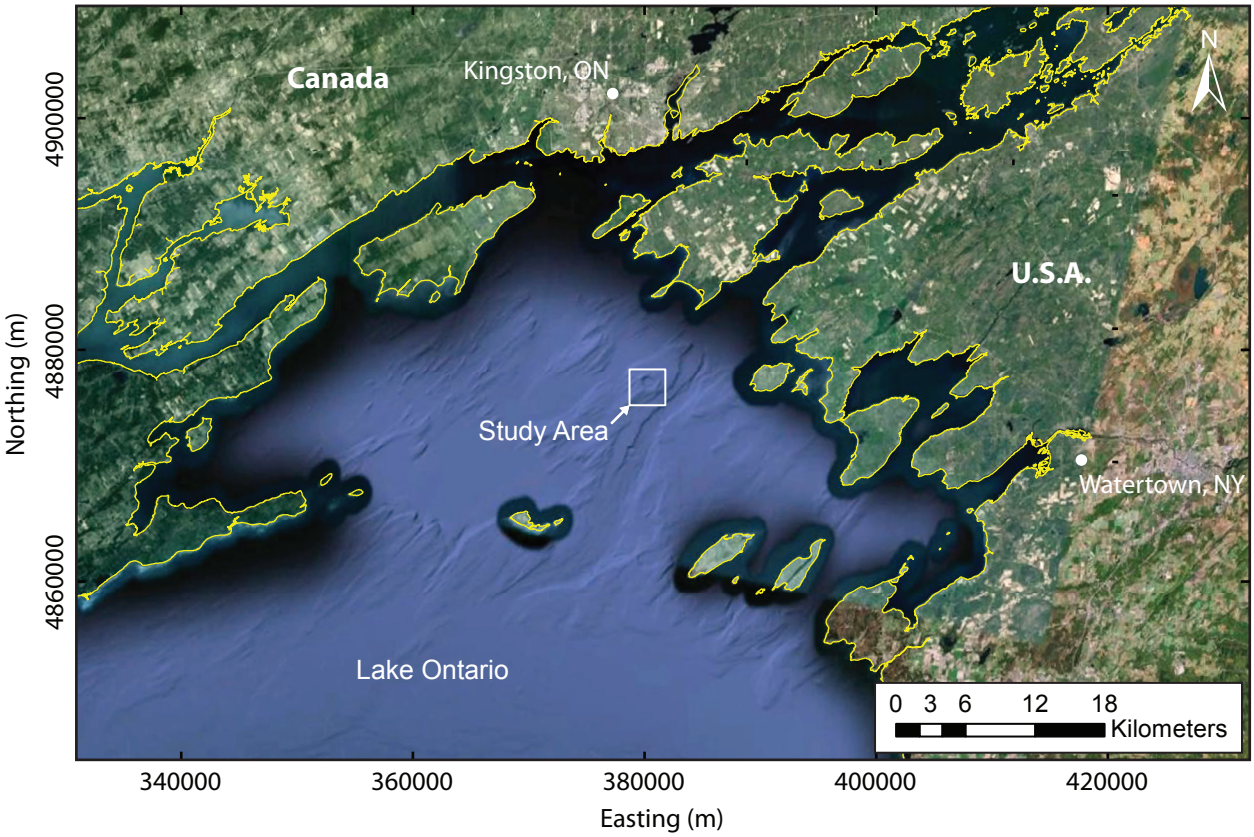
Canada
Kingston, ON
U.S.A.
Study Area
Watertown, NY
Lake Ontario
N
0 3 6 12 18
Kilometers
4900000
4880000
4860000
Northing (m)
340000
360000
380000
400000
420000
Easting (m)

In Chapter #3, high-resolution lake-based magnetic and seismic surveys are employed to investigate the origin of the Charity Shoal Structure (CSS), a suspected meteorite impact crater. The specific objectives were:

1) to map the TMI anomaly and to determine the subsurface structure and depth of the CSS using seismic and magnetic data,
2) to test various geological models for the crater origin using 2-D potential field modelling, including a previously proposed impact crater origin.

3. Methods

High-resolution marine magnetic surveys were acquired at both study areas using a Marine Magnetics SeaSPY^{TM} magnetometer sampling at 2 Hz. The SeaSPY^{TM} employs an omni-directional Overhauser sensor with an accuracy of 0.1 nT and a sensitivity of 0.01 nT. A Marine Magnetics Sentinel^{TM} base-station magnetometer was deployed for the Charity Shoal survey. Seismic reflection profiles and bathymetry data were acquired at both study areas to aid the interpretation of magnetic data. In Küçükçekmece Lagoon seismic data were acquired with an Applied Acoustics AA301 (50-350 Joule) single-channel boomer seismic system. The Charity Shoal survey utilized a 12-24 kHz Knudsen 320BP chirp sub-bottom profiler. The magnetic survey data were processed in Geosoft Oasis Montaj^{TM} using a processing flow that included diurnal and lag corrections and iterative leveling (Pozza, 2002)(see Chapter #2 and #3 for details). Forward modelling was conducted in GM-SYS 2-D and depth estimates were calculated in Geosoft using Euler and analytic signal methods (Reid et al., 1990; MacLeod et al., 1993; Mushayandebvu et al., 2001). Processing of seismic reflection profiles included band-pass filtering and deconvolution to reduce ringing from the water-bottom multiple.

4. Statement on Authorship of Papers

Chapters #2 and #3 are being prepared for publication as journal articles and were co-authored with the supervisor (Boyce) and research collaborators (Alp, Hrvoic). P. Suttak was responsible for data collection, analysis and interpretation of magnetic and seismic data and thesis preparation under the supervision of J. Boyce. P. Suttak processed all geophysical data and prepared all maps and illustrations. Boyce was responsible for thesis research supervision, including design of research projects, editing and preparation of manuscripts and interpretation of research results. D. Hrvoic assisted with magnetic data collection and provided the survey boat for the Charity Shoal survey. H. Alp assisted with the magnetic data collection and performed the seismic data collection during the Avcılar survey.

Chapter Two: Geophysical evidence for extension of active branches of the North Anatolian Fault Zone (NAFZ) below Küçükçekmece Lagoon, Avcılar, Turkey

Philip Suttak[a], Joseph I. Boyce[a], Hakan Alp[b] and Doug Hrvoic[a]

[a] School of Geography and Earth Sciences,

McMaster University, Hamilton, ON L8S 4K1

[b] Dept. of Geophysical Engineering,

Istanbul University, Avcılar, Turkey

Keywords: North Anatolian Fault Zone, magnetic survey, seismic, Marmara Sea, earthquake, Avcılar

Abstract

The Marmara (İzmit) earthquake of 17 August 1999 (M_b = 7.6) caused significant damage across a large area of Metropolitan Istanbul, including the town of Avcılar, which was severely impacted though more than 100 km distant from the epicenter. Earthquake damage has been attributed ruptures on northwest-trending branches of the North Anatolian Fault Zone (NAFZ) but fault locations and co-seismic deformation have not been documented onshore. In this study, a marine geophysical survey was conducted in Küçükçekmece Lagoon (16 km^2) to investigate the possible extension of branches of the NAFZ below the Avcılar area. More than 200 line km of total field magnetic data and 1-10 kHz boomer seismic reflection profiles were acquired to investigate evidence for faulting in the lagoon bottom sediments.

Total magnetic intensity (TMI) maps identify several north-northwest trending (340-350°) magnetic lineaments (L1-L5) that are aligned with strike-slip faults mapped from offshore seismic data. Analytic signal depth estimates indicate magnetic source bodies at ~100 m depth within the Thrace Basin Cenozoic sediments. Forward modelling of TMI data demonstrates that the anomalies (5-10 nT) are consistent with normal fault displacement of Paleozoic Istranca basement rocks and overlying Thrace sediments with vertical displacements of 15-25 m. Seismic profiles revealed faults in the Holocene lake bottom sediments with apparent vertical offsets of 0.5-1 m. Holocene faults are co-located in many instances with magnetic lineaments and are interpreted as normal faults produced by reactivation of more deeply seated faults in the underlying Istranca basement rocks. Seismic and magnetic results confirm the presence of recent active faulting in Küçükçekmece Lagoon and corroborate previous studies that have predicted northwest extension of NAFZ (New Marmara Fault) below the Avcılar area. The pattern of magnetic anomalies in the lagoon is consistent with extensional normal faulting of bedrock and lake sediments. The orientation of the en-echelon extensional faults is consistent with a transtensional regime produced by active northwest-trending strike-slip splay faults of the NAFZ.

1. Introduction

The Marmara Sea region in northwest Turkey has a history of destructive earthquakes associated with the seismically active North Anatolian Fault Zone (NAFZ)(Fig. 1)(Hubert-Ferrari et al., 2000; Bulut et al., 2009). The NAFZ is a major west-east trending continental transform boundary (>1600 km) separating the Eurasian and Anatolian plates (Fig. 1A)(Sengör et al., 2005; Bulut et al., 2009). The transform is characterized by high rates of strain and dextral slip (>20-30 mm yr^{-1}), which accommodates the westward escape of Turkey under the convergence of the Arabian and Eurasian plates (Fig. 1A)(Hergert and Heidbach, 2010). The NAFZ formed sometime between 11 and 13 Ma in the east and propagated westward from the Karliova triple junction through series of seismic ruptures (Armijo et al., 1999; Sengör et al., 2005). In the Marmara region, 70 km to the east of İzmit, the NAFZ splays into three major fault segments; the northern, middle and southern branches (Fig. 1)(Gasperini et al. 2011). The north branch (NAF-NB) passes under the Sea of Marmara entering at the Gulf of İzmit and emerging on the Thrace peninsula in the southwest as the Ganos fault (Fig. 1). The south branch (NAF-SB) remains on land to the south of the Sea of Marmara.

Seismicity along the NAFZ has been observed for over 2000 years. In the past century alone the NAFZ has ruptured 900 km of its length (Huber-Ferrari et al., 2000). Sengör et al. (2005) state that the NAFZ experiences century long seismic cycles that begin in the east and propagate westward. Since the late 1930's a trend of progressive earthquake failures has been observed propagating westward along the NAFZ starting with the 1939 Erzincan earthquake and continuing with the 1999 İzmit and Düzce earthquakes (Stein et al., 1997). The westward propagation of stress and progressive earthquake failures along the NAFZ now places the Marmara region in an area of high seismic risk (Barka, 1992). The recent seismicity in this region has been observed though five earthquakes between M = 6 and M = 7 and three earthquakes greater than M = 7 in the Marmara region between 1990 and 1999 (Huber-Ferrari et al., 2000). Through spatial and temporal modelling it has been

Figure 1. A. Plate boundary map for eastern Mediterranean. Arrows indicate relative plate motion vectors. NAF = Northern Anatolian Fault, EAF = Eastern Anatolian Fault, DSF = Dead Sea Fault, K = Karliova triple junction (after Aksu, 2000). B. Tectonic map of Sea of Marmara region showing branches of NAF. NAF-NB = North Anatolian Fault northern branch, NAF-MB = North Anatolian Fault middle branch. Location of Avcılar study area (Fig. 2) shown in box. C. Schematic cross-section (A-A') across Çınarcık Basin showing interpreted negative flower structures with north and south boundary faults (after Aksu, 2000).

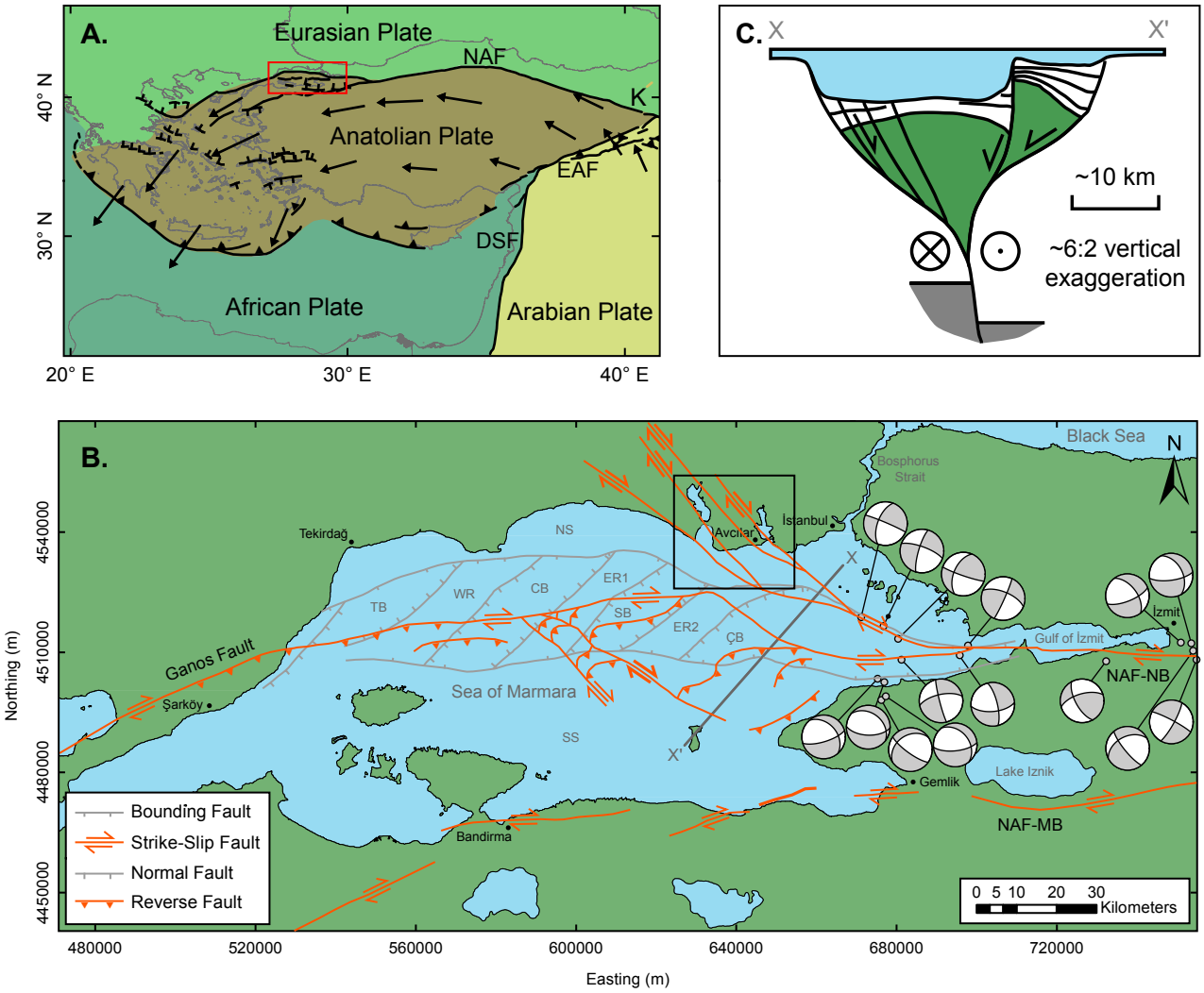
A.
Eurasian Plate
NAF
K
Anatolian Plate
EAF
DSF
African Plate
Arabian Plate
40° N
30° N
20° E
30° E
40° E
C.
X
X'
~10 km
~6:2 vertical
exaggeration
B.
Black Sea
N
Bosphorus
Strait
Tekirdağ
NS
İstanbul
Avcılar
X
ER1
CB
WR
TB
SB
ER2
ÇB
İzmit
Gulf of İzmit
Ganos Fault
Şarköy
Sea of Marmara
NAF-NB
SS
X'
Gemlik
Lake Iznik
NAF-MB
Bandirma
Bounding Fault
Strike-Slip Fault
Normal Fault
Reverse Fault
0 5 10 20 30
Kilometers
Northing (m)
4540000
4510000
4480000
4450000
480000
520000
560000
600000
640000
680000
720000
Easting (m)

predicted that two or more earthquakes of M = 7 or greater will occur in the Marmara region in the next few decades (Huburt-Ferrari et al., 2000). The two most recent earthquakes on the NAFZ occurred in 1999 (İzmit 17 August, M_b=7.6 and Düzce 12 November M_b = 7.2). The İzmit event ruptured the NAF-NB from İzmit to Düzce and the subsequent Düzce event extended the rupture 50 m to the east. The İzmit earthquake resulted in more than 15,000 deaths, 40,000 injuries and the displacement of 150,000 people (U.S.G.S., 2000). Gökaşan et al. (2002) first noticed a perplexing result of the earthquake; Avcılar, a town 20 km west of Istanbul, experienced greater destruction compared to the towns of Zeytinburnu, Bakırköy and Beylikdüzü, which were situated much closer to the epicenter. It has been noted though several studies that the underlying lithologic conditions in these the towns as well as building foundation and structure were all quite similar and could not fully account for the differences in destruction (Dalgic, 2004; Gökaşan et al., 2002; Sen, 2007). This observation led Gökaşan et al. (2002) to suggest that an active branch of the (NAFZ) underlies the Avcılar area.

In this paper, we present the results of a detailed geophysical survey of the Küçükçekmece Lagoon near Avcılar, Turkey (Fig. 2). Previous offshore seismic results indicated the presence of several northwest-trending splay faults from the NAFZ extending below Küçükçekmece Lagoon. Our seismic and magnetic data demonstrates the presence of recent faulting in the Holocene lakebed sediments and underlying bedrock. The lakebed faults are co-located with north-west trending magnetic lineaments that are interpreted as extensional faults in the underlying Cenozoic cover and Paleozoic basement rocks. Forward modelling of the potential field data provides constraints on the depths of magnetic source bodies and fault geometry. The Küçükçekmece lakebed faults and magnetic lineaments (340-350° NW) are sub-parallel to the trends of interpreted NAFZ strike-slip faults and may provide evidence for active fault rupture during the 1999 İzmit earthquake. These results are of importance for seismic risk assessment and understanding the future potential for damaging earthquakes in the Avcılar area. The methods can be applied more broadly to

investigation of fault structures in the Marmara Sea and in other seismically active coastlines.

2. Study Area and Geologic Setting

Küçükçekmece Lagoon (~16 km²) is a shallow coastal lagoon located about 20 km west of Istanbul (Fig. 1B). The lagoon has a maximum water depth of 20 m and is connected to the Sea of Marmara via a narrow navigation channel at its southeast end. The lagoon is located between the heavily urbanized Avcılar and Küçükçekmece districts (Fig. 2), which have a combined population of more than 1 million people. The town of Avcılar (population ~390,000) was subject to extensive damage during the 1999 M_W = 7.4 İzmit earthquake. More than 270 people were killed during the earthquake and 1450 buildings were severely damaged (Tezcan et al., 2002). The damage has been attributed in part to seismic amplification and resonance effects caused by soils and weak bedrock below the Avcılar area. Poor building practices and the widespread use of poor quality concrete was considered an exacerbating factor contributing to widespread damage to infrastructure (Dalgic, 2004). Others have argued, however, that the bedrock and soil characteristics are similar in nearby Istanbul, and that these factors cannot entirely explain the magnitude of the damage experienced in Avcılar (Gökaşan et al., 2002; Şen, 2007).

The geology of the Avcılar area was described recently by Dalgic (2004), Şen, (2007) and Ergintav et al. (2011). The basement rocks below the study area consist of Paleozoic-Mesozoic age metasedimentary rocks of the Istranca (Strandja) Massif in the west and the Paleozoic Istanbul Zone in the east (Dalgiç, 2004). Basement is overlain by a thick sequence (>600 m) of Middle Eocene and younger sedimentary rocks of the Thrace Basin (Figs. 3, 4). The Istranca metamorphics include phylite, schists and granitoid rocks, which are exposed at surface to the west of Büyükçekmece Lake in the Çatalca Fault Zone (CFZ). The CFZ is a northwest-southeast trending horst structure that represents the southern extension of the West Black Sea Fault (WBSF)(Fig. 3)(Ergintav, 2011).

The WBSF is a major north-south transform boundary in the eastern

Figure 2. Map of northeastern shelf of Sea of Marmara (Silivri and Çınarcık basins) and southeastern Thrace Peninsula showing previously mapped faults and topographic lineaments (modified from Gökaşan et al., 2002; 2003; Gasperini et al., 2011; Dalgiç, 2004; Ergintav, 2011). Several northwest-trending dextral-slip strike slip faults (F1-F5) and down to the south normal faults were identified in offshore seismic reflection data. Gökaşan et al. (2002) and interpreted NW-trending strike-slip faults as splays of the NAF-NB. Fault branch F2 underlies the eastern side of Küçükçekmece Lagoon. B. Inset showing terrestrial faults and fault scarps mapped in (from Şen, 2007). BL = Büyükçekmece Lagoon, KL = Küçükçekmece Lagoon. Location of seismic profile MCS-EK9 (Fig. 5) also shown.

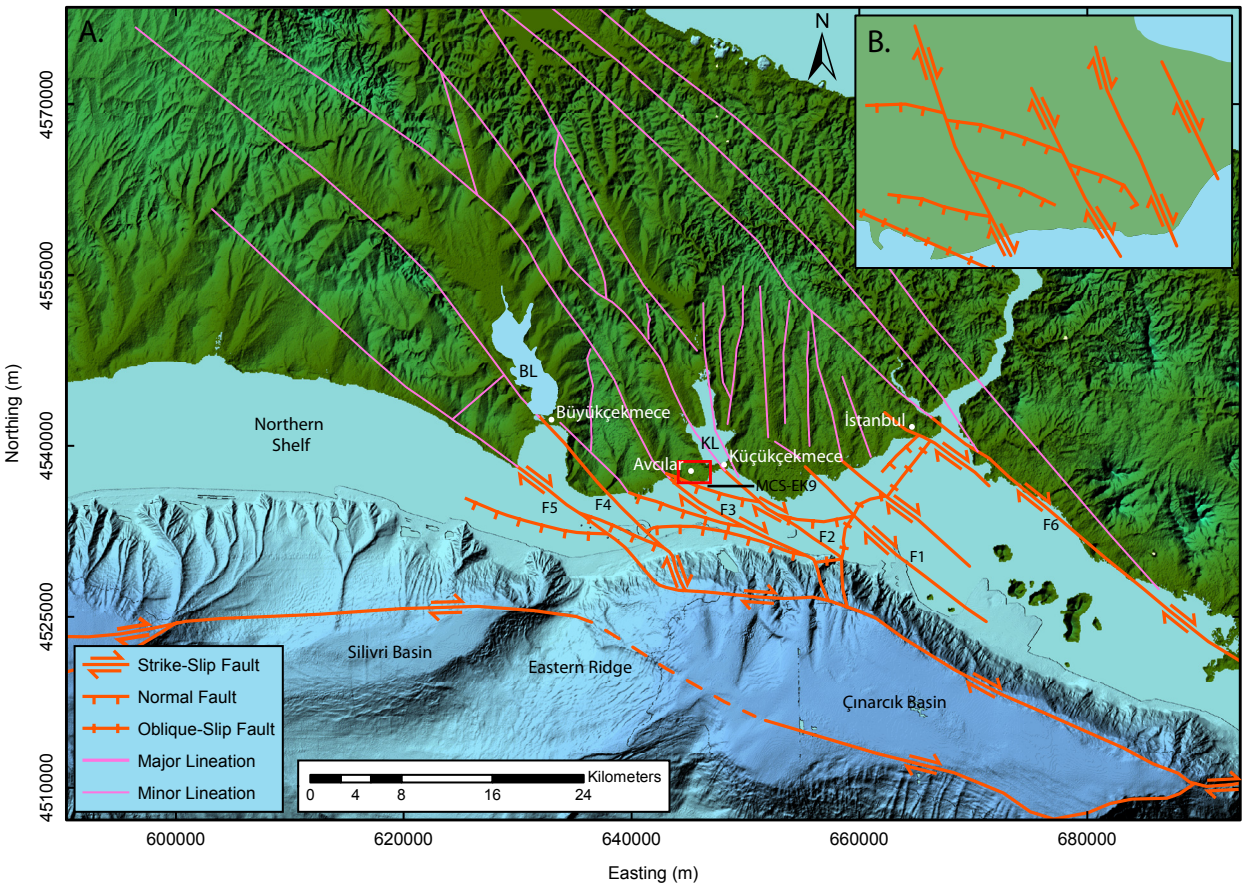
A.
B.
N
BL
Büyükçekmece
KL
Küçükçekmece
Avcılar
İstanbul
MCS-EK9
Northern
Shelf
F1
F2
F3
F4
F5
F6
Silivri Basin
Eastern Ridge
Çınarcık Basin
Strike-Slip Fault
Normal Fault
Oblique-Slip Fault
Major Lineation
Minor Lineation
Kilometers
0
4
8
16
24
4570000
4555000
4540000
4525000
4510000
600000
620000
640000
660000
680000
Northing (m)
Easting (m)

Thrace Peninsula that was active during the Cretaceous to Mid-Eocene (Okay et al., 1994). The Istanbul Zone comprises thick sequence of Carboniferous shale-sandstone turbidites that outcrop to the northwest of Küçükçekmece Lagoon (Fig. 3). The boundary between the Istranca Massif and the Istanbul Zone has been interpreted as a major dextral strike slip fault zone (Dalgiç, 2004). The location of the Istranca/Istanbul Zone contact is unknown, as it is buried below the Thrace Basin sediments but Dalgiç (2004) placed it under Küçükçekmece Lake based on available deep boreholes that intersect the basement (Fig. 4). The Thrace Basin sediments consist of Middle Eocene limestones and overlying Oligocene to Late Miocene clastics (Figs. 3, 4) recording shelf sedimentation, deltaic deposition and fluvial-lacustrine deposition in the Thrace Basin (Şen, 2007). In the Avcılar area, the local bedrock consists of Late Miocene limestones and clastics (Bakırköy, Güngören, and Çukurçeşme Formations) and the underlying Middle Eocene to Early Miocene Gürpinar Group (Figs. 3, 4). The Çukurçeşme, Danişment and Osmancık Formations include thick fluvial conglomerates and coarse deltaic sands, which have a combined thickness of >250 m. These clastic deposits are exposed in shoreline bluffs around the lagoon and form the bedrock below the lakebed (Fig. 4)(Dalgiç, 2004). Thrace Basin sediments dip 10-15° southwest and are overlain by thin Quaternary alluvial and lacustrine sediments (Figs. 3, 4)(Akarvardar et al., 2009; Duman et al., 2005). The Holocene bottom sediments in Küçükçekmece Lagoon consists of gravelly sands with minor clay content (<2%)(Pehlivan and Yilmaz, 2004).

The thickness of the Cenozoic sedimentary cover over the basement is poorly constrained in the Avcılar area due to a lack of deep borehole data. Shear wave studies conducted by Ergintav et al. (2011) indicate that the sedimentary cover is 100-200 m thick to the west of the CFZ and thickens to more than 600 m to the east of Büyükçekmece Lagoon. Dalgiç's (2004) estimated >500 m of Thrace Basin sediments overlying basement in the Avcılar area based on limited drill core data (Figs. 3B, 4).

Several fault zones have been mapped in the Avcılar area (Dalgiç, 2004; Şen, 2007) and on the northern shelf of the Çinarçik Basin to the south of the

study area (Fig. 2A)(Gökaşan et al., 2002; Gökaşan et al., 2003; Şen, 2007; Ergintav et al., 2011). Gökaşan et al. (2002) identified several NW-SE striking dextral strike-slip faults, in seismic profiles from the northern shelf of the Silivri and Çınarcık basins (F1-F5; Figs. 2, 3A). The northwest trending faults cut and displace an older set of E-W striking oblique and normal faults on the northern shelf, which led Gökaşan et al. (2002) to interpret the northwest strike slip faults as active splays of NAFZ (New Marmara Fault). They argued that the severe damage to Avcılar during the August 17, 1999 İzmit earthquake was a direct result of rupturing of these fault segments. Active rupturing and recent activity on these fault segments was also indicated by the pattern of aftershock events and microseismic activity in the Avcılar area, focused around the Büyükçekmece and Küçükçekmece lagoons (KOERI, 2000; Gürbüz et al., 2000; Gökaşan et al. 2002). Şen (2007) identified two sets of faults within Avcılar area; the now inactive CFZ (the continuation of the West Black Sea Fault; Figs. 2A, 3) and several north-northwest trending faults in the area southwest of Küçükçekmece Lagoon (Fig. 2B). The NNW faults cut and displace older west-east oriented normal fault scarps, indicating dextral strike-slip displacement (Şen, 2007). Ergintav et al. (2011) identified several northwest trending normal and dextral strike slip faults in seismic data from the Çınarcık basins, to the south of Küçükçekmece Lagoon (Fig. 5). The seismic data clearly shows steeply dipping normal faults and oblique faults that offset the thin Quaternary/Pliocene shelf sediments and underlying Miocene-Oligocene age Thrace Basin sediments (Fig. 5). Ergintav et al. (2011) argued that the extensive landslides on the west bank of the Küçükçekmece Lagoon and offshore slumping were a result of co-seismic deformation produced by rupturing of northwest NAFZ fault splays during the 1999 İzmit event.

3. Methods

3.1. Geophysical Survey

A total field magnetic survey was conducted in Küçükçekmece Lagoon in June 2011 (Fig. 6A). 210-line-km of magnetic data were acquired with a Marine

Figure 3. A. Surficial and bedrock geology of Avcılar area (modified from Dalgic, 2004; Ergintav et al., 2011). CFZ = Çatalca Fault Zone, WBSF = West Black Sea Fault. B. Stratigraphic column (modified from Dalgiç, 2004; Şen, 2007).

A.

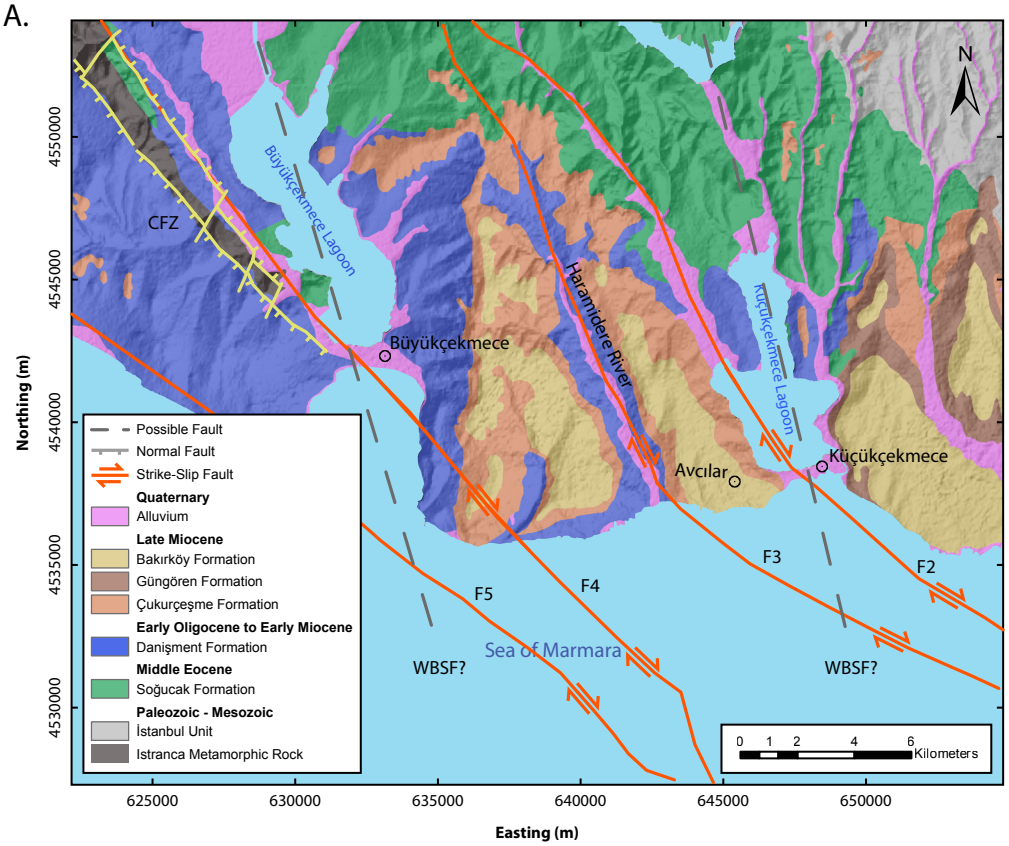
N
CFZ
Büyükçekmece Lagoon
Büyükçekmece
Haramidere River
Küçükçekmece Lagoon
Küçükçekmece
Avcılar
F2
F3
F4
F5
WBSF?
WBSF?
Sea of Marmara
0 1 2 4 6 Kilometers
Possible Fault
Normal Fault
Strike-Slip Fault
Quaternary
Alluvium
Late Miocene
Bakırköy Formation
Güngören Formation
Çukurçeşme Formation
Early Oligocene to Early Miocene
Danişment Formation
Middle Eocene
Soğucak Formation
Paleozoic - Mesozoic
İstanbul Unit
Istranca Metamorphic Rock
Northing (m)
4550000
4545000
4540000
4535000
4530000
625000
630000
635000
640000
645000
650000
Easting (m)

B.

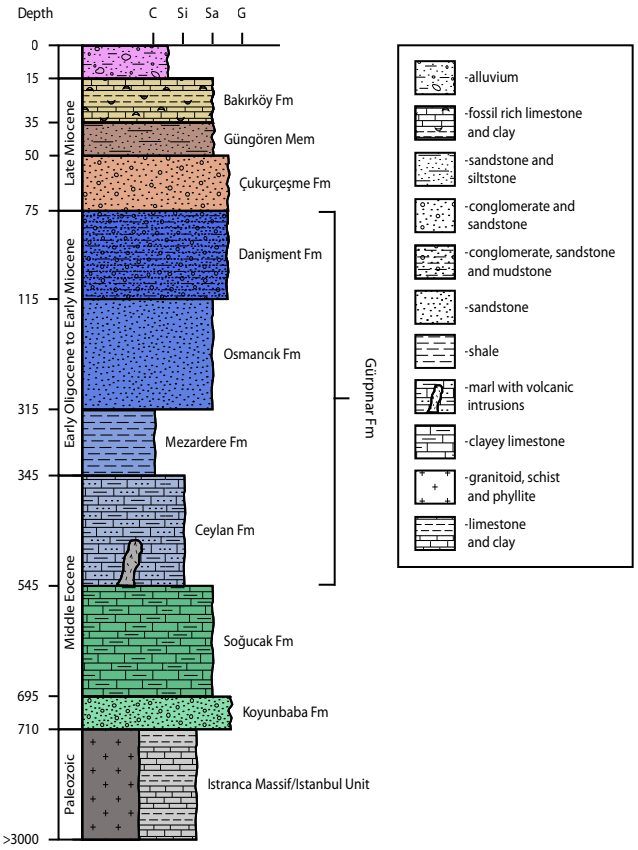
Depth
C Si Sa G
0
15
35
50
75
115
315
345
545
695
710
>3000
Late Miocene
Early Oligocene to Early Miocene
Middle Eocene
Paleozoic
Bakırköy Fm
Güngören Mem
Çukurçeşme Fm
Danişment Fm
Osmancık Fm
Mezardere Fm
Ceylan Fm
Soğucak Fm
Koyunbaba Fm
Istranca Massif/Istanbul Unit
Gürpınar Fm
-alluvium
-fossil rich limestone and clay
-sandstone and siltstone
-conglomerate and sandstone
-conglomerate, sandstone and mudstone
-sandstone
-shale
-marl with volcanic intrusions
-clayey limestone
-granitoid, schist and phyllite
-limestone and clay

Figure 4. Schematic W-E stratigraphic profile (modified from Dalgiç, 2004). Dalgiç (2004) interpreted boundary between Istranca Massif and Istanbul Zone to lie below Küçükçekmece Lagoon.

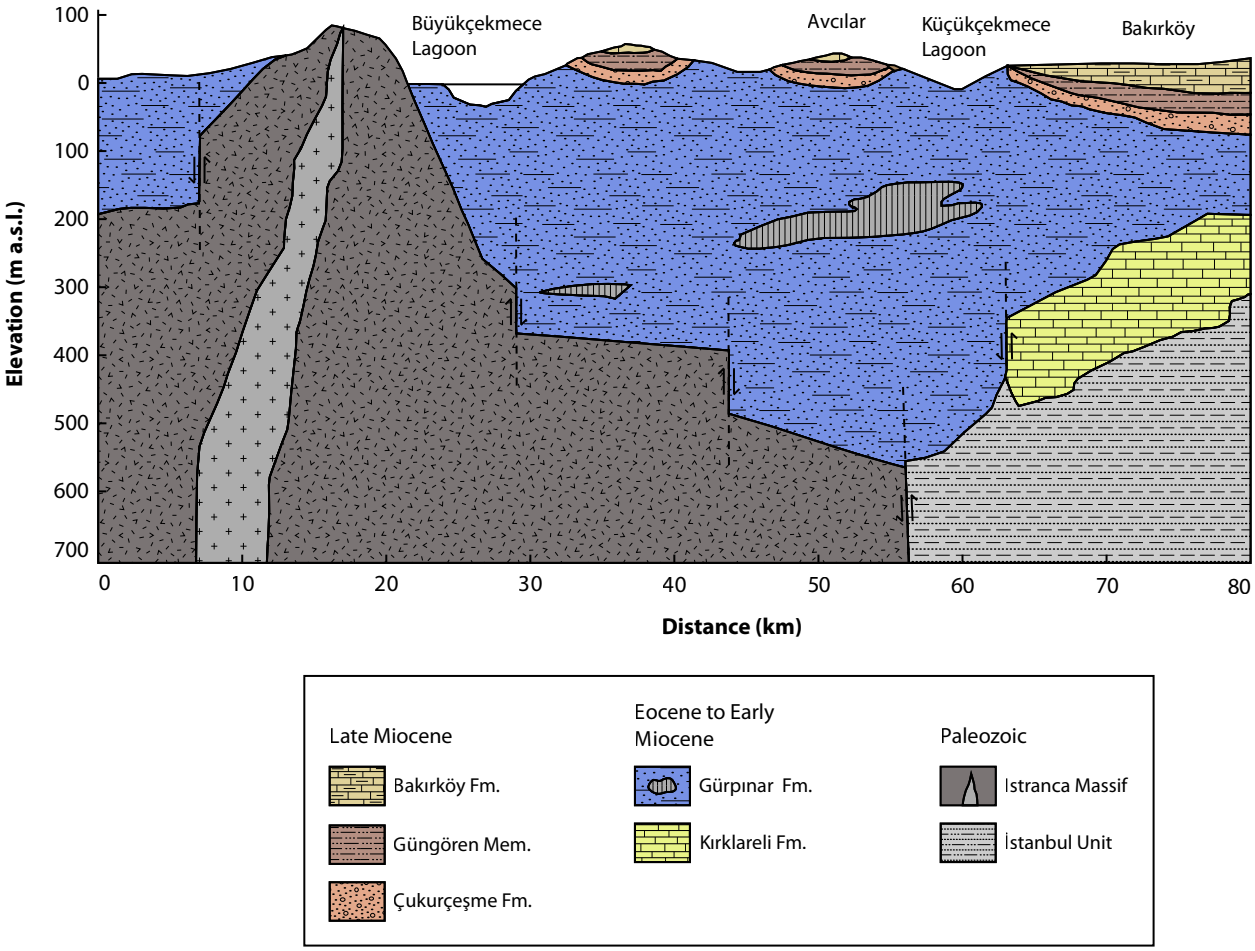
Büyükçekmece
Lagoon
Avcılar
Küçükçekmece
Lagoon
Bakırköy
Elevation (m a.s.l.)
100
0
100
200
300
400
500
600
700
0
10
20
30
40
50
60
70
80
Distance (km)
Late Miocene
Bakırköy Fm.
Güngören Mem.
Çukurçeşme Fm.
Eocene to Early
Miocene
Gürpınar Fm.
Kırklareli Fm.
Paleozoic
Istranca Massif
İstanbul Unit

Figure 5. W-E seismic profile MCS-EK9 showing faulting in Thrace Basin sedimentary rocks on north shelf of Çınarcık basin (modified from Ergintav et al. 2011). The faults have been interpreted as active strike slip faults, splaying off the NAFZ. The seismic data show that the faults also have a dip-slip component, as indicated by normal-slip displacements of several reflectors. Location of seismic profile shown in Figure 2.

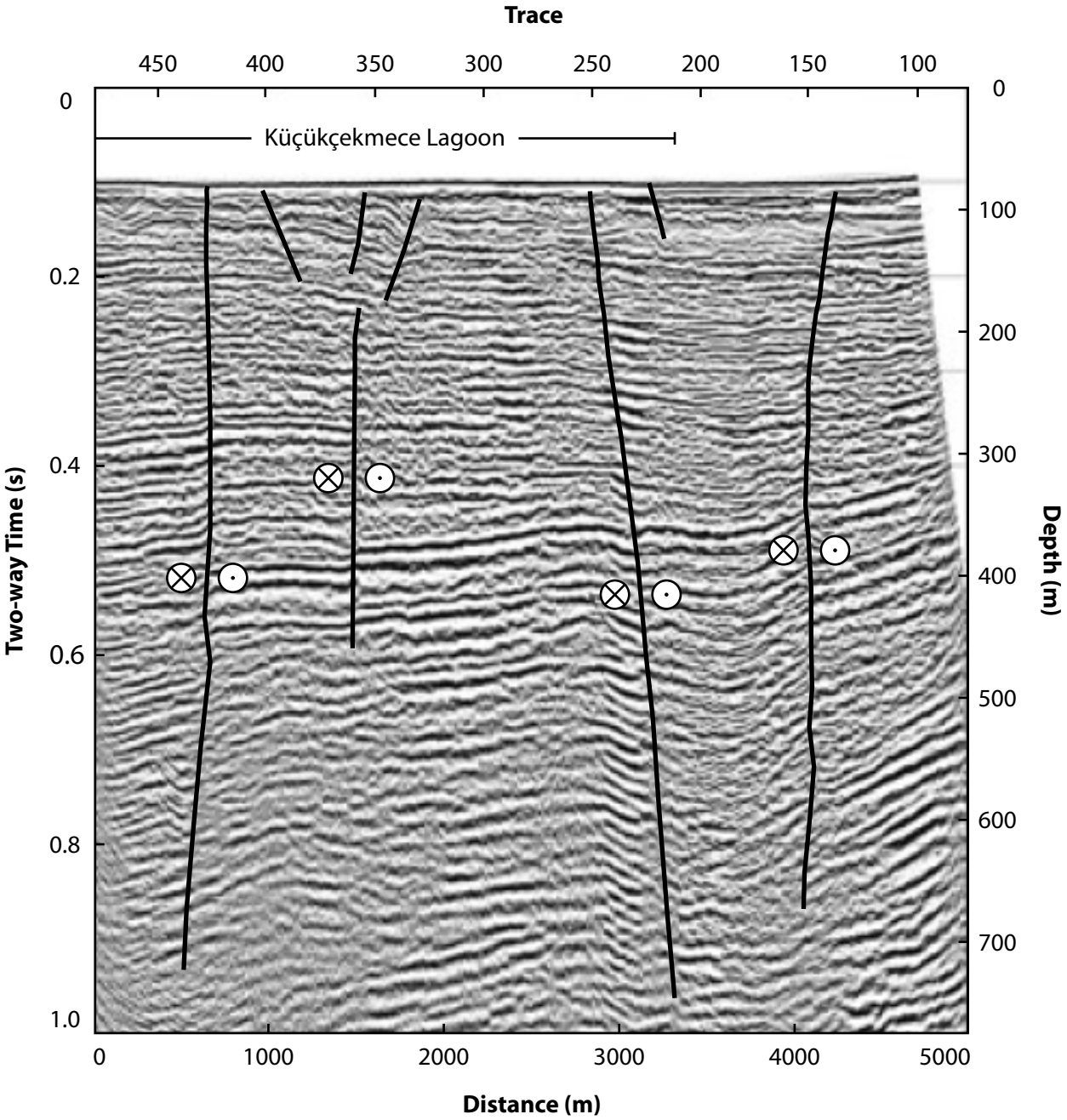
Trace
450
400
350
300
250
200
150
100
0
Küçükçekmece Lagoon
0.2
0.4
0.6
0.8
1.0
Two-way Time (s)
0
100
200
300
400
500
600
700
Depth (m)
0
1000
2000
3000
4000
5000
Distance (m)

Figure 6. A. Magnetic and seismic survey track lines. Location of seismic profile in Fig. 10 indicated. B. Bathymetry map interpolated from 200 kHz echosounder data.

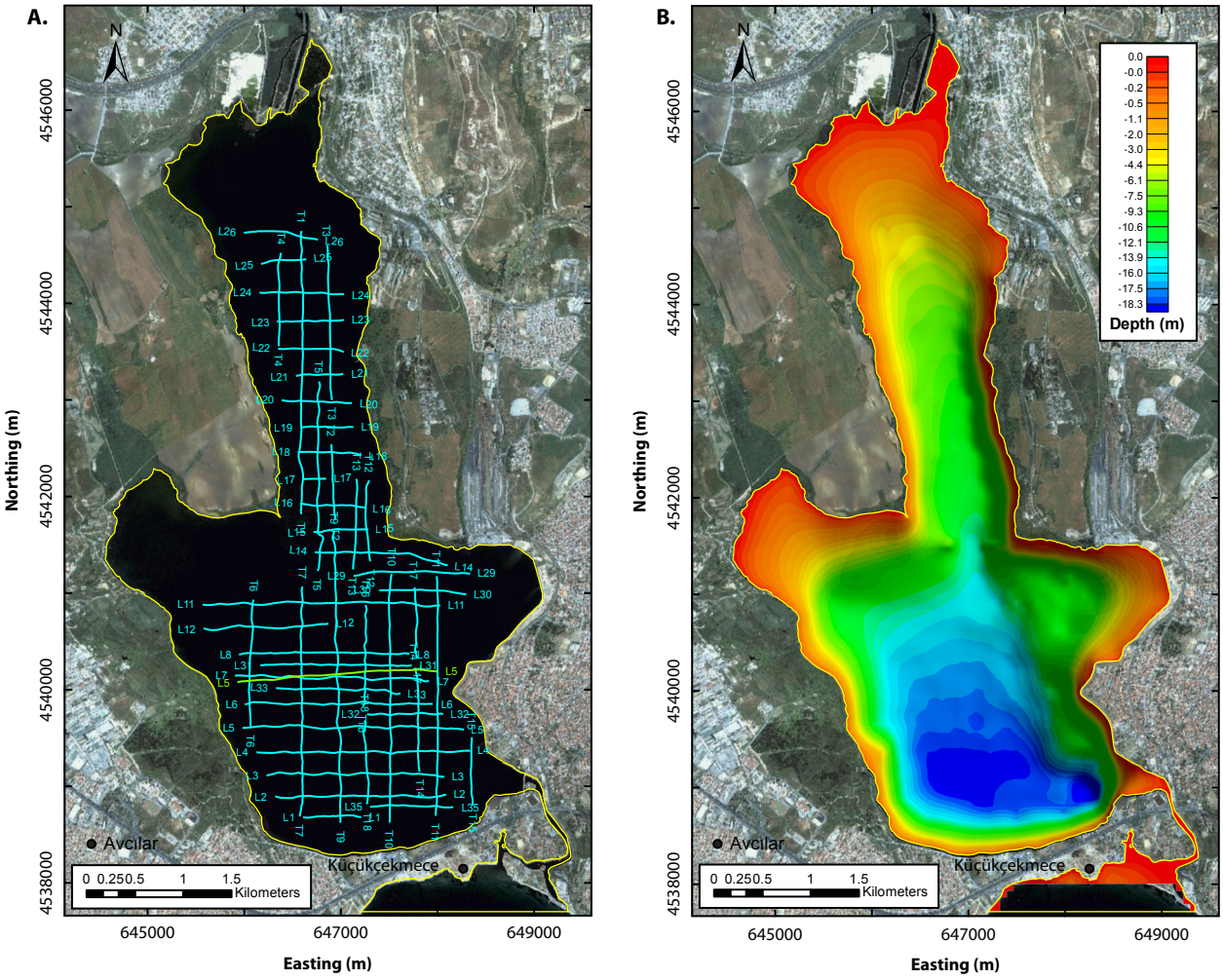
A.
B.
N
Northing (m)
Easting (m)
4546000
4544000
4542000
4540000
4538000
645000
647000
649000
Avcılar
Küçükçekmece
0 0.250.5 1 1.5
Kilometers
Depth (m)
0.0
-0.0
-0.2
-0.5
-1.1
-2.0
-3.0
-4.4
-6.1
-7.5
-9.3
-10.6
-12.1
-13.9
-16.0
-17.5
-18.3

Magnetics Seaspy™ (Overhauser) magnetometer over a 4-day period. The magnetometer was cycled at 2-Hz, providing a nominal inline sampling of 1 m. The magnetometer was towed 40 m behind the vessel. A total of 35 east-west lines and 17 north-south tie-tines were acquired with an average line spacing of 150-200 m (Fig. 6A). Bathymetry data were collected simultaneously with magnetic data using a 200-kHz echosounder mounted on the magnetometer towfish (Fig. 6B). Survey navigation and towfish positioning were determined using an onboard differential-GPS with a positional error of <1 m. Base-station magnetic data for diurnal corrections were obtained from the Kandilli Geomagnetic Observatory (ISK, 41.063N, 29.062E) at Boğaziçi University, Istanbul.

Sub-bottom seismic profiles were acquired in May 2012 using an Applied Acoustics AA301 broadband (0.5-10 kHz) boomer source with a 6-channel hydrophone array (Fig. 6A). The boomer catamaran was towed a distance of 5 m behind the survey boat and operated at 50-350 Joules per shot. The survey lines were acquired at nominal 300 line spacings in both the N-S and E-W directions.

3.2. Data Processing

Magnetic and bathymetry data were processed in Geosoft Oasis Montaj™ using the processing flow shown in Figure 7. The processing flow included signal editing/de-spiking, sensor layback, diurnal correction as well as tie-line and microlevelling (Luyendyk, 1997).

Drape corrections were applied to account for changes in water depth using the Geosoft Compudrape™ extension (Paterson et al. 1990) and a new calculated observation height of 0 m (lake level). The fully-corrected total and levelled magnetic intensity (TMI) data were gridded using a 50 m cell size using a simple Kriging algorithm with a spherical variogram model (Fig. 8A). The residual magnetic intensity (RMI) grid (Fig. 8B) was obtained through subtraction of a 200 m upward continued total field grid from the original total field grid. Analytic signal amplitude (ASA) was calculated on the TMI grid to permit depth estimation using the anomaly half-width method (Nabighian, 1972, 1974; Roest et al., 1992;

MacLeod et al., 1993)(Section 3.3.; Fig. 9). Processing of seismic data in Kingdom Suite™ included layback corrections, bandpass filtering (550-8000 Hz) and deconvolution to suppress direct wave arrivals and water-bottom multiples. Depth conversion of seismic data was performed using a water column velocity of 1450 ms^{-1} and estimated sediment velocity of 1550 ms^{-1}.

The 200 kHz bathymetry data were gridded at a 50 m cells using a minimum curvature algorithm (Briggs, 1974) following tie line levelling and editing of spurious depth values.

3.3. Magnetic Source Depth Estimation

The magnetic source body depth was estimated for several magnetic lineaments using the analytic signal amplitude (ASA) half-width method (Roest et al., 1992; MacLeod et al., 1993). The ASA or the energy envelope of the magnetic field intensity is employed widely as an interpretative tool, as it produces maxima, which are centered over the magnetic source bodies regardless of the direction of magnetization. The ASA is derived from the three orthogonal gradients of the TMI using the expression:

Eq. 1. $$|A(x,y)| = \sqrt{\left(\frac{dT}{dx}\right)^2 + \left(\frac{dT}{dy}\right)^2 + \left(\frac{dT}{dz}\right)^2}$$

Where A(x,y) is the amplitude of the analytic signal at (x,y) and T is the observed total magnetic intensity (TMI) at (x,y). As shown by Nabighian (1972), the ASA anomaly for a 2-D magnetic contact located at x=0 and depth *h* is given by:

Eq. 2. $$|A(x)| = \alpha \frac{1}{(h^2+y^2)^{\frac{1}{2}}}$$

Where α is the amplitude factor given by

Eq. 3. $$\alpha = 2Msind(1 - cos^2(I)sin^2(A))$$

Figure 7. Processing flow employed in magnetic and raw bathymetric data processing.

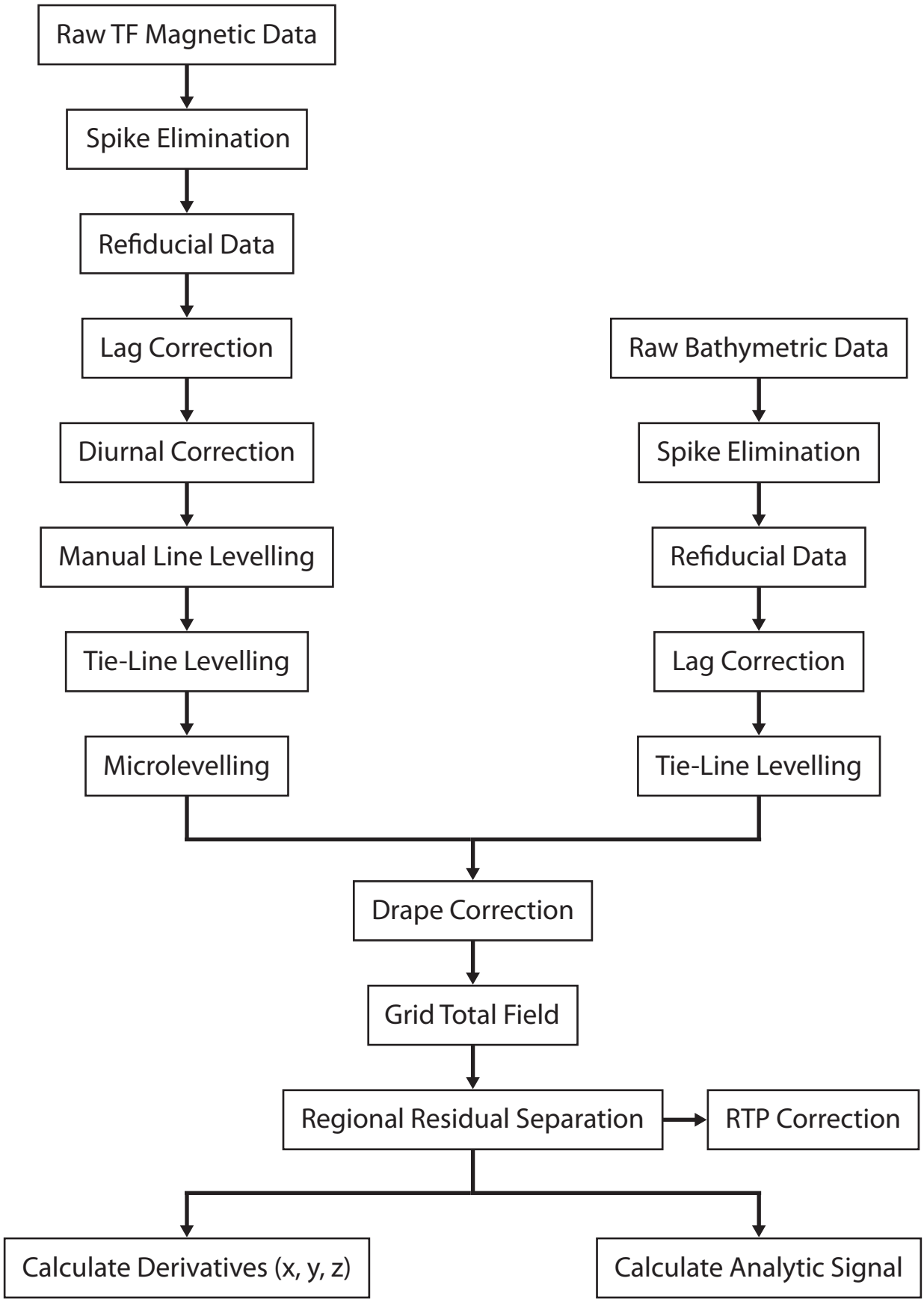
Raw TF Magnetic Data
Spike Elimination
Refiducial Data
Lag Correction
Diurnal Correction
Manual Line Levelling
Tie-Line Levelling
Microlevelling
Raw Bathymetric Data
Spike Elimination
Refiducial Data
Lag Correction
Tie-Line Levelling
Drape Correction
Grid Total Field
Regional Residual Separation
RTP Correction
Calculate Derivatives (x, y, z)
Calculate Analytic Signal

Figure 8. A. Total magnetic intensity (TMI) map. B. Residual magnetic intensity (RMI) map with interpreted magnetic lineaments (L1-L5).

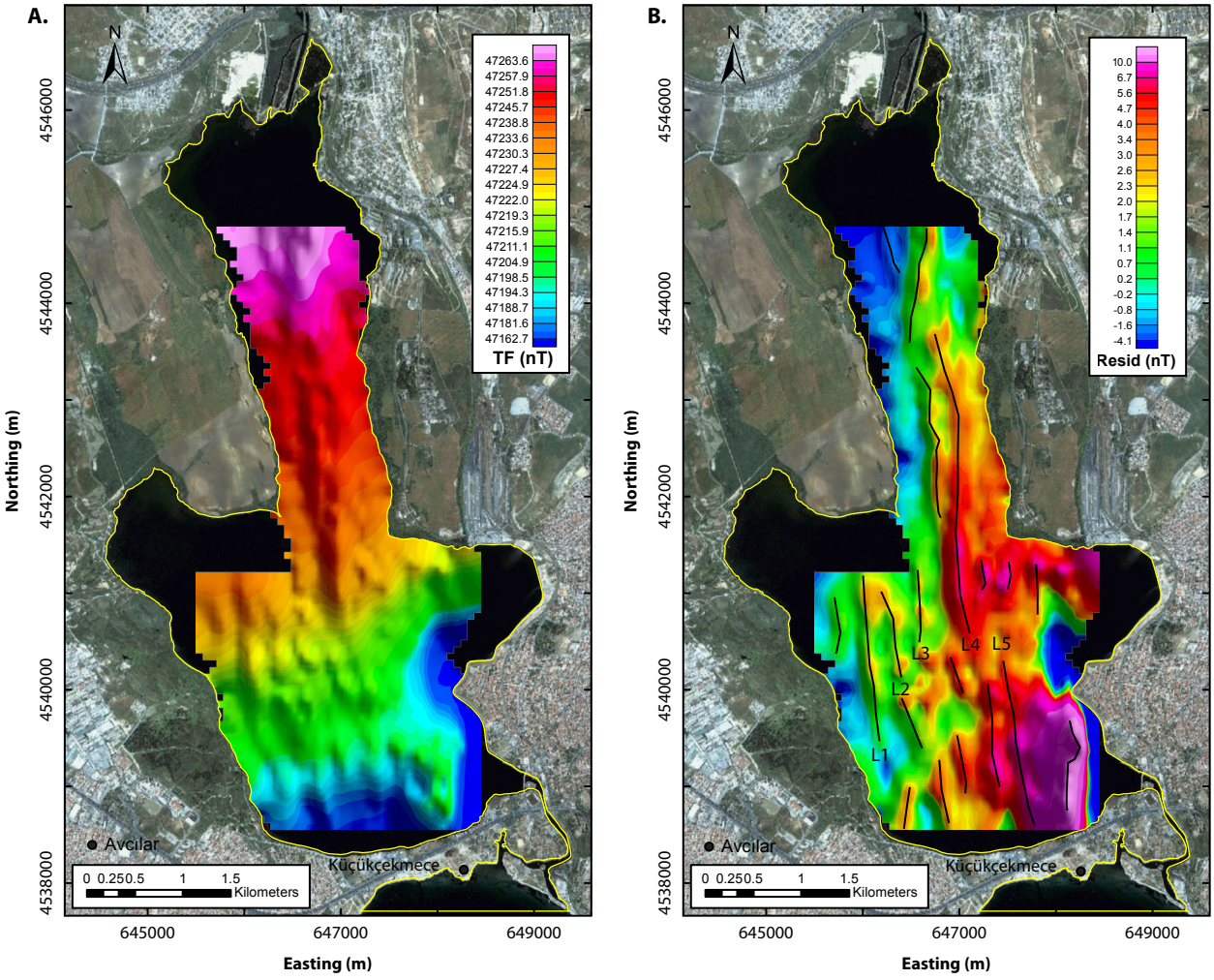
A.
N
47263.6
47257.9
47251.8
47245.7
47238.8
47233.6
47230.3
47227.4
47224.9
47222.0
47219.3
47215.9
47211.1
47204.9
47198.5
47194.3
47188.7
47181.6
47162.7
TF (nT)
Avcilar
Küçükçekmece
0 0.250.5 1 1.5
Kilometers
Northing (m)
4546000
4544000
4542000
4540000
4538000
645000
647000
649000
Easting (m)
B.
N
10.0
6.7
5.6
4.7
4.0
3.4
3.0
2.6
2.3
2.0
1.7
1.4
1.1
0.7
0.2
-0.2
-0.8
-1.6
-4.1
Resid (nT)
L1
L2
L3
L4
L5
Avcilar
Küçükçekmece
0 0.250.5 1 1.5
Kilometers
Northing (m)
4546000
4544000
4542000
4540000
4538000
645000
647000
649000
Easting (m)

Figure 9. A. First vertical derivative map calculated on residual magnetic intensity (Fig. 8B). B. Analytic signal amplitude (ASA) map calculated from TMI grid.

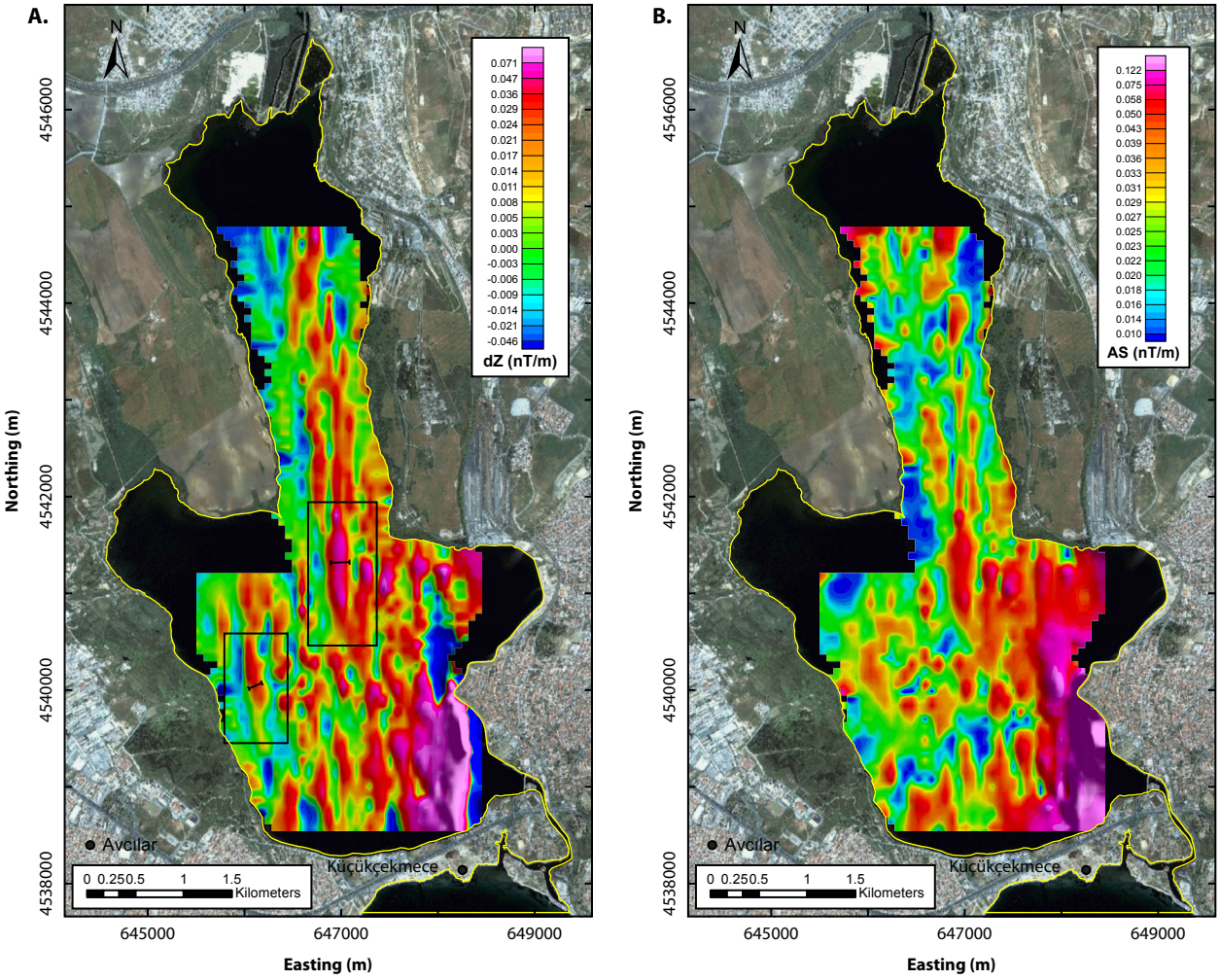
A.
N
0.071
0.047
0.036
0.029
0.024
0.021
0.017
0.014
0.011
0.008
0.005
0.003
0.000
-0.003
-0.006
-0.009
-0.014
-0.021
-0.046
dZ (nT/m)
Avcılar
Küçükçekmece
0 0.250.5 1 1.5
Kilometers
Northing (m)
4546000
4544000
4542000
4540000
4538000
645000
647000
649000
Easting (m)
B.
N
0.122
0.075
0.058
0.050
0.043
0.039
0.036
0.033
0.031
0.029
0.027
0.025
0.023
0.022
0.020
0.018
0.016
0.014
0.010
AS (nT/m)
Avcılar
Küçükçekmece
0 0.250.5 1 1.5
Kilometers
Northing (m)
4546000
4544000
4542000
4540000
4538000
645000
647000
649000
Easting (m)

h is the depth to the top of the contact,
M is the source body magnetization,
d is the dip of the contact
I is the inclination of the magnetization vector, and
A is the direction of the magnetization vector.

For a vertical contact, the ASA anomaly width at half the peak amplitude (X½)is related to the anomaly depth as (Roest et al., 1992):

Eq. 4 $X_{1/2} = 2\sqrt{3h} = 3.46h$

MacLeod et al. (1993) modified this approach by using the distance between inflection points on the ASA anomaly, as this method is less susceptible to errors due to interference from overlapping magnetic anomalies. They showed that the anomaly width between adjacent inflection points (X_i) on the ASA anomaly were related to the source depth h as:

Eq. 5. $X_i = \sqrt{2h} = 1.41h$

To simplify the measurement of anomaly width X_i, a Laplacian filter (3x3) was applied to the ASA grid and the across-strike distance between inflection points was measured (MacLeod et al., 1993).

3.4. 2-D Forward Modelling

In order to investigate the nature of interpreted fault structures, 2-D forward models were constructed using Oasis Montaj™ GM-SYS 2-D™. A west-east profile (Line 5; Fig. 6A) was extracted from the TMI grid and two geologic scenarios were modelled: 1) a simple two-layer model, consisting of faulted low magnetic susceptibility Thrace Basin sediments (κ = $1x10^{-5}$ SI) overlying high susceptibility (κ = $4x10^{-2}$ SI) Istranca metamorphic basement at shallow depth, and 2) a four layer model with moderately magnetized (κ = $2x10^{-2}$ SI) layer within the Thrace Basin sediments (Gürpinar Group; Fig. 4) overlying more magnetized

Istranca metamorphics at depth. Magnetic susceptibilities were assigned based on lithology and basement depth estimated from the profile of Dalgiç (2004)(Fig. 5).

4. Results

4.1. Magnetic and Bathymetric Surveys

The lagoon bathymetry is shown in Figure 6B and the magnetic survey results in Figures 8 and 9. The water depth in the lagoon is on average 5-7 m and reaches a maximum of 20 m within a broad 2-km^2 basin at the south-end of the lake (Fig. 6B). The bathymetry profiles indicate a relatively smooth sediment-floored lakebed with only minor bathymetric relief. The eastern margin of the main lake basin is delineated by a linear scarp that extends 2 km northeastward from the southeastern outlet of the lagoon (Fig. 6B). The scarp rises 5-10 m above the lake basin floor and is contiguous with the eastern shore of the north arm of the lagoon (Fig. 6B). Bathymetry profiles across the scarp show localized areas of more rugged bottom relief, indicating the presence of outcropping bedrock. The western margin of the lake, in contrast, has a much more gradual slope and shows no evidence of scarps or other bedrock structural features.

The variation in total magnetic intensity (TMI) across the lagoon is about 100 nT with a well defined south to north increase in intensity (Fig. 8A). The residual magnetic intensity (RMI) has a variation of about 17.5 nT (Fig. 8B) and shows distinct zones of higher residual magnetic intensity in the central and south-eastern areas of the lagoon. Five major north-northwest trending magnetic lineaments (L1-L5) and several minor lineaments were identified in both the TMI and RMI maps (Figs. 8A, B). The lineaments strike 340-350° northwest, paralleling the long axis of the northern embayment and the bedrock scarp defining the eastern edge of the main lake basin (Fig. 8). The best defined of the lineaments (L4; Fig. 8B) corresponds with central axis of the lake basin. West-east magnetic profiles transecting the five major lineaments are shown in Fig 10A. The profiles show the inline TMI and RMI calculated by subtraction of a 200 m upward continuation. The magnetic lineaments have typical cross-strike

Figure 10. A. Total magnetic intensity (TMI) and calculated residual magnetic intensity profiles for survey Line 8. B. Corresponding boomer seismic profile showing location of small 0.25-0.5 m fault offsets in lakebed Holocene sediments. C. Expanded view of faulted zones.

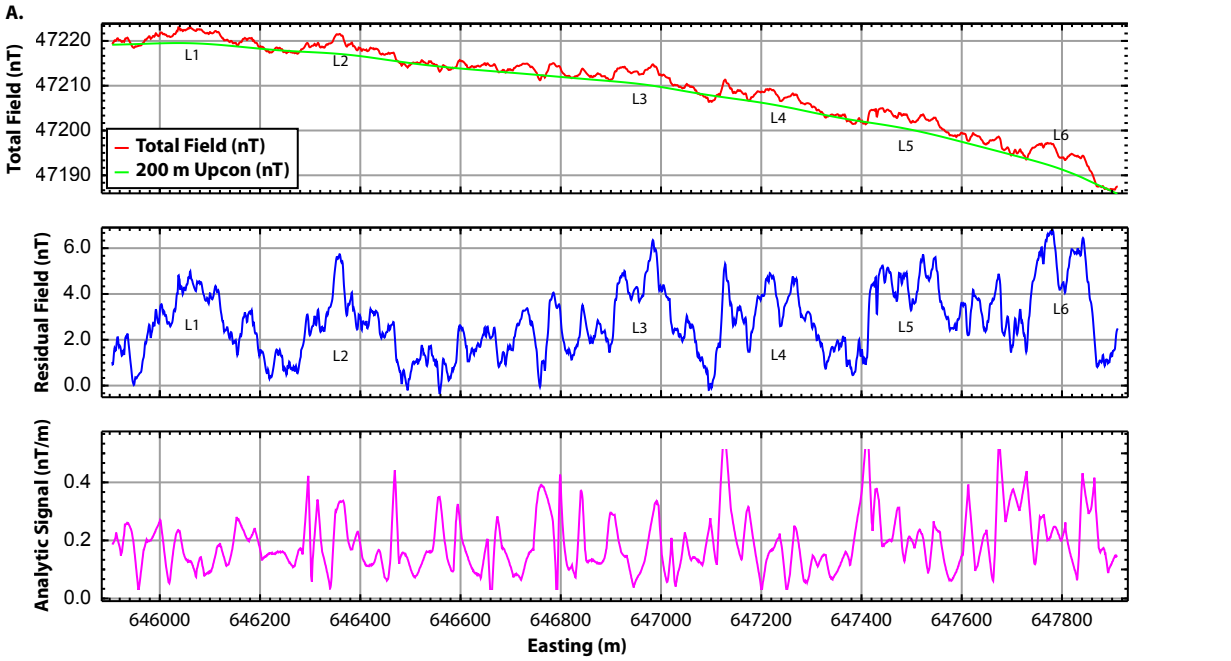
A.
Total Field (nT)
47220
47210
47200
47190
Total Field (nT)
200 m Upcon (nT)
L1
L2
L3
L4
L5
L6
Residual Field (nT)
6.0
4.0
2.0
0.0
Analytic Signal (nT/m)
0.4
0.2
0.0
646000
646200
646400
646600
646800
647000
647200
647400
647600
647800
Easting (m)

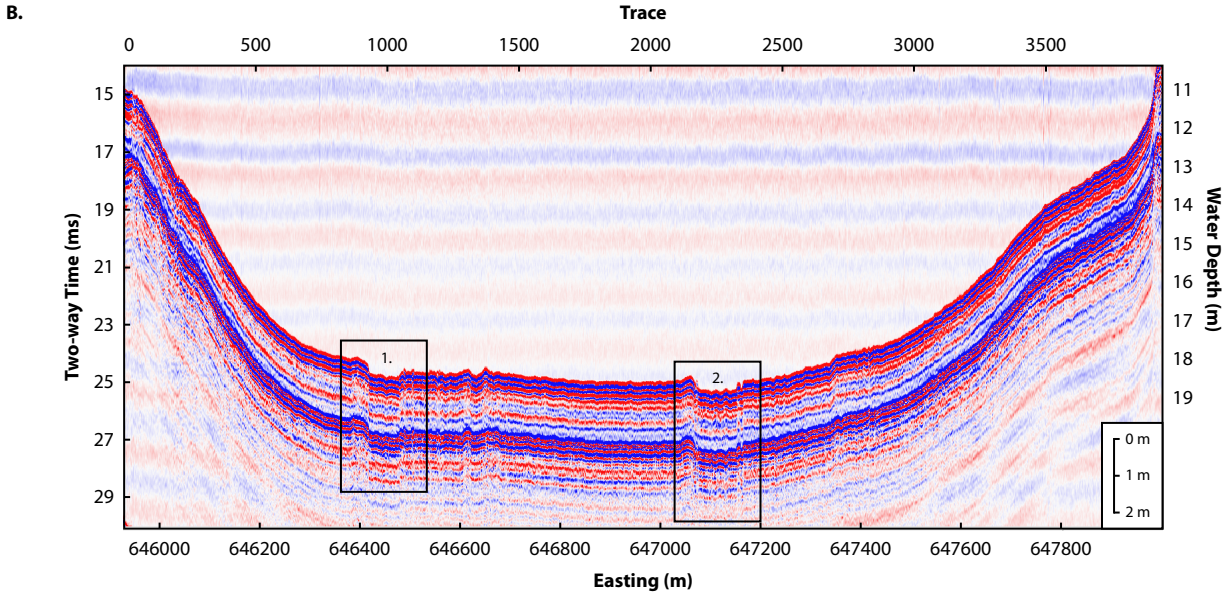
B.
Trace
0
500
1000
1500
2000
2500
3000
3500
Two-way Time (ms)
15
17
19
21
23
25
27
29
Water Depth (m)
11
12
13
14
15
16
17
18
19
1.
2.
0 m
1 m
2 m
646000
646200
646400
646600
646800
647000
647200
647400
647600
647800
Easting (m)

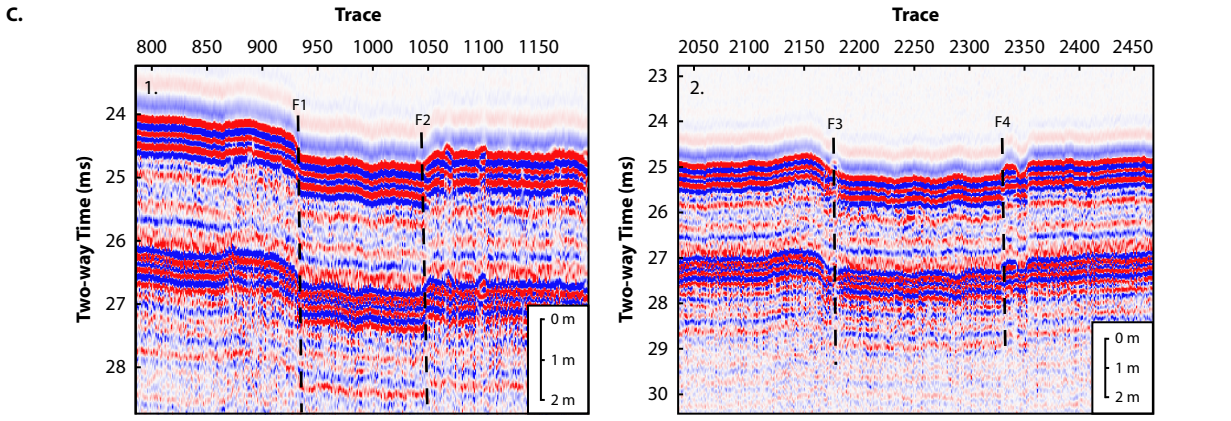
C.
Trace
800
850
900
950
1000
1050
1100
1150
1.
F1
F2
Two-way Time (ms)
24
25
26
27
28
0 m
1 m
2 m
Trace
2050
2100
2150
2200
2250
2300
2350
2400
2450
2.
F3
F4
Two-way Time (ms)
23
24
25
26
27
28
29
30
0 m
1 m
2 m

wavelengths of 100-200 m and amplitudes of 3-6 nT. A number of small amplitude, shorter wavelength anomalies are superimposed on the lineaments (1-2 nT, 20-50 m wavelengths) but are not imaged in the RMI and TMI maps as they are below the grid resolution (50 m cells).

Anomaly depth estimates obtained using the AS half-width method (Eq. 5) are shown in Figure 11. The estimated AS anomaly widths (X_i) range between 120-200 m, yielding source body depth estimates of 85 to 140 m. The estimates indicate that the north-northwest trending magnetic lineaments are the result of shallow magnetic source bodies within the Thrace Basin Cenozoic sequence (Figs 3B, 4). The estimated depth interval (85-150 m) corresponds with the Gürpinar Group, which includes thick interbedded conglomerates, sandstone and south-eastern areas of the lagoon. Five major north-northwest trending magnetic lineaments (L1-L5) and several minor lineaments were identified in both the TMI and RMI maps (Figs. 8A, B). The lineaments strike 340-350° northwest, paralleling the long axis of the northern embayment and the bedrock scarp defining the eastern edge of the main lake basin (Fig. 8). The best defined of the lineaments (L4; Fig. 8B) corresponds with central axis of the lake basin. West-east magnetic profiles transecting the five major lineaments are shown in Fig 10A. The profiles show the inline TMI and RMI calculated by subtraction of a 200 m upward continuation. The magnetic lineaments have typical cross-strike wavelengths of 100-200 m and amplitudes of 3-6 nT. A number of small amplitude, shorter wavelength anomalies are superimposed on the lineaments (1-2 nT, 20-50 m wavelengths) but are not imaged in the RMI and TMI maps as they are below the grid resolution (50 m cells).

Anomaly depth estimates obtained using the AS half-width method (Eq. 5) are shown in Figure 11. The estimated AS anomaly widths (X_i) range between 120-200 m, yielding source body depth estimates of 85 to 140 m. The estimates indicate that the north-northwest trending magnetic lineaments are the result of shallow magnetic source bodies within the Thrace Basin Cenozoic sequence (Figs 3B, 4). The estimated depth interval (85-150 m) corresponds with the Gürpinar Group, which includes thick interbedded conglomerates, sandstone and

mudstone units (Çukurçeşme, Danişment, Osmancık Formations)(Dalgiç, 2004). The conglomerates beds within the sequence are the most likely source of the magnetic contrast, as fluvial gravels are typically rich in titanomagnetic, illmenite and other magnetic carrier minerals. The magnetic sources may also represent coarse-grained Quaternary alluvial sand and gravel deposits within lagoon sediment fill.

4.2. Seismic Survey

Sub-bottom penetration was limited to 2-5 metres due to the presence of gasified sediments at shallow depth and the overall high reflectivity of the sandy gravels that make up the lake bed deposits (Fig. 10B). The lakebed sediments were characterized by a parallel-planar and draped seismofacies, which are interpreted as stratified sand and gravel deposits. Despite the poor penetration, the seismic profiles revealed a number of zones of active faulting and fold and slump structures in the lakebed Holocene sediment fill (Fig. 10B, C). The faults clearly displace the modern lakebed with fault offsets of up to 0.75 m. Most faults appear to be small normal faults but reverse faults were also observed in some locations. Figure 12 shows the mapped distribution of faults and bottom sediment deformation structures in the lagoon with mudstone units (Çukurçeşme, Danişment, and Osmancık Formations)(Dalgiç, 2004). The conglomerates beds within the sequence are the most likely source of the magnetic contrast, as fluvial gravels are typically rich in titanomagnetic, illmenite and other magnetic carrier minerals. The magnetic sources may also represent coarse-grained Quaternary alluvial sand and gravel deposits within lagoon sediment fill.

The overlay analysis shows that magnetic lineaments are in many instances co-located with faults and sediment deformation features, suggesting that the lake bed faults are contiguous with more deeply-seated faults in the bedrock. An alternative explanation is that the faulting is a result of differential compaction of the lake sediments or foundering of the lake side slopes but this is not consistent with the apparent correlation between magnetic lineaments and lake bed faulting (Fig. 12).

Figure 11. Magnetic source depth estimates for lineaments L1 and L4 calculated using the (ASA) half amplitude (Roest et al., 1992). ASA anomaly half width (X½) determined using a 3x3 Laplacian filter (MacLeod et al., 1993).

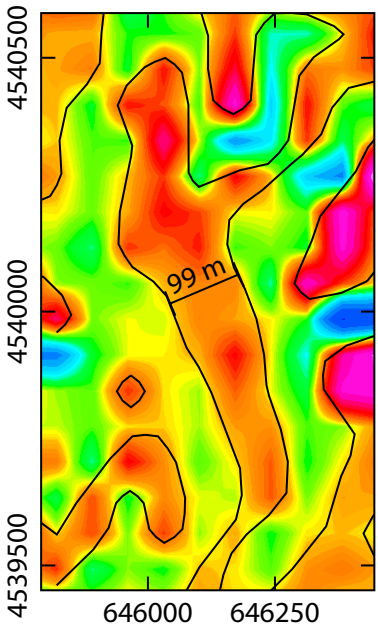
4540500
4540000
4539500
99 m
646000
646250

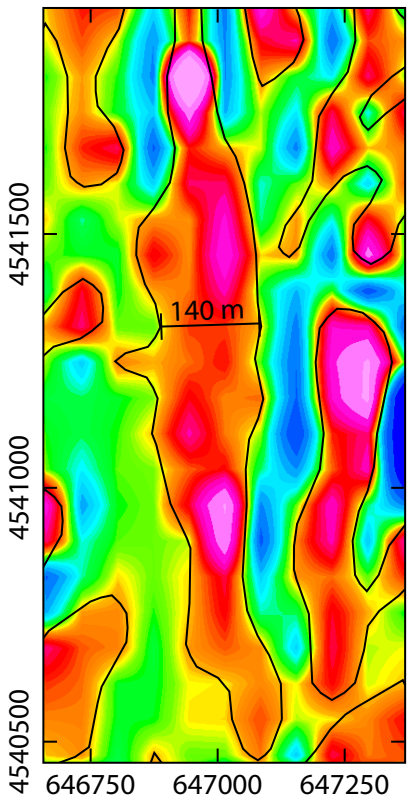
4541500
4541000
4540500
140 m
646750
647000
647250

Figure 12. Seismic survey track lines showing location of faults, slumps and gas chimneys in Holocene bottom sediments. Location of magnetic lineaments (L1-L5) shown for comparison.

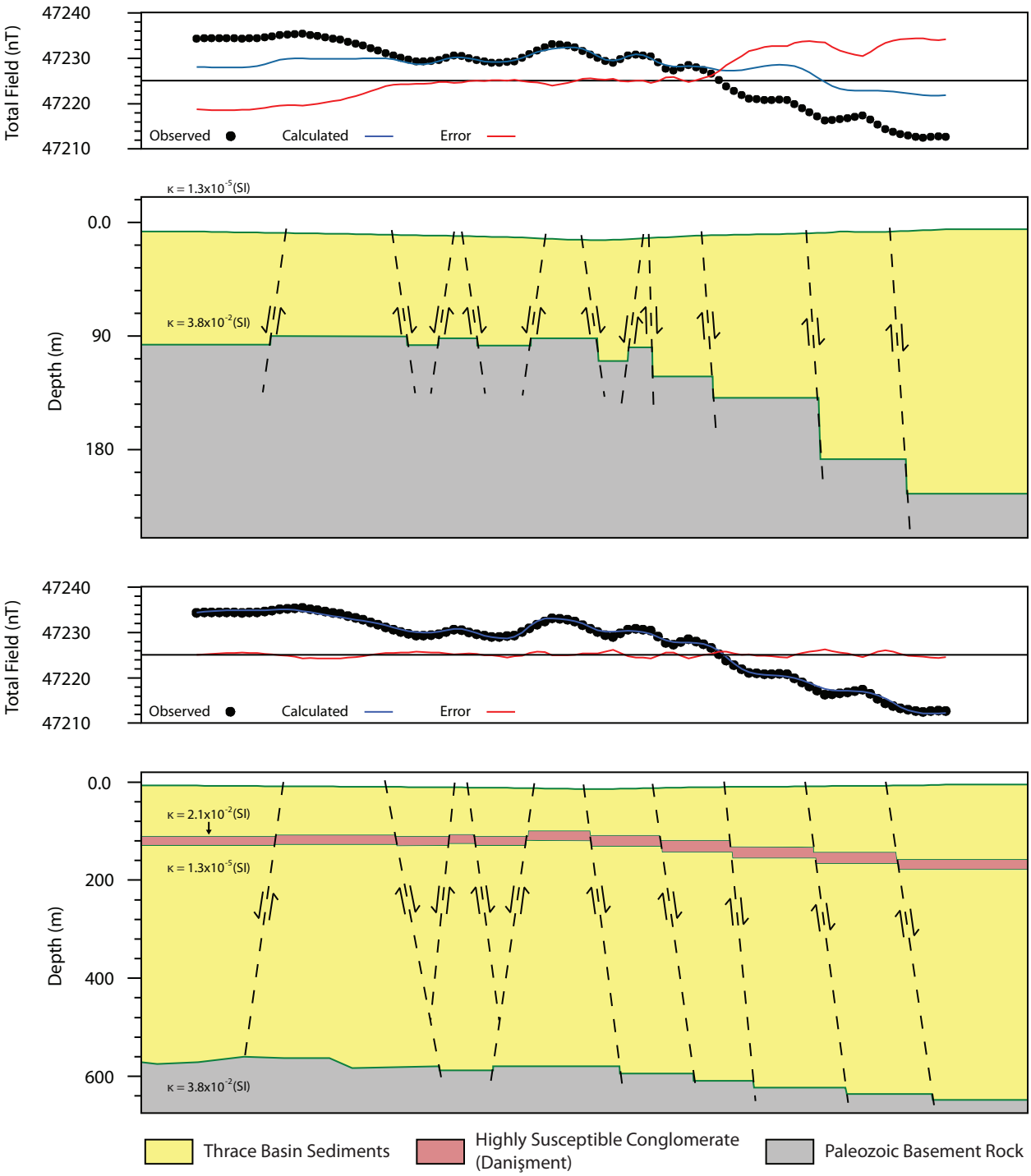
Total Field (nT)
47240
47230
47220
47210
Observed
Calculated
Error
κ = 1.3x10-5(SI)
0.0
κ = 3.8x10-2(SI)
90
180
Depth (m)
Total Field (nT)
47240
47230
47220
47210
Observed
Calculated
Error
0.0
κ = 2.1x10-2(SI)
κ = 1.3x10-5(SI)
200
400
600
Depth (m)
κ = 3.8x10-2(SI)
Thrace Basin Sediments
Highly Susceptible Conglomerate (Danişment)
Paleozoic Basement Rock

4.3. 2-D Forward Models

The results of 2-D forward magnetic modelling are shown in Fig. 13. In both models, the observed TMI anomalies were assumed to result from normal (block) faulting of the Istranca basement rocks and overlying Thrace Basin sediments (Fig. 4). As with all forward models, the solutions are non-unique and there a number of possible fault geometries and configurations that could reproduce the observed TMI signal. The seismic results (Fig. 10) identify the presence of active normal faulting in the lake bottom sediments but we cannot rule out other fault geometries based on the 2-D seismic data. Regardless of whether the faults are purely normal or have a strike slip (oblique) component, the 2-D forward models (Fig. 13) are instructive, as they help to constrain the depths of the faulted layers and the depth to basement.

In an initial two-layer model (Fig. 13A) we tested a scenario in which the magnetic response was a result of a large magnetic contrast between the Istranca basement rocks ($\kappa = 4x10^{-2}$ SI) and overlying Thrace Basin sediments ($\kappa = 1x10^{-5}$ SI) (Fig. 13A). The best fit to the observed TMI signal was achieved when the basement was placed at a shallow depth of 120-150 m with normal fault offsets of 10-45 m on modelled horst and graben structures. This model was rejected, however, as it reproduced the short wavelength anomalies but not the longer wavelength regional gradients. The model was also inconsistent with the available borehole and shear wave data, which indicate a depth to basement of >500 m to the west the CFZ (Fig. 4). In the second model (Fig. 12B), we tested a more geologically feasible scenario where the basement is at depth (>550 m) and the magnetic contrast results from a shallow source body (i.e. conglomeratic unit) in the Thrace Basin sediments (Fig. 12B). The model requires a moderately magnetized layer ($\kappa = 2x10^{-2}$ SI) at a depth 120-170 m with fault offsets of 5-15 m to reproduce short wavelength magnetic anomalies (Fig. 13B). A best fit for the regional west-east component was achieved when the basement ($\kappa = 4x10^{-2}$ SI) was placed at depth of 580-650 m, which is consistent with geological data (Dalgiç, 2004). The results of the second model are also more consistent with the ASA source depth estimates (Fig. 11), which indicate shallow magnetic sources.

It should be noted that the forward models are relatively insensitive to the orientation of the fault planes, and while the second model achieves a good fit with extensional block faulting, other fault geometries with similar offsets could produce a similar result. The lakebed normal faults in seismic data have much smaller vertical displacements (<0.5 m), which may indicate syn-sedimentary fault reactivation (i.e. growth faults).

5. Discussion

5.1. Implications for Seismic Risk Assessment

Geophysical results from Küçükçekmece Lagoon provide evidence for active faulting in the lakebed sediments. Compilation of the previously known faults and lineaments in the study area show that at least 2 of the splay faults are suspected to run under Küçükçekmece Lagoon (Fig. 2)(Gökaşan et al., 2002; 2003). The position and orientation of the suspect faults are based on the continuation of observed marine faults along terrestrial lineaments. The magnetic survey and seismic surveys add additional merit to this theory though the acquisition and modelling of geophysical data in the lagoon. The TMI data from Küçükçekmece Lagoon has several linear anomalies, hundreds of metres to kilometres long, with a strike of ~350-170. The anomalies are also present in the residual field data. Depth estimation using the ASA indicate the source of the anomalies to be 118 metres on average. Several en-echelon faults cutting the bedrock beneath the lagoon are a likely source of the linear anomalies found within the magnetic signal. Faults can produce lineaments in the total field data when the displacement of highly susceptible rock units occurs through faulting. The possibility of a susceptibility contrast created by steeply dipping geologic contacts is rejected because the dip of the sedimentary cover and basement rock units is shallow (10-15°) in the study area. The seismic data add to the evidence of faulting in the lagoon. The weak penetration of the seismic survey only allowed for the soft lakebed sediment to be imaged. In several of the E-W seismic profiles faulting and slumping/folding is observed which may be indications of deeper faults. The fault offsets are quite small (15-30 cm) in the lakebed sediment. This

Figure 13. 2-D forward magnetic models computed for single W-E profile (extracted from TMI grid (Line 5; Fig. 6A). A. Two-layer model with block-faulted Istranca metamorphic basement rocks ($\kappa = 4x10^{-2}$ SI) at shallow depth (<200 m). Note short wavelength magnetic anomalies are reproduced but the longer wavelength regional W-E gradient cannot be produced. B. Four-layer model with Istranca basement at depth (>550 m). The Thrace Basin sediments are modeled as low magnetic susceptibility layer ($\kappa = 1x10^{-5}$ SI) with a block faulted layer (conglomerate) of high magnetic susceptibility ($\kappa = 2x10^{-2}$ SI) at shallow depth (120-150 m). Note both short and long wavelength anomalies can be reproduced by small normal fault displacements (10-20 m).

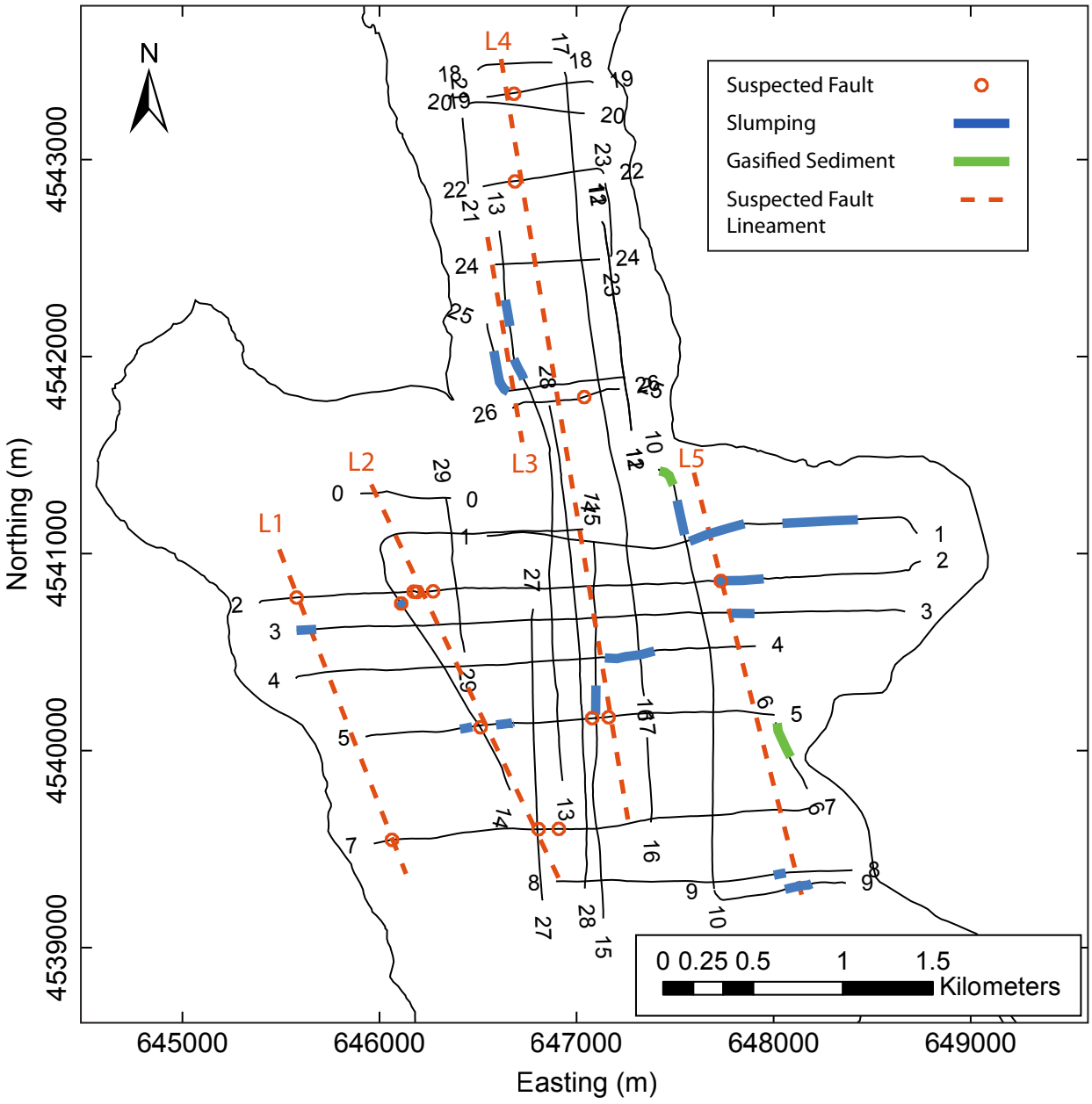
N
Suspected Fault
Slumping
Gasified Sediment
Suspected Fault Lineament
L1
L2
L3
L4
L5
0 0.25 0.5 1 1.5
Kilometers
Northing (m)
4543000
4542000
4541000
4540000
4539000
Easting (m)
645000
646000
647000
648000
649000

may be due to the occurrence of syn-depositional faulting where only the most recent displacement along the faults is seen. The lineaments proposed on the seismic map show the spatial correlation of these observed features in the sediments (Fig. 13). The lineaments observed in the seismic data have similar size and orientation to the lineaments observed in the magnetic data (Fig. 8).

5.2. Origin of Fault Structures

The Marmara Sea region is a structurally complex and tectonically active section of the NAFZ. Pınar (1942) first suggested a major fault zone situated in the Marmara Sea, stretching from the Gulf of İzmit to the Ganos Mountains. This discovery sparked a magnitude of research in the Marmara Sea region. Historically researchers have described the basins formation and present day tectonics with one kinematic model. It was first suggested that the Marmara Sea basin was created as a result of pull-apart tectonics (Barka and Kadinsky-Cade, 1988; Barka, 1992; Ergün and Özel, 1995; Smith et al., 1995; Straub et al., 1997; Wong et al., 1995). During this time it was also suggested that the basin's creation was a function of an en-echelon fault system (Parke et al, 1999; Okay et al, 2000). Research completed by İmren et al. (2001) suggests an alternate explanation of the active tectonics occurring in the region. İmren et al. (2001) found through multibeam bathymetry and seismic interpretation that a single fault zone runs from the Gulf of İzmit to the Ganos Mountains. High resolution seismic data collected in response to the 1999 İzmit earthquake and interpreted by Gökaşan et al. (2001), Kuşçu et al. (2002) and Alpar & Yaltırak (2002) has confirmed the observations of İmren et al. (2001). This research has led to a general acceptance of a single dextral master fault as the driving force behind the regions active tectonics (Okay et al., 1999; Okay et al., 2000; Aksu et al., 2000; İmren et al., 2001; Gökaşan et al., 2002; 2003; Kuşçu et al., 2002; Alpar & Yaltırak, 2002; Yaltırak et al., 2002). The research performed by İmren et al. (2001) also found that the master fault had been active for approximately 200,000 years and not active during the time of the Marmara Sea basin formation. This led Gökaşan et al. (2002; 2003) to state that researchers have

attempted to describe two independent tectonic events with a single tectonic model. Gökaşan et al. (2002; 2003) hypothesizes that the Marmara Sea basin was created during an N-S extensional. During this extensional regime an E-W trending graben opened creating the Marmara Sea Basin (Gökaşan et al., 2003). Strain exerted by the NAFZ then caused a dextral shear regime to take over (Gökaşan et al., 2003). This dextral shear caused en-echelon folding with a fold axis of NNE-SSW, progressing to N60-E50, within the Marmara Sea basin (Gökaşan et al., 2003). The folding resulted in the creation of Çınarcık, Silivri and Tekirdağ Basins and the Eastern and Western Ridges in the Marmara Sea (Gökaşan et al., 2003). The progressive dextral shear caused synthetic Riedel shears to form in the NW-SE direction (Gökaşan et al., 2003). Fault bounding blocks were formed along basin margins and were rotated clockwise by this progressive shear (Gökaşan et al., 2003). The most recent structure generated by the dextral shear is the E-W trending dextral strike-slip fault often called the New Marmara Fault (NMF) (Gökaşan et al., 2003). The NMF cuts all previously formed structures.

The full geometry of the NMF is controversial but several observations are generally accepted. It is shown that the NMF is continuous, with an ENE-WSW trend, along the western section of the Marmara Trough from the Ganos Mountains to offshore Büyükçekmece and Küçükçekmece Lagoons (Okay et al., 1999; Okay et al., 2000; Aksu et al., 2000; Gürbüz et al., 2000; Gazioğlu et al., 2002; Siyako et al., 2000; İmren et al., 2001; Le Pichon et al., 2001; Alpar & Yaltırak, 2002; Yaltırak et al., 2002). The NMF is also found in the Gulf of İzmit (Okay et al., 2000; İmren et al., 2001; Gökaşan et al., 2001; Le Pichon et al., 2001; Kuşçu et al., 2002; Alpar & Yaltırak, 2002). At Çınarcık Basin, one of the several basin in the Marmara Sea, the NMF diverges along two branches which run along the basis's north and south slopes (Aksu et al., 2000; Okay et al., 2000). During the creation of the Çınarcık basin normal bounding faults ran along the basins slopes but were during the formation of the NMF they were reactivated as strike-slip faults (Gökaşan, 2003). It has been proposed that the northern branch of the NMF extends in a NW direction, running through Eastern

Thrace (Okay et al., 2000; Gökaşan et al., 2002; 2003) while the southern branch extends west and then SW where it continues to the Ganos Mountains (Gökaşan et al., 2002).

5.3. Proposed Seismotectonic Model

The faults and lineaments found within the study area can be characterized by their type and orientation. The northern branch of the NMF and the faults splaying from it has been identified as dextral strike-slip faults with a NW-SE strike. Several of the faults identified by Şen (2007) are also dextral strike-slip faults with a NW-SE strike. Normal faults with an E-W strike are located both offshore and west of Küçükçekmece Lagoon on land (Şen, 2007). The terrestrially located normal faults are cut and displaced by the NW-SE trending dextral strike-slip faults. The NNW-SSE trending lineaments and the NNW-SSE trending faults found in Küçükçekmece Lagoon are grouped together.

The E-W trending normal faults found within the study area are likely caused by the now inactive N-S extensional regime. This is shown by several of the NW-SE faults, cutting the E-W faults (Fig. 2-inset). Recent microseismic activity on these faults (Gökaşan et al., 2002) suggests that the E-W normal faults have been reactivated as oblique-slip or strike-slip faults within the dextral shear tectonic regime.

Several tectonic models were considered to explain the relationship between the NW-SE dextral faults and the proposed NNW-SSE faults, including block rotation, Riedel shears, negative flower and transtensional shear. These structures all can be found within a dextral shear regime so they maybe describe the tectonics of the Avcılar region. (Aksu et al., 2000; Gökaşan et al., 2003; Cunningham and Mann, 2007). The block rotation model consists of blocks rotating along dextral zone bounding faults and sinistral block bounding faults (Oktay et al., 2002). Implementation of this model in the study area requires sinistral block bounding faults, which are not observed. The Riedel shear model requires conjugate shears, denoted as R and R', arranged in en echelon arrays (Riedel, 1929; Katz et al., 2004). R makes a 10-30° angle while R' makes an 80-

60° angle to the master strike-slip fault (Dresden, 1991; Katz et al., 2004). The NMF corresponds to R, but there are no sinistral strike-slip faults present. A flower structure consists of dip-slip faults at surface, which are en-echelon or braided to a sub-surface strike-slip fault. In the study area no dip-slip faults are found in an en-echelon or braided configuration to the NMF. A transtensional fault-kinematic model may best explain the faults seen in the study area (Fig. 14). In this model, transtension produced by dextral shear on NW-SE strike-slip faults is accommodated by extension-dominated block faulting. This stress orientation would include NW-SE extension (σ3), NS-SW intermediate stress (σ2) and sub-vertical shortening (σ1) as shown in Figure 14.

6. Conclusion

The magnetic survey performed in Küçükçekmece Lagoon revealed several lineaments with a trend of 350-170° under the lagoon. Seismic survey results and forward modelling suggests that these lineaments are en-echelon normal faults propagated upward from the underlying Istranca basement. Forward modelling has shown that the lineaments are consistent with fault displacements of a magnetized sediment layer at ~100 m depth. Compilation of previously-mapped faults and lineaments shows several NW-SE striking dextral strike-slip faults splaying off the NMF and suggests they continue on land. We propose the NW-SE dextral strike-slip faults have created localized extensional basins through transtensional fault kinematics within the study area. These results are important in understanding the tectonic setting of the Avcılar and need to be considered in future seismic risk assessments. Further analysis of the magnetic field data would provide information on faults kinematics and depth. There is a need for further land based structural studies within the Avcılar area to confirm the existence of terrestrial faults which were inferred through lineament analysis and the extension of marine faults.

Figure 14: Conceptual seismotectonic model for the Küçükçekmece Lagoon. Transtension produced by dextral shear on NW-SE strike-slip faults is accommodated by extension-dominated block faulting. North-northeast trending magnetic lineaments (Fig. 8) are interpreted as en-echelon normal faults displacing Thrace Basin sediments and underlying Paleozoic basement rocks (modified from Allen et al., 1998; Waldron, 2005).

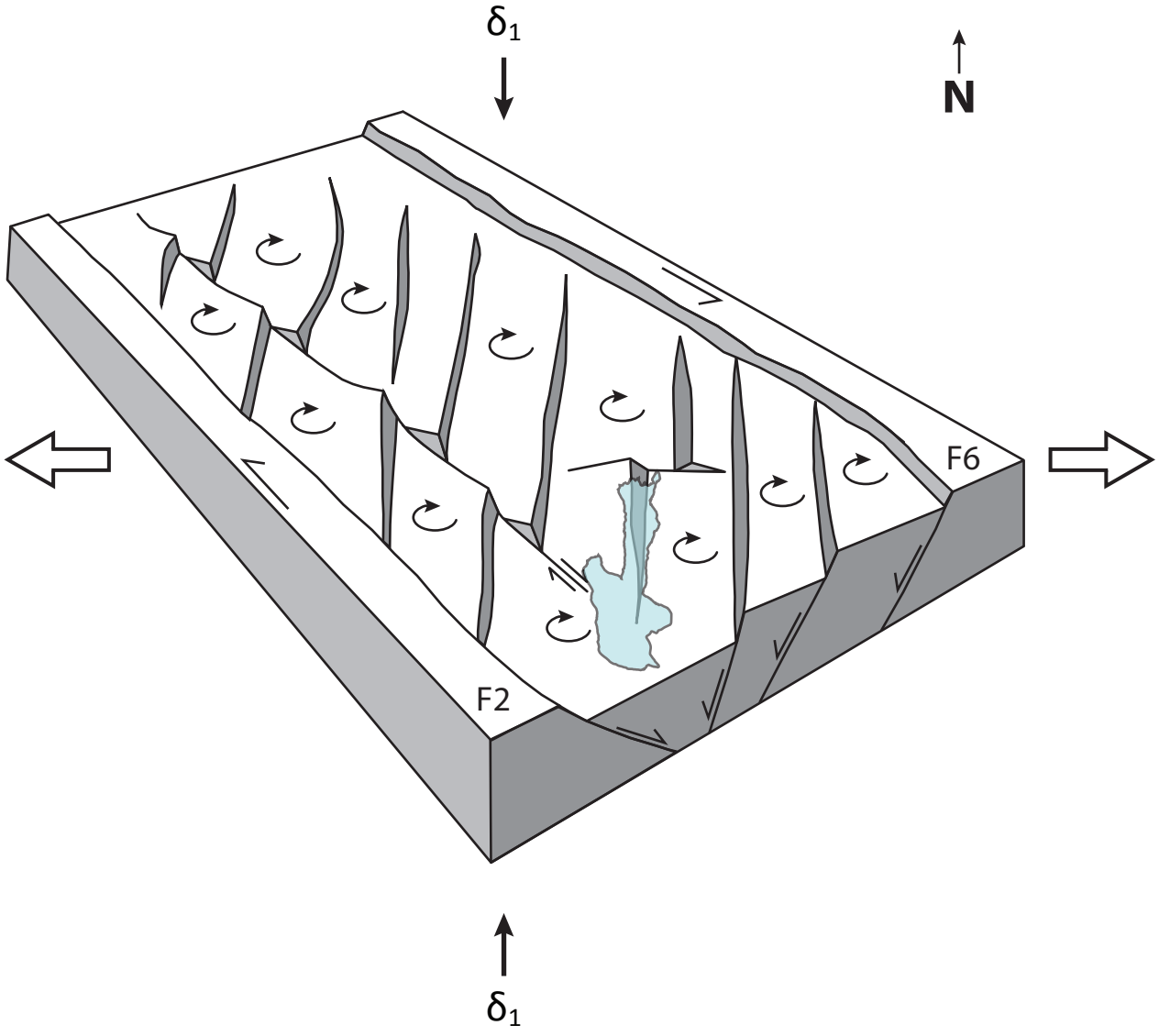
δ1
N
F6
F2
δ1

Acknowledgments

Research work was supported by grants from Istanbul University (Scientific Research Projects Coordination Unit, project #13154) to H. Alp and a Natural Sciences and Engineering Research Council of Canada (NSERC) Discovery Grant to J. Boyce. We thank Savas Karabulut and Erdinç Öksüm for assistance with fieldwork and Ferhat Özçep and Mümtaz Hisarlı for discussions. Research was facilitated by academic software grant from Geosoft Ltd. and field equipment provided by Marine Magnetics Ltd.

Chapter Three: Geophysical investigation of the Charity Shoal structure: a suspected meteorite impact crater in northeastern Lake Ontario.

Suttak, P.[a], Boyce, J.I. [a] and Hrvoic, D.[a]

[a] School of Geography and Earth Sciences,
McMaster University, Hamilton, ON L8S 4K1

Keywords: Charity Shoal, meteorite impact, geophysicalsurvey, magnetic anomaly

Abstract

The Charity Shoal structure (CSS) is a 1.4 km in diameter, crater-like depression discovered in northeastern Lake Ontario in 1999 through bathymetric mapping. The structure is delineated by an elevated 300-500 m wide circular bedrock rim enclosing a 19-m deep basin. The CSS has been interpreted as a meteorite impact based on multi-beam imaging of the lakebed bedrock morphology but details of the crater's subsurface structure were unknown. In 2011, detailed magnetic, sub-bottom seismic and bathymetric surveys (>400 line km) were conducted across a 9-km^2 area of Charity Shoal to investigate its subsurface structure. Magnetic 2-D forward models and Euler depth to basement estimates were used to constrain the crater depth and geometry and to evaluate several possible geological models.

Total magnetic intensity (TMI) data reveal a large (>1400 nT) parabolic-shaped magnetic anomaly centered over the crater basin and a ring-like magnetic high (40-50 nT) corresponding with the basin rim. Sub-bottom seismic profiles revealed 10-12 m of stratified glacial/post-glacial sediments overlying Simcoe Group limestone bedrock. Depth to basement below the centre of the structure was estimated at ~600 m using extended Euler deconvolution. Forward 2-D models verify that the observed TMI anomaly requires a deep (>450 m) depression in Precambrian basement or a source body (e.g. diatreme) with a remanent magnetization opposing the main field. A diatreme origin less likely than an impact origin, as the source body produces complex, short wavelength anomalies not present in the observed signal. A simple structural depression (3-D syncline) in the Precambrian basement does not produce a large enough magnetic susceptibility contrast to create to anomaly. The impact crater model best reproduces the observed TMI anomaly when the basin is modeled as a 450 m deep parabolic impact crater in the Late Proterozoic basement rocks. The modelling results exclude the origin of the CSS as a shallow glacial erosional or karst sinkhole feature and are most consistent with a meteorite impact or diatreme origin.

1. Introduction

Impact catering is an important surface-modification process on terrestrial planets (Grieve and Pilkington, 1996; French & Koeberl, 2010) and has played a significant role in the evolution of Earth's biosphere (Ganapathy, 1982; Sleep et al., 1989; Norris et al., 1999; Krona, 2000; Cockell and Lee, 2002; Schmitz et al., 2008; Schultze et al., 2008; Schultze et al., 2010). The identification of impact craters on Earth is important for understanding the past frequency of impact events and their role in planetary geological and biological processes (French & Koeberl, 2010). On the Moon and other planetary bodies lacking atmospheres and active tectonics, impact craters are often well preserved, and can be identified based on surface morphologic criteria. On Earth, however, post-impact erosion, tectonism, and deep burial often obscure or completely destroy surface morphologic evidence of impact cratering (Grieve and Pesonen, 1996). As a result, the geological record of impact events on Earth is incomplete and is biased towards young (<200 Ma) and large impact structures (>2 km) exposed in continental settings (Grieve and Pesonen, 1996). Identification of impact structures often relies on assessment of a broad range of criteria, including crater morphology (where present), diagnostic macroscopic features (e.g. fracturing, presence of breccia layers, meteorite fragments, suevites, siderophile elements) and distinctive shock-metamorphic effects and structures in target rocks (e.g. planar microstructures, high-pressure polymorphs, diaplectic glasses)(Ferrière et al., 2009; French & Koeberl, 2010).

Where impact craters are deeply buried, or have been modified significantly by post-impact erosion, geophysical methods are an important tool for detecting the signatures of impact structures (Hildebrand et al., 1991; Scott et al., 1997; Sturkell and Ormo, 1998; Pilkington et al., 2002; Therriault et al., 2002). Gravity and magnetic surveys are used most widely, as impact processes often produce well-defined gravity and magnetic anomalies (Therriault et al., 2002). Simple (bowl-shaped) craters are typically associated with well-defined Bouguer gravity lows, as a result of the low density of post-impact sedimentary fill, impact breccia deposits and fracturing of the host rock (Pilkington and Grieve, 2002).

Magnetic anomalies are less diagnostic, due to a wide variation in the magnetic properties of target rocks (Pilkington and Grieve, 2002). Simple impact craters are often associated with circular magnetic lows (<100-1000nT), although some craters do not show any significant magnetic anomalies (Pilkington & Grieve, 2002). The reduction in magnetic intensity in impact craters has been ascribed to a number of effects, including the presence of low susceptibility crater infill, shock demagnetization effects and thermal demagnetization/remagnetization of target rocks (Pilkington and Grieve, 2002).

In this paper, we present the results of a detailed geophysical survey of the Charity Shoal structure (CSS), a suspected 1.4 km diameter impact crater located on the lakebed of northeastern Lake Ontario (Fig. 1). Charity Shoal has been previously mapped as a bedrock shoal in hydrographic charts and in 1999 was identified as anomalous crater-like feature in bathymetric mapping compiled by the Canadian Hydrographic Service (CHS) and National Oceanic and Atmospheric Administration (NOAA)(Fig. 2)(Virden et al., 1999). The improved resolution of the 1999 mapping clearly showed a 1200-1400 m annular bedrock ridge with a central crater-like basin (Figs. 2A, 2C). Holcombe et al. (2001) described the morphology of the CSS and considered the origin though several geological models, including a glacially-eroded kettle hole, a karstic sink hole, a volcanic intrusive and a meteorite impact crater. A meteorite impact origin was the favoured hypothesis, as it was deemed most consistent with the crater morphology and a subtle negative magnetic anomaly (~250 nT) observed in regional aeromagnetic data (Holcombe et al., 2001). Holcombe et al. (2013) subsequently conducted a high-resolution multi-beam bathymetric survey at Charity Shoal in order to map the detailed crater morphology and bedrock structure. In the new multi-beam data, the crater bedrock rim was identified as a ring anticline structure, with Paleozoic strata dipping into the basin and away from the rim. Using the bedrock structural information and stratigraphic relationships they interpreted the CSS as a Middle Ordovician age impact crater resulting from a bollide impact into a shallow marine environment (e.g. Dypvik and Jansa, 2003). The shallow crater relief (depth <20 m) and the ring anticline

rim structure were attributed to the successive burial of the impact crater by post-impact marine sediments.

Our magnetic and seismic results provide the first details of the subsurface structure of the CSS and geophysical constraints for evaluating several possible models for its origin. Magnetic forward modelling and depth to basement estimates indicate that the crater structure is ~600 m in depth and is seated within the Late Proterozoic Grenville basement rocks. The magnetic results are most consistent with an origin as a Pre-Paleozoic simple impact crater or volcanic intrusive (diatreme). The nearby (Late Proterozoic-Cambrian) Holleford impact crater (2.1 km diameter) is a potential structural analog for the CSS, and may indicate a possible multiple impact event during the Late-Proterozoic-Cambrian period. The proposed origin of the CSS as a Middle Ordovician age impact crater (Holcombe et al., 2013) cannot be ruled out but is not supported by the new geophysical data. Confirmation of the impact origin and timing of the CSS event awaits further detailed seismic survey work together with sampling and structural studies of the crater fill and host rocks.

2. Physical and Geologic Setting

Charity Shoal is located about 20 km south of the City of Kingston on the Duck-Galloo Ridge, an area of shallow water bedrock shoals in northeastern Lake Ontario (Fig. 1). The CSS is situated on a 9-km long southwest-northeast trending bedrock ridge on the north side of the St. Lawrence Channel (Fig. 2A). The structure is defined by a continuous bedrock rim that rises 10-15 m above the surrounding lakebed, enclosing a roughly circular central basin (Fig. 2A). The rim is about 300-500 m in width and rises to within 1 m of the water surface in the northwestern section of the shoal and is at 5-12 m depth the rest of the way around. The basin has diameter of about 800-1000 m and lies in a water depth of 15-19 m (Fig. 2C)(Virden et al., 1999; Holcombe, 2001). Two smaller sub-basins are present on the crater floor and are separated by a 2-3 m central rise (Fig. 2C). A 2.5 km long raised ridge of sediment and/or bedrock extends in southwesterly direction from the southwestern section of the crater rim. The ‘tail’

Figure 1: Bathymetry map of eastern Lake Ontario showing bedrock geology (NOAA National Geophysical Data Centre; Holcombe et al., 2013). Location of Charity Shoal study area (9-km^2) and Holleford crater shown

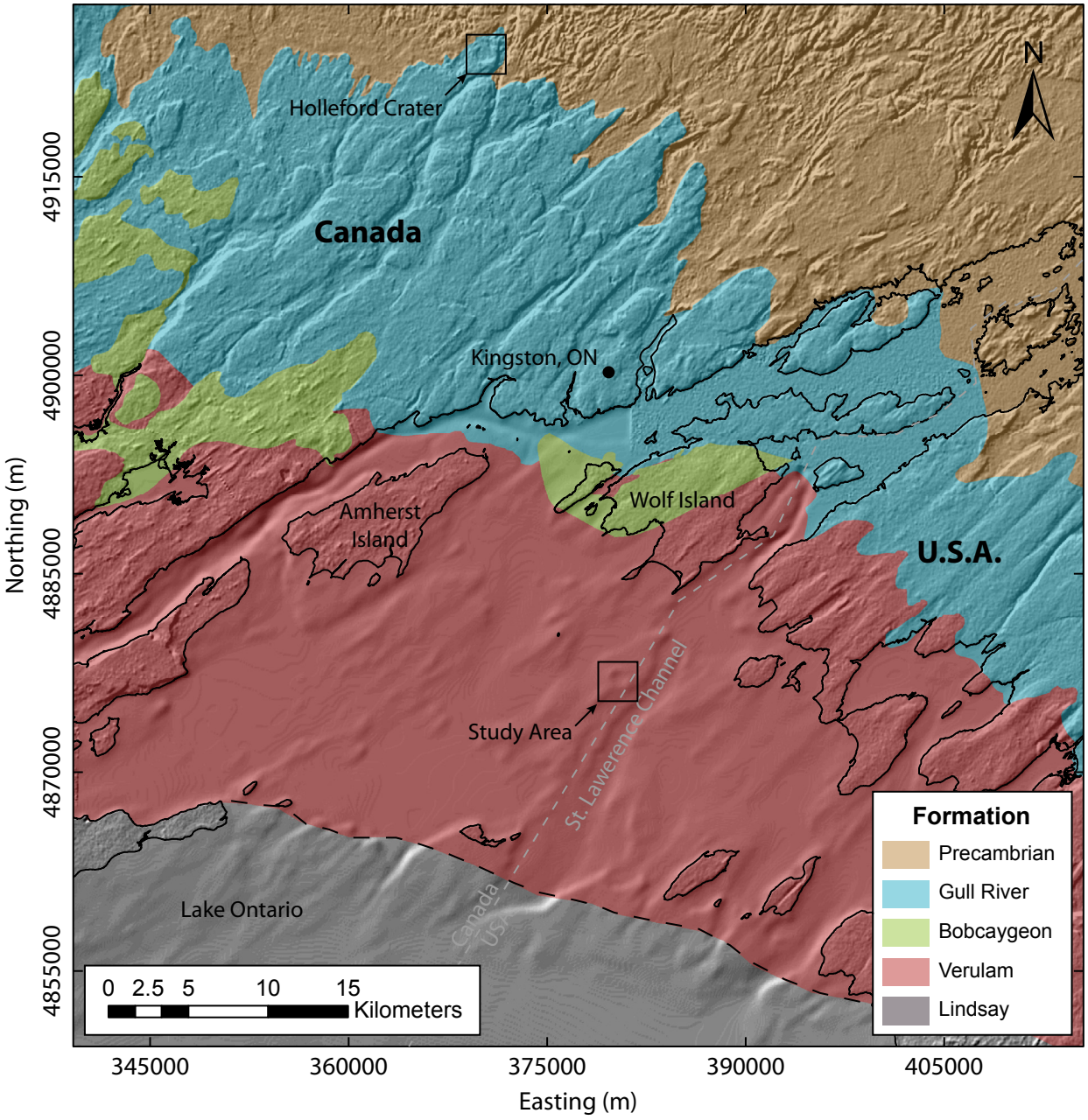
Holleford Crater
Canada
Kingston, ON
Amherst Island
Wolf Island
U.S.A.
Study Area
St. Lawerence Channel
Lake Ontario
Canada
US
N
0 2.5 5 10 15
Kilometers
Formation
Precambrian
Gull River
Bobcaygeon
Verulam
Lindsay
Northing (m)
4915000
4900000
4885000
4870000
4855000
345000
360000
375000
390000
405000
Easting (m)

Figure 2. A. Bathymetric map of northeastern Lake Ontario showing location of Charity Shoal and other physiographic features on the lakebed. The structure is located on bedrock ridge between the Simcoe Island Channel and main St. Lawrence Channel (source NOAA National Geophysical Data Centre). B. Geophysical survey track lines (>400 line km). Location of sub-bottom chirp seismic profile in Figure 5 shown. C. Bathymetry map interpolated from 200 kHz single-beam echosounder data.

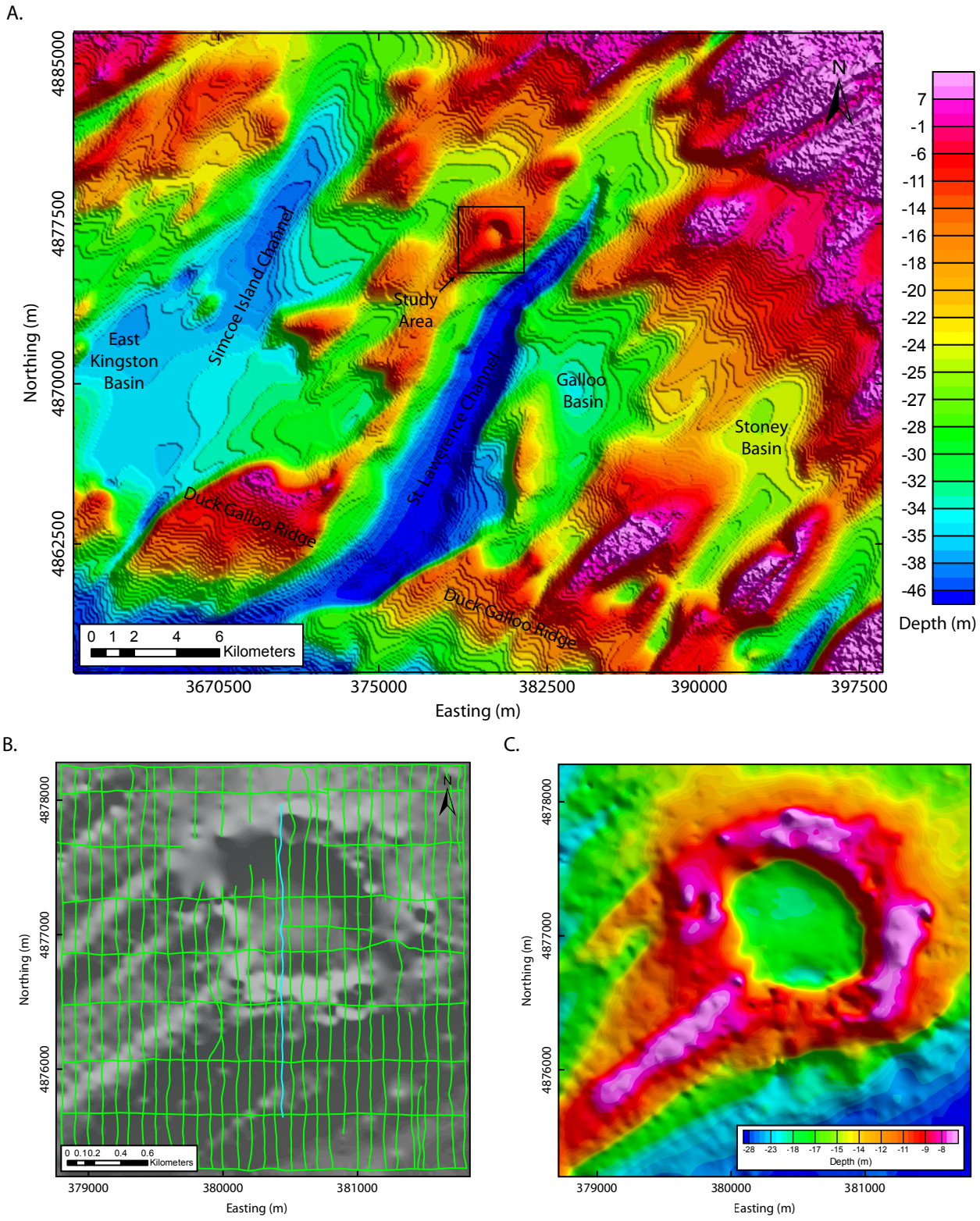
A.
Northing (m)
4885000
4877500
4870000
4862500
3670500
375000
382500
390000
397500
Easting (m)
N
East Kingston Basin
Simcoe Island Channel
Study Area
St. Lawrence Channel
Galloo Basin
Stoney Basin
Duck Galloo Ridge
Duck Galloo Ridge
0 1 2 4 6
Kilometers
7
-1
-6
-11
-14
-16
-18
-20
-22
-24
-25
-27
-28
-30
-32
-34
-35
-38
-46
Depth (m)
B.
Northing (m)
4878000
4877000
4876000
379000
380000
381000
Easting (m)
N
0 0.10.2 0.4 0.6
Kilometers
C.
Northing (m)
4878000
4877000
4876000
379000
380000
381000
Easting (m)
-28 -23 -18 -17 -15 -14 -12 -11 -9 -8
Depth (m)

feature is oriented parallel with other streamlined erosional feature in the lake floor and likely represents a till-cored ridge or bedrock fluting (crag-and-tail feature) formed below the southwestward flowing Laurentide Ice sheet during the last glaciation (Kerr and Eyles, 2007). A number of smaller crag-and-tail features are present on the west side of the CSS indicating that the feature has been modified by glacial erosion (Fig. 2A).

The bedrock below Charity Shoal consists of Mid-Ordovician (450-470 ma) sedimentary rocks overlying Late Proterozoic (1.0-1.2 Ga) metasediments of the Grenville province (Sandford and Baer, 1981; Easton, 1992; McFall, 1993; Armstrong, 2007; Holcombe et al., 2013)(Fig. 1). The crater rim is composed of fossiliferrous limestones of the Mid-Ordovician Simcoe Group (Holcombe et al., 2001). The exact stratigraphic position in the Mid-Ordovician sequence is uncertain, but based on the strike of the Paleozoic strata onshore, the limestones are provisionally identified as belonging to the Verulam Formation (Holcombe et al., 2001) The Paleozoic strata have a regional dip of about 4-5° southwestward (McFall, 1993) and locally, according to Holcombe et al. (2013), dip into and away from the CSS bedrock rim, forming a ring anticlinal structure. The rim anticlinal structure was attributed by Holcombe et al. (2013) to draping of Mid-Ordovician sediments over a raised crater rim, such that the relief on the original impact crater would have been attenuated over time.

The total thickness of the Paleozoic strata at Charity Shoal is unknown but data from oil and gas wells in nearby Prince Edward County, Ontario and Upper State New York suggest a thickness of 150-200 m (OGSR, 2013). The Mid-Ordovician strata overlie thin Cambrian sandstones, which in turn rest unconformably on Late Proterozoic basement rocks. The basement rocks belong to the Frontenac Terrane of the Grenville Province, which consists of high-grade gneisses, marble and quartzite (Forsyth, 1981; Easton, 1992).

3. Methods

3.1. Geophysical Survey

A marine magnetic survey was conducted across a 9-km^2 square area of Charity Shoal in July 2012. A total of 410-line kilometres of data were acquired along N-S lines at 100 m spacing and W-E tie-lines at 400 m spacing (Fig 2B). Total field magnetic data were acquired with a Marine Magnetics SeaSPY^{TM} Overhauser magnetometer cycling at 2 Hz. The Overhauser magnetometer has a sensitivity of 0.01 nT/√Hz and is an omni-directional sensor, free of heading errors that complicate the use of optically-pumped magnetometers. The magnetometer was towed at 40 m behind a 10 m long survey boat travelling at an average speed of 2 knots, providing an inline sample interval of 0.5 m. A Marine Magnetics Sentinel^{TM} base station Overhauser magnetometer was deployed in northwest area of the site in a water depth of 2 m for the duration of the survey (Fig. 2B). Bathymetric data were collected simultaneously using a 200 kHz echosounder mounted on the survey boat. Seismic profiles were acquired with a Knudsen 320BP sub-bottom profiler using a swept frequency (12-24 kHz) chirp pulse. Survey navigation and sensor positioning were provided by an onboard differential-GPS with a horizontal positional error of <1 m.

3.2. Data Processing

Magnetic survey data were processed in Geosoft Oasis Montaj^{TM} using the scheme shown in Figure 3. The processing flow included corrections for diurnal variation, sensor layback and tie-line leveling using an iterative least squares algorithm (Luyendyk, 1997; Green, 1983). Microlevelling was then applied to remove remaining uncompensated residual errors in line and tie-line amplitudes (Minty, 1991). The fully levelled total magnetic intensity (TMI) data were then gridded using a minimum curvature algorithm with 20 m grid cells. (Briggs, 1997). Drape corrections for water-depth related changes in signal amplitude were applied using the chessboard technique Cordell (1985) as implemented in Compudrape^{TM} software (Patterson et al., 1990). A new observation height of 0 m (lake level) was produced from the drape correction.

Figure 3. Processing steps used in correction of magnetic and bathymetric data.

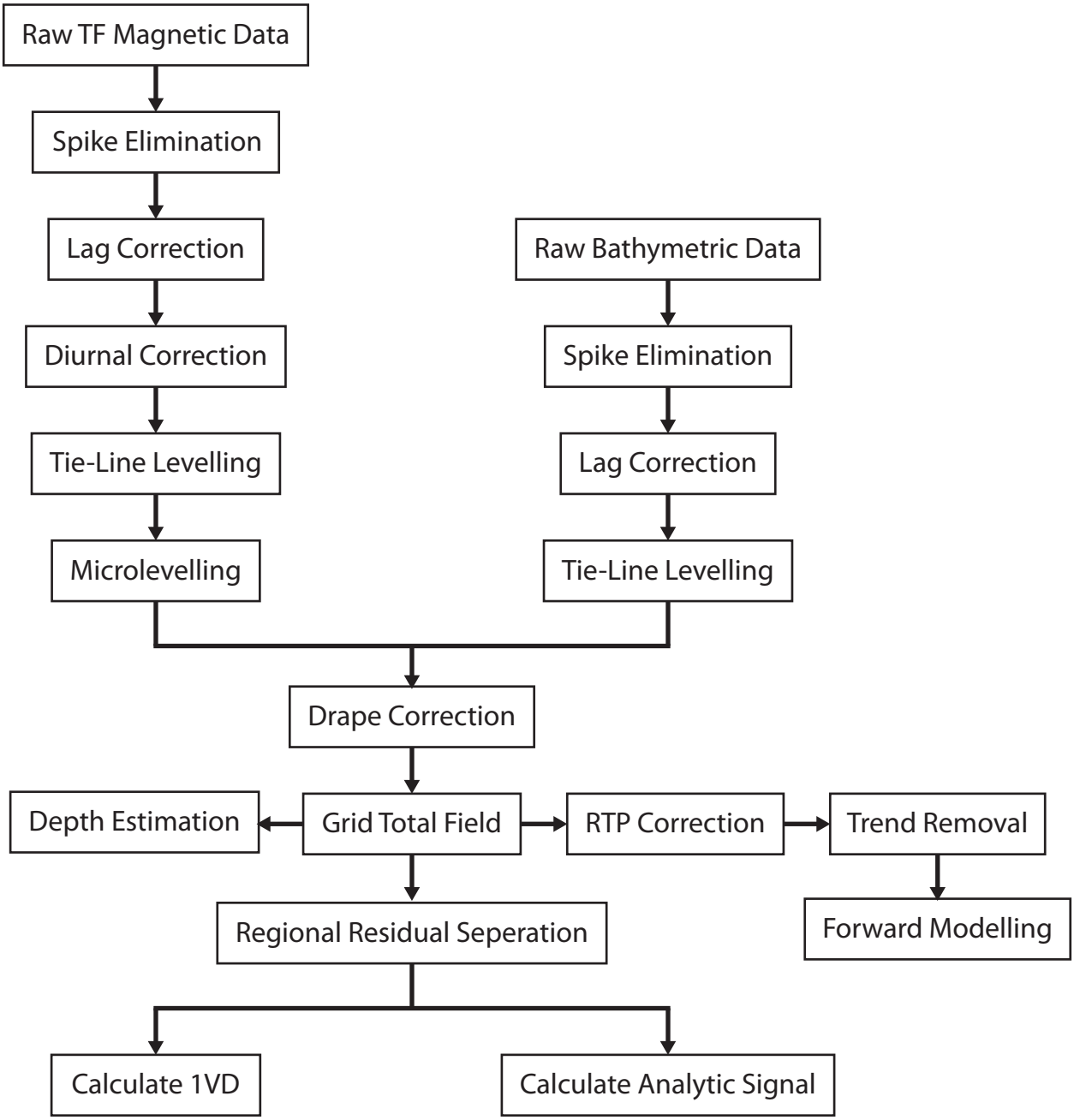
Raw TF Magnetic Data
Spike Elimination
Lag Correction
Diurnal Correction
Tie-Line Levelling
Microlevelling
Raw Bathymetric Data
Spike Elimination
Lag Correction
Tie-Line Levelling
Drape Correction
Depth Estimation
Grid Total Field
RTP Correction
Trend Removal
Forward Modelling
Regional Residual Seperation
Calculate 1VD
Calculate Analytic Signal

The magnetic residual grid was obtained by subtraction of a 200-m upward continuation of the TMI grid from the original TMI grid. In a final step, the 1st vertical derivative and analytic signal amplitude (ASA) grids were calculated with a 2-D FFT filter applied to the fully-corrected TMI grid.

Post-survey processing of seismic profiles in HIS Kingdom Suite™ software included application of bandpass filters and deconvolution to suppress water bottom multiples and ringing.

3.3. Depth Estimation and 2-D Forward Modelling

To assist interpretation of magnetic data, the depth to magnetic source bodies were estimated using 3-D Euler deconvolution (Thompson, 1982; Reid et al., 1990). Euler deconvolution is a semi-automated method for estimation of source body depth and location. The method is based on Euler's homogeneity equation, which relates the source body location (x_0, y_0, z_0) to the magnetic total field intensity T, measured at a position x, y, z as:

Eq. 1 $$(x - x_0)\frac{\delta T}{\delta x} + (y - y_0)\frac{\delta T}{\delta x} + (z - z_0)\frac{\delta T}{\delta x} = -N(B - T),$$

where B is the regional value of the total magnetic field and N is the structural index (Thompson, 1982). The structural index *N* describes the rate the magnetic field decays with distance based on source geometry and is assigned based on expected target geometry in standard Euler deconvolution (Reid et al., 1990). The total-field anomaly produced by a dipolar source decreases as inverse distance cubed and the corresponding structural index is *N* = 3; for a cylinder *N*= 2, a dyke has *N*= 1 and a con- tact has *N* = 0 (Thompson, 1982). Euler solutions for depth to basement estimation typically use N=0, 0.5, or 1 but the choice of the index can be arbitrary, depending on a priori knowledge of the source body characteristics and geometry. The relative clustering or spraying of the Euler solutions is used as a guide to selecting the correct value of N. 3-D Euler depth solutions were calculated in Geosoft Oasis Montaj™ using a moving window of 1000 m. An initial value of N=0 for contacts and N=1 for vertical dike was used in

the calculation. A 3-5 fiducial non-linear filter was applied to smooth the vertical and horizontal derivatives prior to Euler depth calculations.

Four geological models proposed for the CSS (Fig. 4) were evaluated using 2-D magnetic profile models constructed with Geosoft GM-SYS^{TM} 2-D. The software allows forward and inverse modelling of 2-D and 2¾ -D profiles using the Talwani 2-D polygon method (Talwani et al., 1959; Talwani and Heirtzler, 1964) with optional inversion of model parameters using a linear optimization routine (Marqardt, 1963). The production of accurate models required several constraints and assumptions. The depth estimation results from Euler deconvolution were used to constrain the depth to the Precambrian Basement surface. The susceptibility value for the basement was initially assigned using the average for the Grenville basement rocks ($\kappa = 7.2x10^{-2}$ SI) but was found to be too low to reproduce the observed magnetic anomaly. Instead, the magnetic susceptibility was estimated by constraining the crater depth dimensions to the Euler calculated depths and freeing the susceptibility parameter in the model inversion. The inversion indicated an optimum value of $\kappa = 7.2x10^{-2}$ SI for the Precambrian basement. Magnetic susceptibility (κ) values for the Paleozoic strata were assigned a uniformly low value of susceptibility ($\kappa = 1.7x10^{-6}$ SI) based on average values for the Bobcaygeon Formation, a bioclastic limestone which is lithologically similar to the Simcoe Group fossiliferous limestone (O'Dowd and Eaton, 2005). Several other parameters and constraints used in the forward modelling are summarized in Table 1.

Model A (Fig. 4A1), simulates a 1.2 km diameter simple impact crater penetrating the Precambrian basement to a depth of 450 m. The crater depth and impact breccia layer thickness were estimated from the crater diameter using scaling functions (Fig. 5A)(Melosh,1988; Grieve, 1997). The true depth (Ht), apparent depth (Ha) and the rim high (hr) of the crater were calculated (Melosh, 1989)(Grieve, 1997)(Fig. 5A). The calculated floor to rim depth allowed for the maximum breccia depth (Bd) to be calculated (Melosh, 1989)(Fig. 5A). A younger crater situated in the Ordovician limestone is unlikely as the depth to basement estimate and forward modelling indicate that the magnetic source bodies are at a

Figure 4. Schematic geological models for Charity Shoal structure evaluated in this study. A1. Late Proterozoic to Cambrian age impact structure in basement rocks infilled by Ordovician and younger strata. A2. Ordovician-age impact penetrating into underlying basement rocks. B. Volcanic intrusion (Jurassic age diatreme) penetrating Grenville basement and overlying Ordovician-age cover rocks. C. 3-D syncline in Grenville basement draped by Ordovician sedimentary strata. D. Cavity in Paleozoic bedrock produced by glacial erosion or karst dissolution and infilled with glacial/post-glacial sediments.

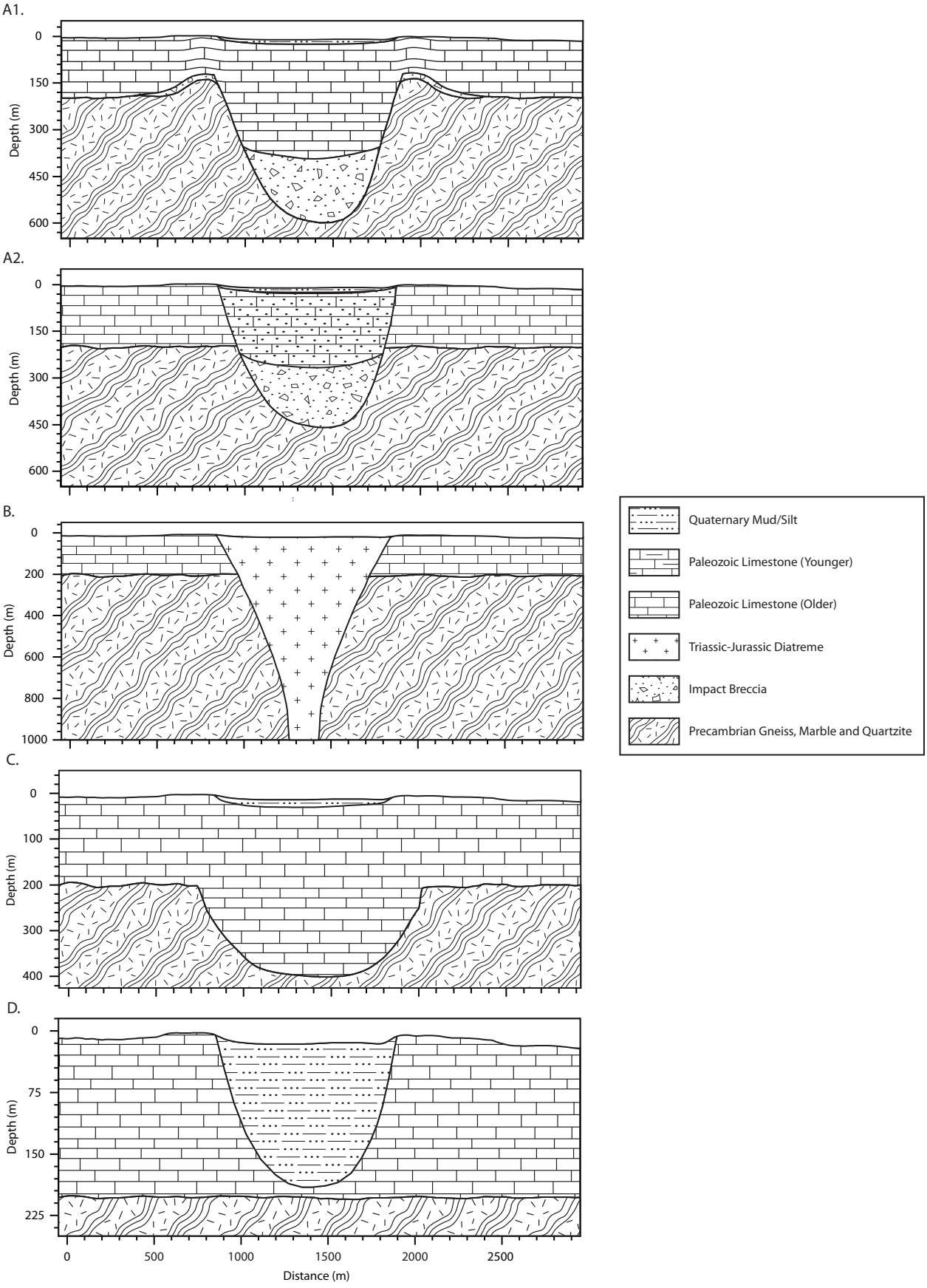
A1.
A2.
B.
C.
D.
Depth (m)
0
150
300
450
600
200
400
800
1000
100
75
225
0
500
1000
1500
2000
2500
Distance (m)
Quaternary Mud/Silt
Paleozoic Limestone (Younger)
Paleozoic Limestone (Older)
Triassic-Jurassic Diatreme
Impact Breccia
Precambrian Gneiss, Marble and Quartzite

Table 1. Forward modelling parameters and constraints.

Constraint	Value	Source
Depth to Precambrian Basement	200 m	Suttak et al., 2013
Susceptibility of Glacial Till	2.6×10^{-3} SI	Gravenor, 1974
Susceptibility of Paleozoic Bedrock	1.7×10^{-6} SI	Dowd and Eaton, 2005
Susceptibility of Precambrian Basement	Average: 1.8×10^{-2} SI Experimental: 7.7×10^{-2} SI	Muir, 2013 Suttak et al., 2013
Susceptibility of Impact Breccia	2.8×10^{-3} SI	Suttak et al., 2013
Susceptibility of Diatreme	2.2×10^{-2} SI	Muir, 2013
Scaling of Impact Crater	See Fig. 5	Melosh, 1998 Grieve, 1997
Remanent Magnetization of Diatreme	Inclination: -68° Declination: 198°	Barnett er al., 1984
Field Intensity of Diatreme	0.5 A/m	Van Fossen and Kent, 1993

Figure 5. A. Crater scaling functions used to construct simple impact crater forward model. B. Simple crater geometry with scaling parameters defined (from Melosh, 1989; Grieve, 1997)

A.

	Equation	Dimension	Source
Average Diameter (D)		1400 m	
True Depth (Ht)	$Ht = 0.28D^{1.02}$	394.65 m	Grieve, 1997
Apparent Depth (Ha)	$Ha = 0.13D^{1.06}$	185.71 m	Grieve, 1997
Rim Height (hr)	$hr = 0.036D^{1.014}$	55.78 m	Melosh, 1989
Floor to Rim Depth (H)	H = Ht + hr	450.43 m	
Max Breccia Depth (Bd)	½ rim to floor depth	225.22 m	Melosh, 1989

B.

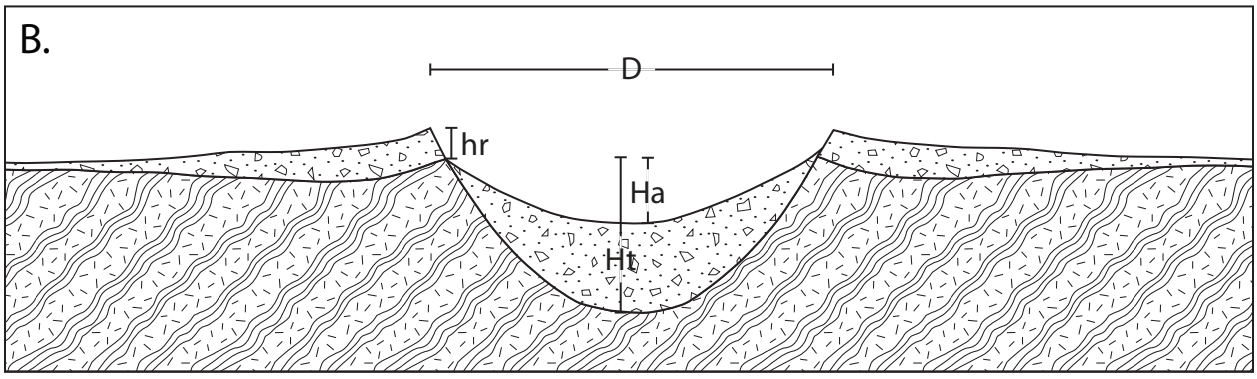

depth that exceeds the thickness of the Simcoe Group limestones (Fig 4A2). This scenario is not modelled

Model B simulates a diatreme intruding the Grenville basement and overlying Ordovician strata (Fig. 4B). Post-Paleozoic age intrusives have been identified at Varty Lake and at Picton, Ontario (Hon, 1970; Barnett et al., 1984) and in several locations in Upper State New York (Fossen and Kent, 1993). The intrusives are typically thin kimberlitic and lamproitic dikes (1 cm – 200 cm wide) intruded into joints and fractures in the Paleozoic sediments but pipes up to 10 m in diameter have also been identified (Fossen and Kent, 1993). The ultramafic intrusives were emplaced during the Middle to Late Jurassic (Barnett et al., 1984) and have been ascribed to hotspot volcanism (Crough, 1981) or to Late Jurassic continental rifting and fault reactivation during the re-opening of the Atlantic basin (Parrish and Lavin, 1982). In the forward modelling, the diatreme is modeled as a 'prairie type' kimberlite pipe (Field and Scott-Smith, 2006) with a broad 1.2-km diameter, bowl-shaped crater fed by a 200 m diameter neck at depth (Fig. 4B). The diatreme magnetic susceptibility and remanence values ($\kappa = 2.2 \times 10^{-1}$ SI, M_r = 0.5 A/m) were assigned based on data from Jurassic-age ultramafic intrusives in southern Ontario and New York State (Van Fossen and Kent, 1993; Muir, 2013) and using average remanence directions (inclination: -68, declination: 198) determined by Barnett et al. (1984). The layer magnetic parameters were held constant while the geometry of the pipe was freed in the inversion.

Model C (Fig. 4C), evaluates the magnetic response of a simple bowl-shaped synclinal basin structure in the Grenville basement infilled with Paleozoic strata ($\kappa = 1.7 \times 10^{-6}$ SI). High relief erosional surfaces, comprising monadnocks and intervening swales with local relief <200 m, are a common feature on the Precambrian shield rocks to the north of the study area (e.g. Algonquin Highlands)(Chapman and Putnam, 1985; Di Prisco and Springer, 1991). 3-D basement synclines and anticlines with similar amplitude also produced by regional folding, and produced arches and basins on the Grenville basement surface. The depth of the synclinal feature was set to 200 m to simulate some of the largest reliefs seen in the Precambrian surface.

Model D (Fig. 4D) simulates 1-km wide cavity in Paleozoic bedrock formed by glacial erosion or a sinkhole produced by karst dissolution. The Paleozoic strata ($\kappa = 1.7 \times 10^{-6}$ SI) were assigned a thickness of 200 m and the cavity infilled with low magnetic susceptibility ($\kappa = 2 \times 10^{-5}$ SI) glacial and post-glacial sediments.

4. Results

4.1. Seismic Profiles

Model D (Fig. 4D) simulates 1-km wide cavity in Paleozoic bedrock formed by glacial erosion or a sinkhole produced by karst dissolution. The Paleozoic strata ($\kappa = 1.7 \times 10^{-6}$ SI) were assigned a thickness of 200 m and the cavity infilled with low magnetic susceptibility ($\kappa = 2 \times 10^{-5}$ SI) glacial and post-glacial sediments.

Sub-bottom seismic profiles reveal a maximum of 10-12 m of crudely stratified unconsolidated sediments overlying a high amplitude basal reflector that is interpreted as the top of the Simcoe Group limestones (Fig. 6A). The upper 2-3 m of the sediment fill is characterized by planar parallel reflections interpreted as laminated (post-glacial-Holocene?) muds and silt. The muds unit overlies an acoustically transparent unit that is largely devoid of reflections, that represents poorly-stratified unconsolidated sediment, possibly sand and gravel. The bedrock reflector shows a low relief bedrock surface with a symmetric, parabolic-shaped crater (Fig. 6A). The depth of the crater as measured from the rim to the top of bedrock in the crater base is about 20 m.

Seismic profiles show a number of vertical offsets in the bedrock surface, indicating either the presence of faults or erosional channels cut into the bedrock surface. The bedrock offset at the north end of the profile in Figure 6A shows an apparent normal fault with an offset of 3 m. The offset coincides with a 5-10 nT TMI anomaly (Fig. 6A) and is evident in the vertical and horizontal gradient profiles (Fig. 6C). The co-located magnetic anomaly and bedrock offset in seismic data suggest that the structure is most likely a fault that extends into and displaces the Grenville basement rocks.

Figure 6. A. South-north sub-bottom chirp profile (12-24 kHz) acquired across CSS (location in Fig. 2A.). Ordovician bedrock indicated below 10-12 m thick sediment fill by high amplitude reflector. Note offset in bedrock surface at north end of profile indicated by arrow. B. Total magnetic intensity (TMI) along same survey line. C. Residual magnetic intensity. D. Horizontal and vertical 1st derivatives of TMI. Note the anomaly in both the vertical and horizontal derivatives (1900 m) coinciding with apparent fault offset imaged in seismic profile. E. 1-D analytic signal amplitude (ASA) calculated on TMI. F. Forwarded modelled depth to basement with extended Euler depth solutions for comparison.

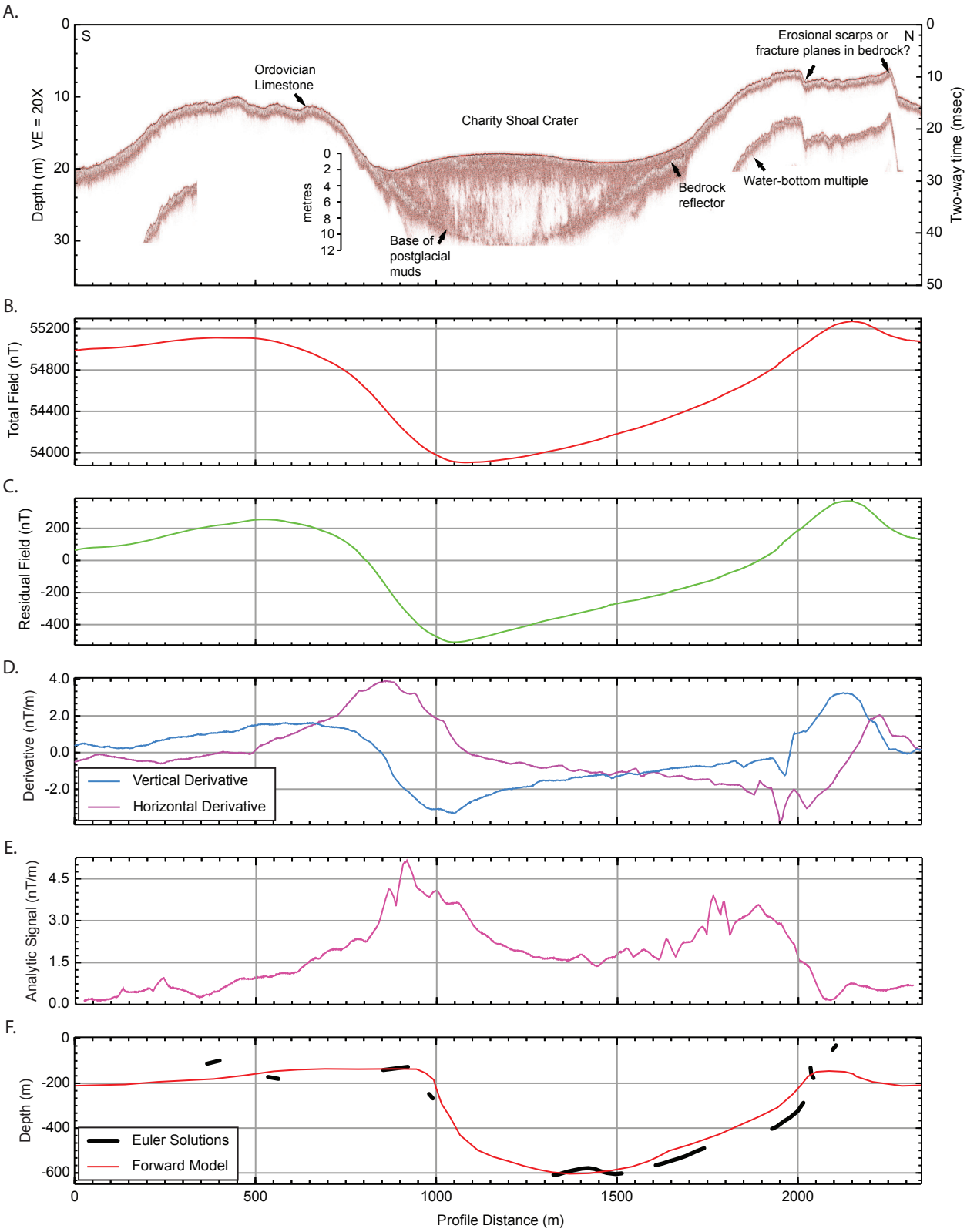
A.
S
N
Ordovician Limestone
Charity Shoal Crater
Erosional scarps or fracture planes in bedrock?
Bedrock reflector
Water-bottom multiple
Base of postglacial muds
metres
Depth (m) VE = 20X
Two-way time (msec)
B.
Total Field (nT)
C.
Residual Field (nT)
D.
Derivative (nT/m)
Vertical Derivative
Horizontal Derivative
E.
Analytic Signal (nT/m)
F.
Depth (m)
Euler Solutions
Forward Model
Profile Distance (m)

4.2. Magnetics

The TMI and residual magnetic maps are shown as colour-shaded images (Fig. 7A, B). The TMI map shows a large amplitude (~ -1400 nT), roughly circular negative magnetic anomaly centered over the CSS. The variation in magnetic intensity across the 9-km^2 study area is >1800 nT, with a general increase in intensity from west to east. The residual magnetic map (Fig. 7B) shows a well-defined annular magnetic anomaly corresponding with the rim of the structure. The anomaly is interrupted in the southwestern quadrant of the structure by a southwest-northeast trending magnetic low that coincides with the tail feature of the CSS (Figs. 2C, 6B). The annular magnetic anomaly of the rim is well defined in the 1st veridical derivative and analytic signal amplitude (ASA) maps (Fig. 8). The ASA is a useful tool for magnetic interpretation as it produces maxima over magnetic contrasts, regardless of the direction of magnetization. The ASA transform of the TMI produces a more uniformly circular anomaly and shows that the source body is coincident with rim crest. In 2-D profile, the ASA clearly shows that the ring anomaly is centered below the broader bedrock rim.

The extended Euler depth solutions are shown in profile in Figure 6E. Depth to basement outside the CSS is ~200 m and rises to ~150 m at the rim of the structure. The depth estimate falls to ~600 m in the centre of the CSS. The solutions define an 800-1000 m wide parabolic basin structure in the basement that is apparently offset from the overlying crater in the Paleozoic bedrock.

4.3. Forward Magnetic Models

The GM-SYS^{TM} forward models are shown in Figure 9A-D. The upper pane in each model window shows the observed magnetic response (black dots), the modeled response (green line) and the RMS error (red line) in nT (calculated - observed signal). The lower pane shows the layer geometry obtained by linear optimization.

The impact crater model (Model A; Fig. 9A) was created using an estimated crater true depth of 450 m with an impact breccia layer scaled to one half the rim to floor depth (225 m) and constituting about 40% of the crater

volume (Grieve, 1997; Melosh, 1987). The geometry of the crater was freed in the model inversion while the crater and bedrock depth were held constant. The best model fit (average RMS Error = 6.5) was achieved after optimization of the crater and bedrock geometry through inversion (Fig. 9A). Inversion of the model produced a 450 m deep parabolic-shaped crater in the 200 m deep Precambrian basement with well defined rim that rises 50 m above the surrounding basement.

The diatreme model (Model B; Fig. 9B) produced a large negative TMI anomaly that occurred when the intrusive body had a remanent magnetization (inclination: -68, declination: 198) that opposed the main field direction. A good fit (average RMS error = 25.4, maximum error = 131 nT) to the observed TMI anomaly was obtained when geometry of the bowl-shaped crater was optimized to extended to a depth 600 m and join with a 200 m in diameter feed pipe. The model reproduces the long-wavelength component of the TMI quite well but also generates a number of short wavelength anomalies at the edges of the crater. These short wavelength anomalies are not present in the observed signal. The model is considered to be geologically plausible but has a more complex magnetic response than the observed TMI anomaly.

In Model C, a 3-D basement syncline was modelled by constraining the susceptibility values of the Paleozoic and Precambrian rock units and the depth of the Paleozoic/Ordovician surface to 200 meters. The geometry of the depression was determined by optimization (Fig. 9C). It was found that the shape of the 1400 nT anomaly observed at the CSS could be reproduced but the amplitude of the anomaly could not be produced given the constraints (average RMS error = 244.6, maximum error = 532 nT). The results show that a syncline or erosional relief on the Precambrian surface can reproduce the shape of the CSS anomaly, but very large susceptibility values are needed to reproduce the amplitude, which make this model unlikely.

The erosional/dissolutional cavity simulation (Model D; Fig. 9D) demonstrates that a 190 m deep sediment-filled cavity will produce a small positive magnetic anomaly (~40 nT), due to the low magnetic contrast between limestone bedrock and unconsolidated sediment fill. This model was rejected, as

Figure 7. A. Total magnetic intensity (TMI) map. B. Residual magnetic intensity map.

A.

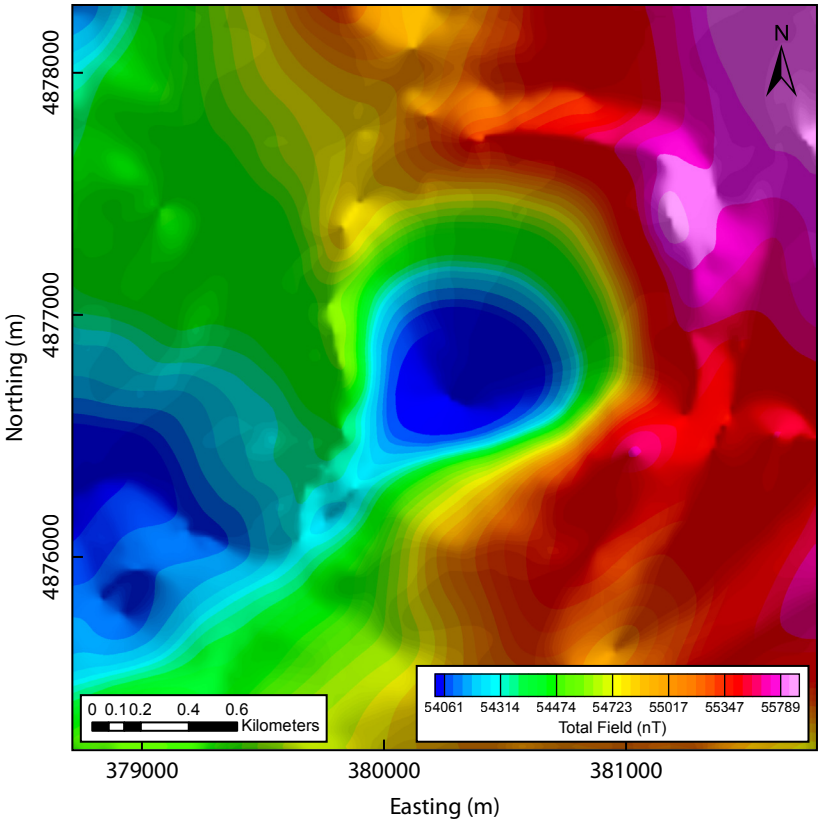
N
4878000
4877000
4876000
Northing (m)
0 0.10.2 0.4 0.6
Kilometers
54061 54314 54474 54723 55017 55347 55789
Total Field (nT)
379000
380000
381000
Easting (m)

B.

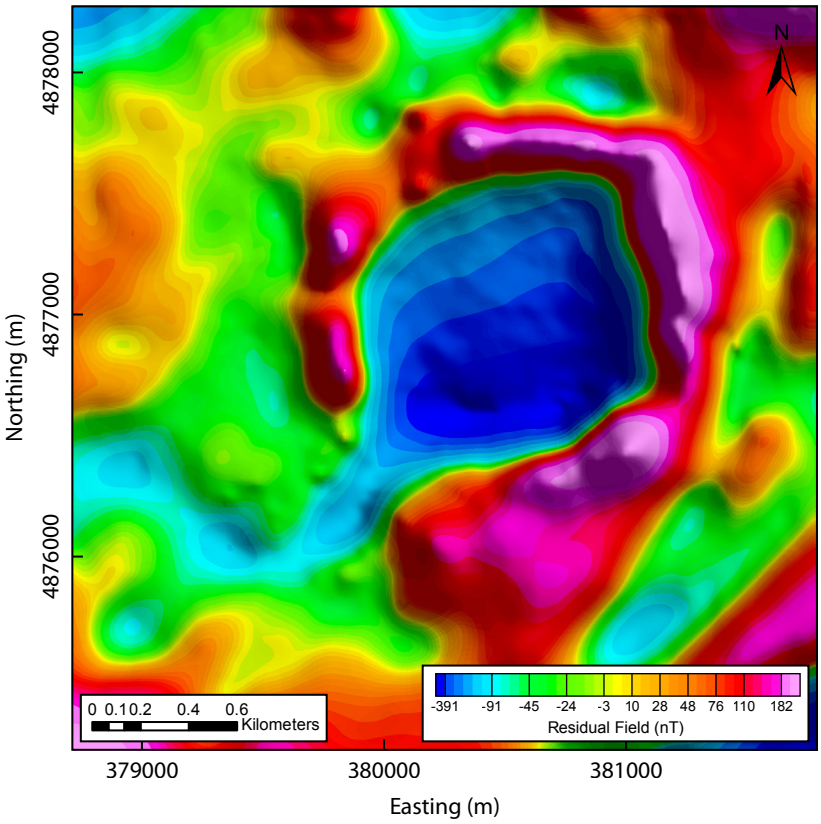
N
4878000
4877000
4876000
Northing (m)
0 0.10.2 0.4 0.6
Kilometers
-391 -91 -45 -24 -3 10 28 48 76 110 182
Residual Field (nT)
379000
380000
381000
Easting (m)

Figure 8. A. 1st vertical derivative of TMI. B. Analytic signal calculated on TMI grid.

A.

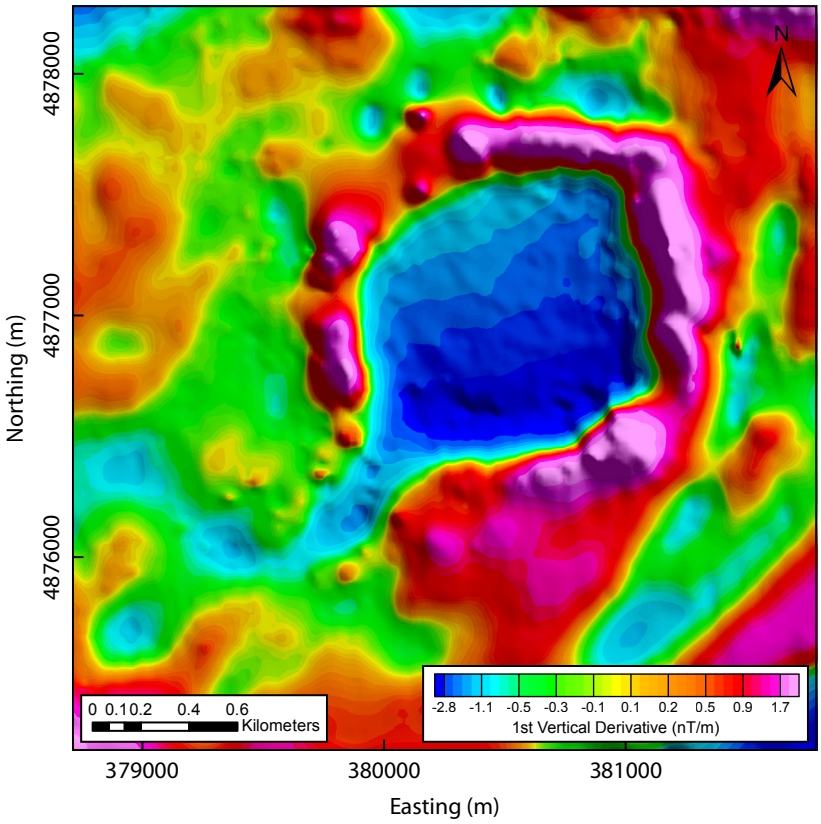
N
4878000
4877000
4876000
Northing (m)
0 0.10.2 0.4 0.6
Kilometers
-2.8 -1.1 -0.5 -0.3 -0.1 0.1 0.2 0.5 0.9 1.7
1st Vertical Derivative (nT/m)
379000
380000
381000
Easting (m)

B.

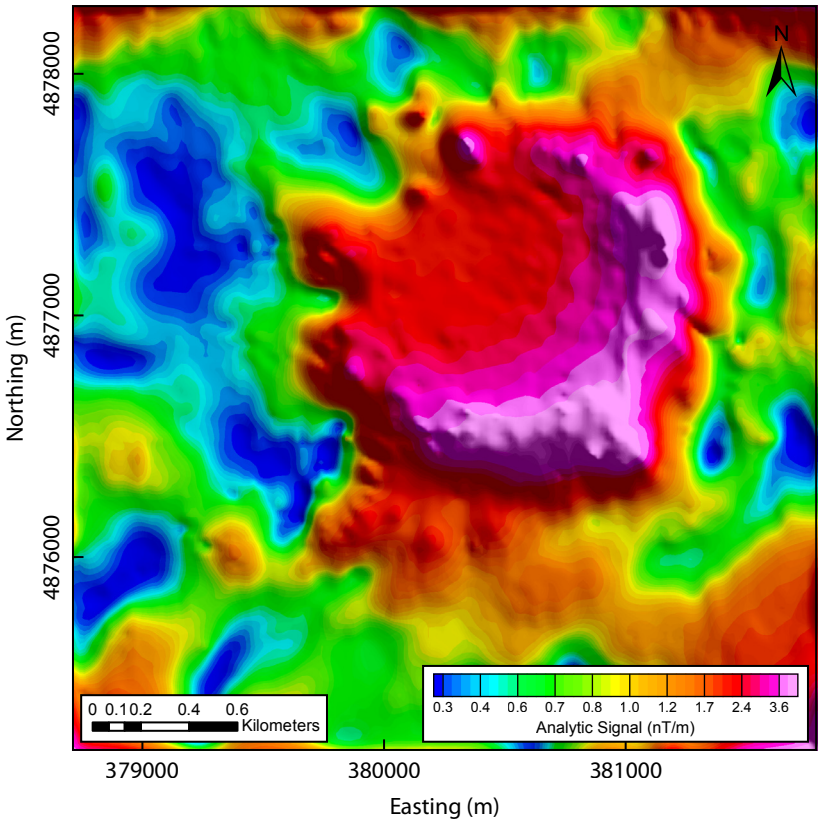
N
4878000
4877000
4876000
Northing (m)
0 0.10.2 0.4 0.6
Kilometers
0.3 0.4 0.6 0.7 0.8 1.0 1.2 1.7 2.4 3.6
Analytic Signal (nT/m)
379000
380000
381000
Easting (m)

Figure 9. Forward 2-D magnetic models generated in GM-SYS™ using west-east and north-south profiles extracted from the RTP corrected total magnetic intensity grid. A. Impact structure in Precambrian basement. B. Volcanic intrusion (diatreme). C. 3-D synclinal structure in Precambrian basement. D. Kettle/sink hole with 100 m deep basin infilled by glacial/post-glacial sediments.

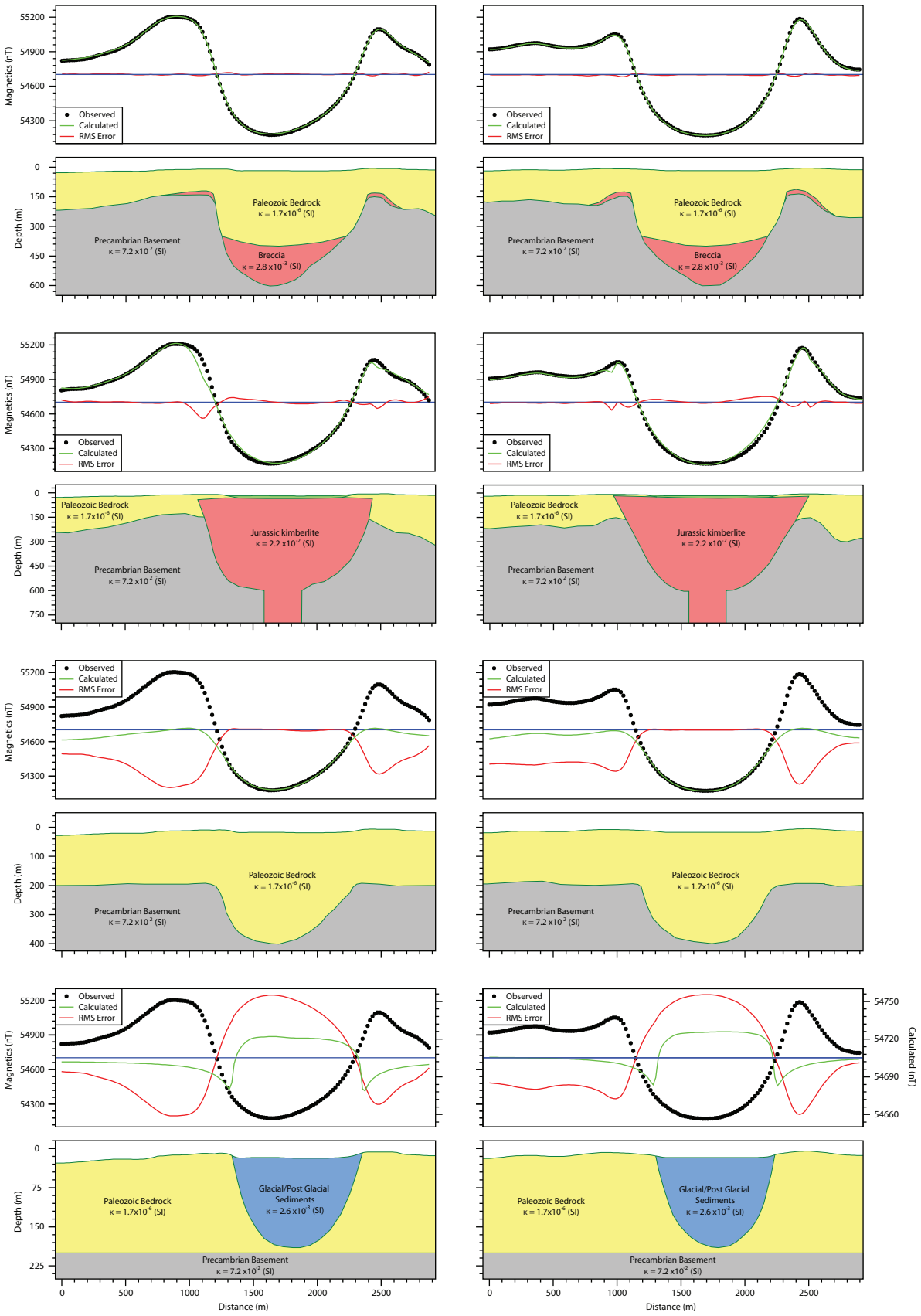
Magnetics (nT)
Observed
Calculated
RMS Error
Depth (m)
Paleozoic Bedrock
κ = 1.7x10⁻⁶ (SI)
Precambrian Basement
κ = 7.2 x10⁻² (SI)
Breccia
κ = 2.8 x10⁻³ (SI)
Jurassic kimberlite
κ = 2.2 x10⁻² (SI)
Glacial/Post Glacial
Sediments
κ = 2.6 x10⁻³ (SI)
Calculated (nT)
Distance (m)
S-N
E-W

it is impossible to recreate the observed TMI anomaly with this scenario (average RMS error = 355.2, maximum error = ~1400 nT)

4.4. Grenville Basement Topography

The Euler depth and 2-D forward modelling results confirm that the CSS is deep-seated structure, which fully penetrates the Paleozoic cover strata and affects the underlying Precambrian basement. Inversion using constraints from the Euler depth estimation found the average depth to the Precambrian basement to be 200-250 m, larger than previously estimated by Holcombe et al. (2001).

5. Discussion

5.1. Origin of the CSS

The geophysical results and 2-D profile models provide geophysical constraints for evaluating the four geological models considered in this study. Of the four models considered, the diatreme and impact crater models are most consistent with the seismic and magnetic field data and results of 2-D potential field modelling (Fig. 9). The diatreme model reproduces many aspects of the TMI anomaly except in the region of the crater rim anomaly, where the model generates short spatial wavelength anomalies not present in the TMI signal (Fig. 9B). The reversed remanence of the diatreme, which we speculate to be coeval with Jurassic ultramafic intrusions (Barnett et al., 1994), does provide a mechanism for creating a large demagnetization effect, and allows for a diatreme crater at shallow depth (Fig. 9B). The model profile shows that the ultramafic volcanics could be within 10-20 m of the lakebed surface, underlying the Quaternary sediment basin fill. In that case, we would anticipate that the Quaternary sediments in the basin should contain eroded volcanic materials. Coring and sampling of the basin sediments, and the crag-and-tail feature, which could contain glacially-transported debris from the basin, could provide confirmation of a volcanic origin.

The impact crater origin is most consistent with forward model results, as

it best reproduces both the central parabolic-shaped anomaly of the crater basin and annular rim anomaly (Fig. 9A) and is the favoured interpretation. The crater depth as estimated using the crater scaling functions is shallower than the depth to basement determined using the Euler method (Fig. 7).

Holcombe et al. (2013) have interpreted the CSS as an impact crater formed by a Middle Ordovician meteorite impact into a shallow marine environment. In their model, the impact crater basin and rim were successively draped and buried by carbonate sediments forming a broad, ring anticline structure recorded by strata dipping into an away from the basin. As a result of post-impact deposition, the relief on crater rim was attenuated over time. The geophysical results in this study, find that an impact crater with a base in the Paleozoic bedrock is unlikely, as it is not consistent with very large magnetic anomaly recorded across the CSS (Fig. 5A). We note that the rim anticlinal structure described by Holcombe et al. (2013) is also not inconsistent with a pre-Paleozoic age for the impact event. The anticlinal structure of the Simcoe Group carbonates can be equally explained by draping of carbonate sediments across a ~50 m high crater rim formed in the Grenville basement rocks.

The Holleford impact crater, located 40 km to the north of the study area may provide a structural analog for the CSS (Fig. 10). The Holleford crater is a ~2.3 km diameter buried impact structure discovered in aerial photographs by Beals(1956). The structure was confirmed as a simple impact structure after magnetic, gravity and seismic surveys were completed (Beals, 1960; Dawson, 1961; MacLennan, 1988) and drill cores revealed consolidated breccias and shocked quartz grains (Beals, 1960). The Holleford crater is just under twice the size of the CSS, with a rim to crater basin relief of about 30 m. The stratigraphy of the crater consists of>250 m of Paleozoic limestone and Cambrian sandstones overlying a 275 m thick impact breccia unit. The impact breccia rests unconformably over Grenville basement gneiss, which led Beals (1965) to suggest a Late Proterozoic-Cambrian age for the impact event. A regional aeromagnetic data survey acquired over the Holleford crater in the 1960's detected a small depression in the TMI but no marked anomaly. The Grenville

Figure 10. Aerial photograph of the 2-km diameter Holleford impact crater (from MacLellan, 1988).


N
1
2
3
300 m

basement below the crater includes quartzite and metapelites units, which may explain the lack of well defined magnetic anomaly. A gravity survey revealed a circular anomaly in the Bouguer gravity of about 2 mGal. The overlying Paleozoic strata dip into the centre of the crater basin and flat-lying or dip gently outward from the rim. The rim structure may be analogous to the Charity Shoal rim anticline described by Holcombe et al. (2013). The basin fill sediments at Holleford include lacustrine sand and shale deposits, which were attributed to shallow lake phase prior to deposition of Ordovician limestones (MacLennan, 1988).

6. Conclusion

The seismic and magnetic data presented provide important new insights into the subsurface structure of Charity Shoal and geophysical constraints for evaluating its origin. Of the four models evaluated, the origins as an impact crater and volcanic intrusive best fit the potential field data and 2-D modelling results. The diatreme model explains many aspects of the crater morphology but the 2-D modelled magnetic response is more complex than the observed smooth, parabolic TMI anomaly. The impact crater model, constructed using the empirical scaling functions, produces the best fit to the potential field models. The CSS analogous in many respects to the Late Proterozoic-Cambrian age Holleford Crater, located 30 km to the north of the study site (Fig. 1), and may represent an impact event of a similar age.

Confirmation of the impact origin of the CSS and its age will require further detailed geophysical survey work and ultimately, drilling and sampling of the crater floor sediments and bedrock to identify diagnostic impact indicators (French and Koeberl, 2010). Future geophysical studies at Charity Shoal should include a 3-D multi-channel seismic survey using a high-energy source to provide details of crater infill stratigraphy and basement structure (e.g. Muller et al., 2011). Collection of additional potential field surveys, using full tensor airborne gravity and marine magnetic gradient surveys, would provide a basis for detailed 3-D modelling and would assist in the interpretation of seismic data.

Acknowledgements

Research supported by a Natural Sciences and Engineering Research Council of Canada (NSERC) grant to Boyce. We thank Marine Magnetics Corporation for access to field instrumentation and Geosoft Ltd. for academic software grant.

Chapter 4: Conclusions

4.1 Summary

The results of this thesis demonstrate that high-resolution marine magnetic surveys allow subsurface geologic structures (<2 km in size) to be imaged and analyzed. This method is important because borehole drilling may be costly and aerial magnetic surveys may not provide to resolution needed for imaging.

Chapter 2 presented the application of utilizing high resolution marine magnetic surveying to map basement faults. The displacement of rock units with high magnetic susceptibility is hypothesized to have created the NNW-SSE trending linear anomalies seen in the TMI data. The observed lineaments within the magnetic signal were combined with lineaments within the seismic survey data to map fault traces. Forward modelling was combined with previously found fault and lineament data in the region allowing for a structural model of the Küçükçekmece Lagoon area to be created. It was found that a transtensional fault regime best described the observed faults in the study area.

Chapter 3 presents the application of utilizing high resolution marine magnetic surveying to image and analyze an undetermined geologic structure. The Charity Shoal structure is an enigmatic crater like depression found in the Ordovician bedrock of Lake Ontario. Analysis of the surveyed magnetic total field data, including regional residual separation and depth estimation, determined that the structure must either be present in the underlying Precambrian bedrock or have a remanent magnetization opposing the present day field. Forward modelling confirmed the validity of the diatreme and impact crater models favoured a meteorite impact as the most plausible origin.

4.2 Limitations

This thesis shows that high-resolution marine magnetic surveying can offer valuable insights into the structure and depth of small scale geologic structures, at a reduced cost and higher resolution than many other methods. There are limitations to high resolution marine magnetic surveying. Geophysical methods work though the detection and measurement of various quantitative physical properties (magnetics, seismics, and gravity). When magnetic surveys are used as the exclusive data source for a study the results are hard to constrain and non-uniqueness is a problem. Geophysical methods are best used when paired with complimentary geophysical methods or ground truthing methods like borehole sampling or field observations. Another limitation of the magnetic method is that as water depth increases the resolution of the survey will decrease as per the attenuation of the induced magnetic field at depth, therefore surveys have greater resolution at shallower water depths. It is important to note that magnetic surveys should always be performed during periods of low solar activity as high solar activity may produce incomprehensible survey data.

4.3 Future Work

The potential applications made possible by high resolution marine magnetic surveying are quite diverse. Magnetic surveying offers an inexpensive way to image and analyze any small scale geologic feature that exhibits a susceptibility contrast with its surroundings Magnetic surveys are an excellent preliminary tool that will suggest depth, structural and compositional properties of a target before more expensive imaging and diagnostic methods are employed. There is great potential for magnetic methods to be used for impact crater, kimberlite and fault identification, analysis and mapping.

References

Aksu, A.E., Calon, T.J., and Hiscott, R.N., 2000. Anatomy of the North Anatolian Fault Zone in the Marmara Sea, Western Turkey: Extensional Basins Above a Continental Transform. *GSA Today*,10(6):2-7.

Akarvardar, S., Feigl, K.L., and Ergintav, S., 2009. Ground deformation in an area later damaged by an earthquake: monitoring the Avcılar district of İstanbul, Turkey, by satellite radar interferometery 1992-1999. *Geophys. J. Int.,* 178: 976-988

Allen, M.B., MacDonald, D.I.M., Xun, Z., Vincent, S.J., and Brouet - Menzies, C., 1998. Transtensional deformation in the evolution of the Bohai Basin, northern China, in: Holdsworth, R.E., Strachan, R.A., Dewey, J.F. (Eds.), Continental Transpressional and Transtensional Tectonics. *Geological Society of London Special Publication*, 135: 215-229.

Alpar, B., and Yaltırak, C., 2002. Characteristic features of the North Anatolian Fault in the Marmara region and its tectonic evolution.*Marine Geology*, 190: 329-350.

Armijo, R., Meyer, B., Hubert, A., and Barka, A., 1999. Westward propagation of the North Anatolian fault into the northern Aegean Sea: Timing and kinematics. *Geology*, 27:267-270.

Armstrong, D.K., and Dodge, J.E.P., 2007. Paleozoic Geology of Southern Ontario.*Sedimentary Geoscience Section,* Miscellaneous Release – Data 219.

Barka, A.A., and Kadinsky-Cade, K., 1988. Strike-slip fault geometry in Turkey and its influence on earthquake activity. *Tectonics*, 7: 663-684.

Barka, A.A., 1992. The North Anatolian Fault Zone. *Ann. Tecton*, 6: 164-195.

Barnett, R.L., Arima, M., Blackwell, J.D., Winder, C.G., Palmer, H.C., and Hayatsu, A. 1984. The Picton and Varty Lake ultramafic dikes: Jurassic magmatism in the St.Lawrence Platform near Belleville, Ontario. *Canadian Journal of Earth Sciences,* 2(1): 1460-1472.

Beals, C.S., Ferguson, G.M., and Landua, A., 1956. A search for analogies between lunar and terrestrial topography on photographs of the Canadian Shield.*Journal of the Royal Astronomical Society of Canada,* 50: 250-261.

Beals, C.S., 1960. A probable meteorite crater of Precambrian age at Holleford, Ontario.*Ottawa Dominion Observatory Publications*, 24(6): 117-142.

Briggs, I.C., 1974. Machine contouring using minimum curvature. *Geophysics*, 39: 39-48.

Boyce, J.I.and Morris, W.A., 2002. Basement controlled faulting of Paleozoic strata in southern Ontario, Canada: new evidence from geophysical lineament mapping.*Tectonophysics*, 353: 151-171.

Boyce, J.I., Pozza, M., Morris, W.A., Eyles, N., Doughty, M., 2002.High-resolution magnetic and seismic imaging of faults in western Lake Ontario and Lake Simcoe. Canada: Proceedings of the Symposium on the Application of Geophysics to Environmental and Engineering Problems (SAGEEP), Las Vegas. 12 pp.

Boyce, J.I., Reinhardt, E.G., Raban, A. and Pozza, M., 2004.Marine magnetic survey of a submerged Roman harbour, Caesarea Maritima, Israel.*International Journal of Nautical Archaeology*, 33: 122-136.

Boyce, J.I., Reinhardt, E.G., and Goodman, B.N., 2009. Magnetic detection of ship ballast mounds and anchorages at Caesarea Maritima, Israel.*Journal of Archaeological Science*, 36: 1516-1526.

Bulut, F., Bohnhoff, M., Ellsworth, W.L., Aktar, M., and Dresen, G., 2009. Microseismicity at the North Anatolian fault in the Sea of Marmara Offshore Istanbul. *J. Geophys. Res.* doi 10.1029/2008JB006244.

Chapman, L.J., and Putnam, D.F., 1984. The Physiology of Southern Ontario. 3rd ed. Toronto, Ontario: Ontario Ministry of Natural Resources.

Cockell, C.S., and Lee, P., 2002. The Biology of Impact Craters - a review. *Biol. Rev*., 77: 279 - 310.

Cordell, L., 1985. Techniques, applications and problems of analytical continuation of New Mexico aeromagnetic data between arbitrary surfaces of very high relief. Institut de Geophysique. University de Lausanne, Switzerland, Bulletin No. 7., pp. 96 – 99.

Crough, S.T., 1981. The Darfur Swell, Africa: Gravity contraints on its isostatic compensation. Geophysical Research Letters 8: doi: 10.1029/0GPRLA00 0008000008000877000001.

Cunningham, W.D., and Mann, P., 2007. Tectonic of strike-slip restraining and releasing bends. *Geological Society, London, Special Publications,* 290:1-12.

Dalgiç, S., 2004. Factors affecting the greater damage in the Avcılar area of İstanbul during the 17 August 1999 İzmit earthquake.*Bull. Eng. Geol. Env*., 63: 221-232.

Dawson, K.R., 1961. The origin of the Holleford Crater breccias.*Can. Mineral,* 6: 634-646.

Del Negro, C., and Napoli, R., 2002. Ground and marine magnetic surveys of the lower eastern flank of Etna volcano (Italy), *J. Volcanol. Geotherm. Res*., 114(3/4): 357-372.

Dehler,S.A.,and Potter, D.P.2002.Determination of nearshore geologic structure off western Cape Breton Island, Nova Scotia, using high-resolution marine magnetics.*Canadian Journal of Earth Sciences*,39:1299–1312.

Di Prisco, G., and Springer, J.S., 1991. The Precambrian-Paleozoic unconformity and related mineralization in southeastern Ontario.*Ontario Geological Survey,* Open File Report 5751, 88 p.

Dresden, G., 1991. Stress distribution and the orientation of Riedel shears. *Tectonophysics,* 188: 239-247.

Duman, T.Y., Can, T., Ulusay, R., Kecer, M., Emre, O., Ates, S., and Gedik, I., 2005. A geohazard reconnaissance study based on geoscientific

information for development needs of the western region of İstanbul (Turkey). *Environ. Geol.,* 48: 871-888.

Dypvik, H., Jansa, L.F., 2003. Sedimentary signatures and processes during marine bolide impacts: a review. *Sedimentary Geology,* 161: 309-337.

Easton, R., 1992.The Grenville Province and the Proterozoic history of central and southern Ontario.pp. 714-904. *In* P. C. Thurston et al. (eds.). Geology of Ontario.Special Volume 4, Part 2.Ontario Geological Survey, Toronto.

Ergintav, S., Demirbag, E., Ediger, V., Saatcilar, R., Inan, S., Cankurtaranlar, A., Dikbas, A., and Bas, M., 2011.Structural framework of onshore and offshore Avcılar, İstanbul under the influence of the North Anatolian fault.*Geophys. J. Int.*, 185: 93-105.

Ergün, M., and Ozel, E., 1995.Structural relationships between the Sea of Marmara basin and the North Anatolian Fault Zone.*Terra Nova*, 7: 278-288.

Ferrière, L., Morrow, J.R., Amgaa, T., and Koeberl, C., 2009. Systematic study of universal-stage measurements of planar deformation features in shocked quartz: Implications for statistical significance and representation of results. *Meteoritics and Planetary Science,* 44: 925–940.

Field, M., Scott Smith, B.H., 1999. Contrasting geology and near-surface emplacement of kimberlite pipes in southern Africa and Canada. *Proc. 7th Int. Kimb. Conf.* (Eds. Gurney et al.) 1: 214-237.

Firestone, R.B., West, A., Kennett, J.P., Becker, L., Bunch, T.E., Revay, Z.S., et al., 2007. Evidence for an extraterrestrial impact 12,900 year ago that contributed to the megafaunal extinction and the Younger Dryas cooling. *PNAS,* 104(41):16016-16021.

French,B.M., and Koeberl,C., 2010.The convincing identification of terrestrial meteorite impact structures; What works, what doesn't, and why*. Earth-Science Reviews, 98: 123-170.*

Ganapathy, R., 1982.Evidence for a major meteorite impact on the earth 34 million years ago; implication for Eocene extinctions.*Science*, 216: 885-886.

Gasperini, L., Polonia, A., Çağatay, N., Bortoluzzi, G., and Ferrante, V., 2011. Geological slip rates along the North Anatolian Fault in the Marmara region. *Tectonics*, 30: TC6001

Gazioğlu, C., Gökaşan, E., Algan, O., Yücel, Z.Y., Tok, B., and Doğan, E., 2002. Morphologic features of the Marmara Sea from multi-beam data.*Mar. Geol.,* 190(1/2): 333-356.

Gökaşan, E., Alpar, B., Gazioğlu, C., Yücel, Z.Y., Tok, B., Doğan, E., and Güneysu, C. 2001. Active tectonics of the İzmit Gulf (NE Marmara Sea): from high resolution seismic and multi-beam bathymetry data. *Marine Geology*, 175(1-4): 271-294.

Gökaşan, E., Gazioğlu, C., Alpar, B., Yücel, Z.Y., Ersoy, S., Gündoğdu, O., Yaltırak, C., and Tok, B., 2002.Evidence of NW extension of the North Anatolian Fault Zone in the Marmara Sea; a new interpretation to the 17 August 1999 Marmara Sea earthquake.*Geo-Mar. Lett*., 21:183-199.

Gökaşan, E., Ustaömer, T., Gazioğlu, C., Yücel, Z.Y., Öztürk, K., Tur, H., Ecevitoğlu, B., and Tok, B., 2003. Morpho-tectonic evolution of the Marmara Sea inferred from multi-beam bathymetric and seismic data, *Geo-Mar. Lett.*, 23(1):19-33.

Grauch, V.J.S., Bauer, P.W. and Kelson, K.I.,2004. Preliminary interpretation of high-resolution aeromagnetic data collected near Taos, New Mexico. *New Mexico Geological Society*, Guidebook 55, p. 244-256.

Gravenor, C.P., and Stupavsky, M., 1974. Magnetic Susceptibility of the Surface Tills of Southern Ontario. *Canadian Journal of Earth Sciences,* 11(5): 658-663.

Green, A.A. 1983. A comparison of adjustment procedures for leveling aeromagnetic survey data.*Geophysics* 48(6): 745-753.

Grieve, R.A.F., and Pesonen, L.J., 1996. Terrestrial impact craters: Their spatial and temporal distribution and impacting bodies. *Earth, Moon, Planets*, 72: 357-376.

Grieve, R.A.F., and Pilkington, M., 1996. The signature of terrestrial impacts.*AGSO Journal of Australian Geology & Geophysics*, 16: 399-420.

Grieve, R.A.F. 1997, Terrestrial impact structures: basic characteristics and economic significance with emphasis on hydrocarbon production. In Johnson K. S. and Campbell J. A. (eds) Ames structure in northwest Oklahoma and similar features: Origin and petroleum production. *Oklahoma Geol. Surv. Circular,* 100:3–16.

Gürbüz, C., Aktar, M., Eyidoğan, H., Cisternas, A., Haessler, H., Barka, A., Ergin, M., Türkelli, N., Polat, O., Üçer, S.B., Kuleli, S., Barış, S., Kaypak, B., Bekler, T., Zor, E., Biçmen, F., and Yörük, A., 2000. The seismotectonics of the Marmara region (Turkey): results from a microseismic experiment. *Tectonophysics*, 316: 1-17.

Hergert, T., and Heidbach, O., 2010. Slip-rate variability and distributed deformation in the Marmara Sea fault system. *Nature Geoscience,* 3: 132-135.

Hildebrand, A.R., Penfield, G.T., Kring, D.A., Pilkington, M., Camargo, A., Jacobsen, S.B., and Boynton, W.V., 1991. Chicxulub crater: a possible Cretaceous/Tertiary boundary impact crater on the Yucatan Peninsula, Mexico. *Geology*, *19*(9): 867-871.

Holcombe, T.L., Warren, J.S., Reid, D.F., Virden, W.T., and Divins, D.L., 2001. Small Rimmed Depression in Lake Ontario: In Impact Crater? *J. Great Lakes Res.* 27(4): 510-517.

Holcombe, T.L., Youngblut, S., and Slowey, N., 2013. Geological structure of Charity Shoal crater, Lake Ontario, revealed by multibeam bathymetry. *Geo. Mar. Lett.,*DOI 10.1007/s00367-013-0322-6

Hon, V., 1970. A Study of Some Post-Cambrian Dike Rocks in Southeastern Ontario; unpublished BSc. Thesis, Carleton University, Ottawa, Ontario, 41p.

Hubert-Ferrari, A., Barka, A., Jacques, E., Nalbant, S.S., Meyer, B., Armijo, R., Tapponnier, P., and King, G.C.P., 2000.Seismic hazard in the Marmara Sea region following the 17 August 1999 İzmit earthquake,*Nature,*404(6775): 269-273.

İmren, C., Le Pichon, X., Rangin, C., Demirbağ, E., Ecevitoğlu, B., and Görür, N., 2001. The North Anatolian Fault within the Sea of Marmara: a new evaluation based on multi-channel seismic and multi-beam data. *Earth Planet Sci Lett* 186: 143-158.

Jacques, J. M., Parsons, M. E., Price, A. D., & Schwartz, D. M. (2003). Improving geologic understanding with gravity and magnetic data: Examples from Gabon, Nigeria and the Gulf of Mexico. *First Break*, 21(11).

Jones, E.J.W., 2001. Marine Geophysics. Blackwell: Wiley.

Katz, Y., Weinberger, R., and Aydin, A., 2004. Geometry and kinematic evolution of Riedel shear structures Capitol Reef National Park, Utah. *Journal of Structural Geology,* 26: 491-501.

Kerr, M., and Eyles, N., 2007.Origin of drumlins on the floor of Lake Ontario and in upper New York State.*Sedimentary Geology,* 193: 7-20.

KOERI, 2000.The earthquake activities of the Marmara region between 1990 and 2000. Bosphorous University Kandilli Observatory, http://www.koeri.

.boun.edu.tr.

Krona, D.A., 2000.Impact events and their effect on the origin, evolution, and distribution of life.*GSA today*, *10*(8): 1-7.

Kuşçu,İ., Okamura, M., Matsuoka, H., and Awata,İ., 2002. Active faults in the Gulf of İzmit on the North Anatolian Fault, NW Turkey: a high resolution shallow seismic study*. Mar Geol,* 190(1/2):421–433.

Le Pichon, X., Şengör, A.M.C., Demirbag, E., Rangin, C., İmren, C., Armijo, R., Gorur,N., Cagatay, de Lepinay, B.M., Meyer, B., Saatcilar, R., and Tok, B., 2001. The active Main Marmara Fault. *Earth and Planetary Science Letters*, 192(4): 595-616.

Luyendyk, A.P.J., 1997. Processing of airborne magnetic data. *AGSO Journal of Australian Geology & Geophysics,* 17(2): 31-38.

MacLennan, M.J., 1988. The Holleford Meteorite Impact Crater.*The Canadian Geographer,* 32(2): 173-177.

MacLeod, I.N., Jones, K., and Dai, T.F., 1993. 3-D Analytic Signal in the Interpretation of Total Magnetic Field Data at Low Magnetic Latitudes. *Exploration Geophysics,* 24:679-688.

Marqardt, D.W., 1963. An algorithm for least-squares estimation of non-linear parametres.*J.SIAM*, 11: 431-441.

McFall, G.H., 1993. Structural elements and neotectonics of Prince Edward County, Southern Ontario.*GeographiePhysique et Quaternaire* 47(3): 303-312.

Melosh, H.J., 1989. Impact Cratering: A Geologic Process. Oxford University Press, New York. p. 126-130.

Minty, B.R.S., 1991. Simple micro-levelling for aeromagnetic data. *Exploration Geophysics*, 22: 591-592.

Muir, T.L., compiler. 2013. Ontario Precambrian bedrock magnetic susceptibility geodatabase for 2001 to 2012. Ontario Geological Survey, Miscellaneous Release-Data 273 - Revised.

Mushayandebvu, M. F., Van Driel, P., Reid, A.B., and Fairhead, J.D., 2001. Magnetic source parametres of two dimensional structures using extended Euler deconvolution: *Geophysics*, 66(3): 814-823.

Musselman, C., Whitehead, N., McDonald, K., 2000. Geosoft Levelling System, processing and enhancing geophysical data, tutorial and user guide. Geosoft Inc.

Nabighian, M.N., 1972. The analytic signal of two-dimensional magnetic bodies with polygonal cross section: Its properties and use for automated anomaly interpretation. *Geophysics*, 37: 507-517.

Nabighian, M.N., 1974. Additional comments on the analytic signal of two-dimensional magnetic bodies with polygonal cross-section.*Geophysics*, 39: 85-92.

NOAA National Geophysical Data Center, Great Lake Bathymetry, Retrieved May 2012, http://www.ngdc.noaa.gov/mgg/greatlakes/greatlakes.html.

Norris, R.D., Huber, B.T., and Self-Trail, J., 1999. Synchroneity of theK–T oceanic mass extinction and meteorite impact: Blake Nose, western North Atlantic. *Geology* 27: 419-422.

O'Dowd, C., Eaton, D., 2005. Field and laboratory measurements of magnetic properties and density, Central Metasedimentary Belt, Ontario.Geological Survey of Canada, Current Resarch 2005-D2, p 12.

Okay, A.I., Şengör, A.M.C., and Görür, N., 1994, Kinematic history of the opening of the Black Sea and its effects on the surrounding regions. *Geology*, 22: 267-270.

Okay, A., Demirbağ, E., Kurt, H., Okay, N., and Kusçu, İ., 1999. An active, deep marine strike-slip basin along the North Anatolian fault in Turkey. *Tectonics*, 18(1): 129-147.

Okay, A.I., Kaşlılar-Özcan, A., İmren, C., Boztepe-Güney, A., Demirbağ, E., and Kuşçu, İ., 2000. Active faults and evolving stike-slip basins in the Marmara Sea, northwest Turkey: a multichannel seismic reflection study. *Tectonophysics*, 321: 189-218.

Oktay, F.Y., Gökaşan, E., Sakınc, M., Yaltırak, C., Imren, C. and Demirbag, E., 2002. The effects of the North Anatolian Fault Zone on the latest connection between Black Sea and Sea of Marmara. *Mar. Geol.,* 190**:** 367–382.

Ontario Oil, Gas and Salt Resources Library (OGSR). 2013. Well Resources Map. Web. Retrieved on March 2013.

Parrish, J.B., and Lavin, P.M., 1982. Tectonic model for kimberlite emplacement in the Appalachian Plateau of Pennsylvania.*Geology [Boulder]*, 10(7): 344-347.

Parke, J.R., Minshull, T.A., Anderson, G., White, R.S., McKenzie, D., Kuşçu, I., Bull, J.M., Görür, N., and Sengör, C., 1999. Active faults in the Sea of Marmara, western Turkey, imaged by seismic reflection profiles. *Terra Nova*, 11: 223-227.

Paterson, N.R., Reford S.W., and Kwan, K.C.H., 1990. Continuation of magnetic data between arbitrary surfaces: Advances and applications. Proceedings of the Society of Exploration Geophysicists, Sixtieth Annual International Meeting, San Francisco, Expanded Abstracts, p. 666-669.

Pehlivan, R., and Yilmaz, O., 2004.Geochemistry and mineralogy of bottom sediments in the Kucukcekmece Lake, Istanbul, Turkey.*Geochemistry International*, 42: 1099-1106.

Phillips, J.D., 1997. Potential-field geophysical software for the PC, version 2.2: *U.S. Geological Survey Open-File Report 9*, 725 p.

Pilkington, M., and Grieve, R.A.F., 2002.The Geophysical Signature of Terrestrial Impact Craters.*Reviews of Geophysics,* 30(2): 161-181.

Pınar, N., 1942. Geologie et meteorologie sismiques du bassin de la mer de Marmara. *Univ Istanbul Sci Fac Bull* 7(3-4): 121-182.

Pozza, M.,Boyce, J.I., and Morris, W.A. 2004.Lake-based magnetic mapping of contaminated sediment distribution, Hamilton Harbour, Ontario, Canada.*Journal of Applied Geophysics*, 57: 23-41.

Reid, A.B., Allsop, J.M., Granser, H., Millett, A.J., and Somerton,I.W., 1990. Magnetic interpretation in three dimensions using Eulerdeconvolution: *Geophysics*, 55: 80-91.

Riedel, W., 1929.Zur Mechanik geologischer Brucherscheinungen.*Zentral-blatt für Mineralogie Abteilung B*, 354-368.

Roest, W.R., Verhoef, J., and Pilkington, M., 1992.Magnetic interpretation using the 3-D analytic signal.*Geophysics,* 57(1):116-125.

Sanford, B.V., andBaer, A.J., 1981. Geological Map of Southern Ontario, GEOLOGICALATLAS 1:1,000,000 (R. J. W. Douglas, coordinator), Geological Survey of Canada, map 1335A, sheet 30S.

Schmitz, B., Harper, D.A., Peucker-Ehrenbrink, B., Stouge, S., Alwmark, C. Cronholm, A., Bergström, S.M., Tassinari, M., and Wang, X., 2008: Asteroid breakup linked to the Great Ordovician Biodiversity Event. *Nature Geoscience* 1: 48-53.

Schulte, P, Speijer, R.P., Brinkhuis, H, Kontny, A, Caleys, P, Galeotti, S, Smit, J,. 2008. Comment on the paper, Chicxulub impact predates K–T boundary: new evidence from Brazos, Texas. by Keller et al., 2007. *Earth Planet Sci Lett* 269: 613-619.

Schulte, P., and 40 others, 2010.The Chicxulub asteroid impactand mass extinction at the Cretaceous–Paleogene boundary.*Science*, 327: 1214-1218.

Scott, R.G., Pilkington, M., and Tanczyk, E.I., 1997. Magnetic investigations of the West Hawk, Deep Bay, and Clearwater impact structures, Canada. *Meteorit. Plan. Sci*., 32: 293-308.

Şen, S., 2007. A fault zone cause of large amplification and damage in Avcılar (west of İstanbul) during 1999 İzmit earthquake.*Nat. Hazards,* 43: 351-363.

Şengör, A.M.C., Tüysüz, O., İmren, C., Sakınç, M., Eyidoğan, H., Görür, N., Le Pichon, X., and Rangin, C., 2005. The North Anatolian Fault: A New Look. *Annual Review of Earth and Planetary Sciences*, 33: 37-112.

Siyako, M., Tanış, T., and Şaroğlu, F., 2000. Marmara Denizi'nin aktif fay geometrisi (Active fault geometry of the Marmara Sea (in Turkish). *Sci Technol*, 388: 66-71.

Sleep, N.H., Zahnle, K.J., Kasting, J.F., and Morowitz, H.J., 1989. Annihilation of ecosystems by large asteroid impacts on the early Earth.*Nature*, 342(6246): 139-142.

Smith, A.D., Taymaz, T., Oktay, F., Yuce, H., Alpar, B., Basaran, H., Gackson, J. A., Kara, S., and Simsek, M., 1995. High-resolution seismic profiling in the

Sea of Marmara (northwest Turkey): Late Quaternary sedimentation and sea-level changes. *Geol. Soc. Am. Bull*., 108: 923-936.

Stein, R.S., Barka, A.A., and Dieterich, J.H., 1997. Progressive failure on the North Anatolian fault since 1939 by earthquake stress triggering.*Geophys. J. Int.*128: 594-604.

Straub, C., Kahle, H.G., and Schindler, C., 1997. GPS and geologic estimates of the tectonic activity in the Marmara Sea region, NW Anatolia.*J. Geophys. Res.*, 102(27):587-601.

Sturkell, E.F.F., and Ormö, J., 1998. Magnetometry of the marine, Ordovician Lockne impact structure, Jämtland, Sweden.*Journal of Applied Geophysics*, 38: 195-207.

Talwani, M., and Heirtzler, J.R., 1964. Computation of magnetic anomalies caused by two dimensional bodies of arbitrary shape, in Parks, G. A., Ed., Computers in the mineral industries, Part 1: Stanford Univ. Publ., *Geological Sciences*, 9: 464-480.

Talwani, M., Worzel, J.L., and Landisman, M., 1959. Rapid gravity computations for two dimensional bodies with application to the Mendocino submarine fracture zone. *J. Geophys. Res*., 64: 49-59.

Tezcan, S.S., Kaya, I. E., Bal, E., and Ozdemir, Z., 2002. Seismic amplification at Avcılar, Istanbul.*Eng. Struct*. 24(5): 661-667.

Therriault, A.M., Fowler, A.D., and Grieve R.A.F., 2002. The Sudbury igneous complex: A differentiated impact melt. *Economic Geology* 97: 1521-1540.

Thompson, D.T., 1982. EULDPH—A new technique for making computer-assisted depth estimates from magnetic data. *Geophysics*, 47: 31-37.

U.S. Geological Survey (USGS), 2000. Implications for Earthquake Risk Reduction in the United States from the Kocaeli, Turkey, Earthquake of August 17, 1999. *U.S. Geological Survey Circular*, 119.

Van Fossen, M., and Kent, D.V., 1993.A palaeomagnetic study of 143 Ma kimberlite dikes in central New York State.*Geophysical Journal International,* 113: 175-185.

Virden, W.T., Warren, J.S., Holcombe, T.L., Reid, D. F., and Berggren, T.L., 1999. Bathymetry of Lake Ontario.National Geophysical Data Center, World Data Center A for Marine Geology & Geophysics, Boulder CO. Rept. MGG–14.

Waldron, J.W.F. 2005. Extensional fault arrays in strike-slip and transtension.*Journal of Structural Geology*, 27: 23-34.

Weiss, E., Ginzburg, B., Cohen, T.R., Zafrir, H., Alimi, R., Salomonski, N., and Shatvit, J., 2007. High resolution marine magnetic survey of shallow water littoral area. *Sensors*, 7: 1697–1712.

Wong, H.K., Luedmann, T., Ulug, A., and Görür, N., 1995. The Sea of Marmara: A plate boundary sea in an escape tectonic regime. *Tectonophysics*, 244: 231-250.

Yaltırak, C., Sakınc, M., Aksu, A.E., Hiscott, R.N., Galleb, B., and Ulgen, U.B., 2002. Late Pleistocene uplift history along the southwestern Marmara Sea determined from raised coastal deposits and global sea-level variations, *Mar. Geol.*, 190(1-2): 283-305.